PORE STRUCTURE ANALYSIS OF LIME PLASTERS THROUGH INVERSE CHARACTERIZATION BASED ON SOUND PROPAGATION MODEL AND LABORATORY TESTS

A THESIS SUBMITTED TO
THE GRADUATE SCHOOL OF NATURAL AND APPLIED SCIENCES
OF
MIDDLE EAST TECHNICAL UNIVERSITY

BY

IŞIN MERİÇ NURSAL

IN PARTIAL FULFILLMENT OF THE REQUIREMENTS
FOR
THE DEGREE OF DOCTOR OF PHILOSOPHY
IN
BUILDING SCIENCE IN ARCHITECTURE

JUNE 2024

Approval of the thesis:

PORE STRUCTURE ANALYSIS OF LIME PLASTERS THROUGH INVERSE CHARACTERIZATION BASED ON SOUND PROPAGATION MODEL AND LABORATORY TESTS

submitted by **IŞIN MERİÇ NURSAL** in partial fulfillment of the requirements for the degree of **Doctor of Philosophy** i**n Building Science in Architecture, Middle East Technical University** by,

Prof. Dr. Naci Emre Altun
Dean, Graduate School of **Natural and Applied Sciences** _____

Assoc. Prof. Dr. Ayşem Berrin Çakmaklı
Head of the Department, **Architecture** _____

Assoc. Prof. Dr. Ayşe Duman
Supervisor, **Architecture, METU** _____

Prof. Dr. Mehmet Çalışkan
Co-Supervisor, **Mechanical Engineering, METU** _____

Examining Committee Members:

Prof. Dr. Ali Murat Tanyer
Architecture, METU _____

Assoc. Prof. Dr. Ayşe Duman
Architecture, METU _____

Assoc. Prof. Dr. Çağla Meral Akgül
Civil Engineering, METU _____

Assist. Prof. Dr. Zühre Sü Gül
Architecture, Bilkent University _____

Assoc. Prof. Dr. Aktan Acar
Architecture, TOBB ETÜ _____

Date: 13.06.2024

I hereby declare that all information in this document has been obtained and presented in accordance with academic rules and ethical conduct. I also declare that, as required by these rules and conduct, I have fully cited and referenced all material and results that are not original to this work.

Name Last name : Işın Meriç Nursal

Signature :

ABSTRACT

PORE STRUCTURE ANALYSIS OF LIME PLASTERS THROUGH INVERSE CHARACTERIZATION BASED ON SOUND PROPAGATION MODEL AND LABORATORY TESTS

Meriç Nursal, Işın
Doctor of Philosophy, Building Science in Architecture
Supervisor: Assoc. Prof. Dr. Ayşe Duman
Co-Supervisor: Prof. Dr. Mehmet Çalışkan

June 2024, 177 pages

Sound absorption of lime plasters is strongly connected to their unique pore structures. This study aims to comprehensively define the pore structures formed by different compositional features in lime plasters. The methodology includes inverse characterization based on sound absorption performance and laboratory tests to define the physical and the physico-mechanical properties, in addition to the pore structure analysis of cross sections under microscope. The inverse characterization study is performed using Johnson Champoux Allard's sound propagation model and Genetics Algorithm.

The interpretation of the data achieved by laboratory tests and inverse characterization shows that the aggregate size distribution is the key compositional property that controls the sound absorption performance. Furthermore, it has a major influence on the viscous and thermal characteristic lengths, fine porosity, tortuosity, airflow resistance, pore size, and morphology of the pore structure. Among different features related to pore structure, only airflow resistivity and thermal characteristic length are significantly affected by the binder-to-aggregate ratio. The effective porosity values estimated by inverse characterization are lower than the measured

total open porosity using the water immersion technique. This indicates that most of the lime plasters' open pores are dead-end type blind pores.

In this study, combining inverse and direct characterization gives valuable insights into the pore structure of lime plasters. Estimating pore structure-related parameters using sound absorption performance offers great promise as a non-destructive tool in material characterization as long as in-situ sound absorption measurement methods are accessible.

Keywords: Lime Plasters, Pore Structure, Sound Absorption Coefficients, Inverse Characterisation, Johnson Champoux Allard Model

ÖZ

SES YAYILIM MODELİNE DAYALI TERS KARAKTERİZASYON VE LABORATUVAR TESTLERİ İLE KİREÇ SIVALARININ GÖZENEK YAPISI ANALİZİ

Meriç Nursal, Işın
Doktora, Yapı Bilimleri, Mimarlık
Tez Yöneticisi: Doç. Dr. Ayşe Duman
Ortak Tez Yöneticisi: Prof. Dr. Mehmet Çalışkan

Haziran 2024, 177 sayfa

Kireç sıvaların ses yutma performansı gözenek yapısı ile doğrudan ilintilidir. Bu çalışma, kireç sıvalarında farklı bileşim özelliklerinin oluşturduğu gözenek yapılarını, ses yutma performansına dayalı ters karakterizasyon yöntemini ve diğer standard laboratuvar testlerini kullanarak, kapsamlı bir şekilde tanımlamayı amaçlamaktadır. Ters karakterizasyon çalışması Johnson Champoux Allard'ın ses yayılım modeli ve Genetik Algoritma kullanılarak gerçekleştirilmiştir. Doğrudan, ölçümlerle gerçekleştirilen karakterizasyon çalışmasında; fiziksel ve fizikomekanik özellikler için yapılan temel laboratuvar testlerinin yanısıra, mikroskop ile alınan kesit görüntüleri üzerinden yapılan gözenek analizlerinden yararlanılmıştır.

Laboratuvar testleri ve ters karakterizasyonla elde edilen verilerin ortak yorumu, agrega boyut dağılımının ses yutma performansını etkileyen temel bileşim özelliği olduğunu göstermektedir. Agrega boyut dağılımının; viskoz karakteristik uzunluk, ısıl karakteristik uzunluk, ince gözeneklilik, hava akışı direnci, kıvrımlılık, gözenek boyutu ve biçimi gibi gözenek yapısı özellikleri üzerinde önemli bir etkisi olduğu gözlenmiştir. Gözenek yapısına ilişkin farklı özellikler arasında bağlayıcı/agrega oranı değişiminden en çok etkilenen özellikler, hava akışı direnci ve termal

karakteristik uzunluktur. Ters karakterizasyonla tahmin edilen etkin gözeneklilik, suya daldırma tekniği ile ölçülen toplam açık gözeneklilikten daha düşüktür. Bu durum kireç sıvalardaki açık gözeneklerin çoğunun, çıkmaz/kör gözeneklerden oluştuğunu göstermektedir.

Bu çalışmada ters karakterizasyon ve doğrudan yapılan ölçümler yoluyla elde edilen verilerin birlikte analizi, kireç sıvalarının gözenek yapısı hakkında ayrıntılı sonuçlara ulaşma imkanı sunmuştur. Yerinde ses yutma katsayısı ölçme yöntemleri erişilebilir olduğu sürece, ses yutma performansına bağlı ters karakterizasyon, gözenek yapısı analizinde tahribatsız bir muayene metodu olarak kullanılabilecektir.

Anahtar Kelimeler: Kireç Sıvalar, Gözenek Yapısı, Ses Yutma Katsayısı, Ters Karakterizasyon, Johnson Champoux Allard Modeli

To my grand mother Nazife Güngör…

ACKNOWLEDGMENTS

I would like to extend my sincere appreciation to my supervisor, Assoc. Prof. Dr. Ayşe Duman and my co-supervisor, Prof. Dr. Mehmet Çalışkan for their support, counsel, critiques, inspirations, and insights during this research. The study came to a satisfactory end thanks to my supervisor's inquisitive perspective and her attention to details together with my co-supervisor's encouraging attitude toward further research, and his comforting attitude throughout this journey.

I would also like to thank the members of thesis study examining committee for their sincere guidance. Prof. Dr. Emine Caner Saltık played an important role during this study with her short to the point remarks originating from her extensive knowledge on material characterization. The development of this study was greatly aided by Assoc. Prof. Dr. Çağla Akgül's supportive remarks and the knowledge she offered regarding contemporary analytical approaches.

I would like to thank Onursal Önen for his assistance in implementing the optimization studies, which are the foundation of this thesis. He answered all my questions regarding Matlab or Genetic Algorithm with great patience and extraordinary speed. My dearest lab mates; Meltem Erdil Bölükbaşı, Negar Madani, Nilüfer Kızılkaya Öküz, Burhan Alam and Gökçe Ulusoy's existence makes this journey the most enjoyable one. And thanks to the members, other friends from from METU Materials Conservation laboratory. A great mention goes to Mezzo Stüdyo and the team mates. Thanks for the facilities and the super fruitful conversations on acoustics.

Finally I would like to express my appreciation to my dearest parents Seher and Rifat, my generous mother in law Nermin İcay and my belowed husband, one of a kind Ali Özgü Nursal. Your assistance is what keeps me going. My cuties Doruk and Neşe, I am now completely available to play.

TABLE OF CONTENTS

ABSTRACT v

ÖZ vii

ACKNOWLEDGMENTS x

TABLE OF CONTENTS xi

LIST OF TABLES xiv

LIST OF FIGURES xix

LIST OF ABBREVIATIONS xxiii

LIST OF SYMBOLS xxiv

1 INTRODUCTION 1

1.1 Argument 1

1.2 Aim and objectives 2

1.3 Disposition 3

2 LITERATURE REVIEW 5

2.1 Propagation of sound in porous materials 5

2.1.1 Acoustical performance parameters associated with sound absorption 5

2.1.2 Material properties related to sound absorption performance 8

2.1.3 Sound propagation theories 14

2.2 Mortar and plaster: Definition and compositional characteristics 20

2.3 Pore structure of mortars and plasters 21

2.4 Acoustic performance in relation to pore structure for consolidated granular materials 27

3 MATERIALS AND METHODS 39
3.1 Raw materials used in plaster sample preparation 39
3.2 Sample preparation 47
3.3 Experimental procedures for direct characterization 50
3.3.1 Determination of bulk density, porosity and fine porosity 50
3.3.2 Determination of pore size and pore morphology by microscopy 51
3.3.3 Determination of water vapor permeability 52
3.3.4 Determination of dynamic modulus of elasticity by ultrasonic pulse velocity 54
3.3.5 Measurement of sound absorption coefficient 55
3.4 Non acoustical parameters estimation using inverse characterization 57
4 RESULTS 61
4.1 Density, porosity and fine porosity of plaster samples 62
4.2 Pore size and morphology of plaster samples 64
4.3 Water vapor permeability of plaster samples 72
4.4 UPV and modulus of elasticity of plaster samples 73
4.5 Sound absorption coefficients of plaster samples 74
4.6 Inverse characterization 76
5 DISCUSSION 81
5.1 Assessing the effect of compositional properties on the pore structure 81
5.2 Discussion on the interrelations between parameters defining pore structure 93
5.3 Performance properties in relation to pore structure and compositional properties 99

5.3.1 Discussion on water vapor permeability and pore structure of plasters 100

5.3.2 Discussion on dynamic modulus of elasticity and pore structure of plasters 104

5.3.3 Discussion of sound absorption performance and pore structure of plasters 109

6 CONCLUSION 117

REFERENCES 123

A. The results of statistical tests conducted on the first plaster set 143

B. The resulst of statistical tests conducted on the second plaster set 168

CURRICULUM VITAE 175

LIST OF TABLES

TABLES

Table 2.1 Type of waves propagating in rigid, elastic and limp frame materials ... 16
Table 2.2 Measured (M) and predicted (P) microstructural pore properties of different granular materials reported in literature ... 35
Table 3.1 Types of building limes and their classification ... 40
Table 3.2 Classification of calcium lime and the minimum amount of CaO+MgO required for classification ... 40
Table 3.3 The origin, procurement form and size of aggregates used in samples ... 42
Table 3.4 Sieved and washed aggregates from second set of samples ... 45
Table 3.5 Water absorption, relative density of SSD aggregates, bulk density of dry aggregates and bulk density of SSD aggregates used in sample preparation ... 46
Table 3.6 Compositional ratios of first set of samples ... 48
Table 3.7 Compositional ratios of second set of samples ... 49
Table 3.8 Water vapor permeability classification ... 54
Table 4.1 Density, porosity (%), fine porosity (%) and fine to total porosity (%) .. 63
Table 4.2 Impregnation status of material samples ... 64
Table 4.3 Average, median, minimum and maximum pore sizes observed visually through microscopy. ... 71
Table 4.4 Water vapour diffusion-equivalent air layer thickness (S_d) and water vapour resistance factor (μ) ... 72
Table 4.5 Measured UPV (m/s) and E_{mod} (MPa) values of samples ... 73
Table 4.6 Results of inverse characterization ... 77
Table 5.1 Pairwise comparison of material samples based on sound absorption data at 100Hz, (a) unadjusted significance results (b) adjusted significance results 111
Table 5.2 Pairwise comparison of material samples based on sound absorption data at 125Hz, (a) unadjusted significance results (b) adjusted significance results 112
Table 5.3 Pairwise comparison of second set based on sound absorption data 116
Table 5.4 SAA and NRC comparison of second set of plasters ... 116

Table A. 1 The result of Kruskal Wallis Test for the data of first plaster set received from low frequency impedance tube measurements …143

Table A. 2 The result of Kruskal Wallis Test for the data of first plaster set received from high frequency impedance tube measurements..... 144
Table A. 3 Abbreviations used for material codes in statistical tests 144
Table A. 4 Pairwise comparison of samples from the first material set based on sound absorption data at 63Hz received from low frequency impedance tube 145
Table A. 5 Pairwise comparison of samples from the first material set based on sound absorption data at 80Hz received from low frequency impedance tube 146
Table A. 6 Pairwise comparison of samples from the first material set based on sound absorption data at 100Hz received from low frequency impedance tube .. 147
Table A. 7 Pairwise comparison of samples from the first material set based on sound absorption data at 125Hz received from low frequency impedance tube .. 148
Table A. 8 Pairwise comparison of samples from the first material set based on sound absorption data at 160Hz received from low frequency impedance tube .. 149
Table A. 9 Pairwise comparison of samples from the first material set based on sound absorption data at 200Hz received from low frequency impedance tube .. 150
Table A. 10 Pairwise comparison of samples from the first material set based on sound absorption data at 250Hz received from low frequency impedance tube .. 151
Table A. 11 Pairwise comparison of samples from the first material set based on sound absorption data at 315Hz received from low frequency impedance tube .. 152
Table A. 12 Pairwise comparison of samples from the first material set based on sound absorption data at 400Hz received from low frequency impedance tube .. 153
Table A. 13 Pairwise comparison of samples from the first material set based on sound absorption data at 500Hz received from low frequency impedance tube .. 154
Table A. 14 Pairwise comparison of samples from the first material set based on sound absorption data at 630Hz received from low frequency impedance tube .. 155

Table A. 15 Pairwise comparison of samples from the first material set based on sound absorption data at 800Hz received from low frequency impedance tube ... 156
Table A. 16 Pairwise comparison of samples from the first material set based on sound absorption data at 1000Hz received from low frequency impedance tube . 157
Table A. 17 Pairwise comparison of samples from the first material set based on sound absorption data at 1250Hz received from low frequency impedance tube . 158
Table A. 18 Pairwise comparison of samples from the first material set based on sound absorption data at 1600Hz received from low frequency impedance tube . 159
Table A. 19 Pairwise comparison of samples from the first material set based on sound absorption data at 1000Hz received from high frequency impedance tube 160
Table A. 20 Pairwise comparison of samples from the first material set based on sound absorption data at 1250Hz received from high frequency impedance tube 161
Table A. 21 Pairwise comparison of samples from the first material set based on sound absorption data at 1600Hz received from high frequency impedance tube 162
Table A. 22 Pairwise comparison of samples from the first material set based on sound absorption data at 2000Hz received from high frequency impedance tube 163
Table A. 23 Pairwise comparison of samples from the first material set based on sound absorption data at 2500Hz received from high frequency impedance tube 164
Table A. 24 Pairwise comparison of samples from the first material set based on sound absorption data at 3150Hz received from high frequency impedance tube 165
Table A. 25 Pairwise comparison of samples from the first material set based on sound absorption data at 4000Hz received from high frequency impedance tube 166
Table A. 26 Pairwise comparison of samples from the first material set based on sound absorption data at 5000Hz received from high frequency impedance tube 167

Table B. 1 The results of Kruskal-Wallis test for the data of second plaster set received from low frequency impedance tube measurements 168
Table B. 2 The results of Kruskal-Wallis test for the data of second plaster set received from high frequency impedance tube measurements 169

Table B. 3 Abbreviations used for material codes in statistical tests..... 169
Table B. 4 Pairwise comparison of samples from the second material set based on sound absorption data at 63Hz received from low frequency impedance tube 169
Table B. 5 Pairwise comparison of samples from the second material set based on sound absorption data at 100Hz received from low frequency impedance tube .. 170
Table B. 6 Pairwise comparison of samples from the second material set based on sound absorption data at 125Hz received from low frequency impedance tube .. 170
Table B. 7 Pairwise comparison of samples from the second material set based on sound absorption data at 315Hz received from low frequency impedance tube .. 170
Table B. 8 Pairwise comparison of samples from the second material set based on sound absorption data at 400Hz received from low frequency impedance tube .. 170
Table B. 9 Pairwise comparison of samples from the second material set based on sound absorption data at 500Hz received from low frequency impedance tube .. 171
Table B. 10 Pairwise comparison of samples from the second material set based on sound absorption data at 630Hz received from low frequency impedance tube .. 171
Table B. 11 Pairwise comparison of samples from the second material set based on sound absorption data at 800Hz received from low frequency impedance tube .. 171
Table B. 12 Pairwise comparison of samples from the second material set based on sound absorption data at 1000Hz received from low frequency impedance tube 171
Table B. 13 Pairwise comparison of samples from the second material set based on sound absorption data at 1250Hz received from low frequency impedance tube 172
Table B. 14 Pairwise comparison of samples from the second material set based on sound absorption data at 1600Hz received from low frequency impedance tube 172
Table B. 15 Pairwise comparison of samples from the second material set based on sound absorption data at 1000Hz received from high frequency impedance tube 172
Table B. 16 Pairwise comparison of samples from the second material set based on sound absorption data at 1250Hz received from high frequency impedance tube 172
Table B. 17 Pairwise comparison of samples from the second material set based on sound absorption data at 1600Hz received from high frequency impedance tube 173

Table B. 18 Pairwise comparison of samples from the second material set based on sound absorption data at 2000Hz received from high frequency impedance tube 173
Table B. 19 Pairwise comparison of samples from the second material set based on sound absorption data at 2500Hz received from high frequency impedance tube 173
Table B. 20 Pairwise comparison of samples from the second material set based on sound absorption data at 3150Hz received from high frequency impedance tube 173
Table B. 21 Pairwise comparison of samples from the second material set based on sound absorption data at 4000Hz received from high frequency impedance tube 174
Table B. 22 Pairwise comparison of samples from the second material set based on sound absorption data at 5000Hz received from high frequency impedance tube 174

LIST OF FIGURES

FIGURES

Figure 2.1. Different pore types in porous materials (Mati-Baouche et al., 2016) ... 9
Figure 2.2. Classification of pore sizes and the size range for different type of pores (Thomson et al., 2007) ... 10
Figure 2.3. Representation of tortuosity (drawn by author, 2023) ... 12
Figure 2.4. A representation of pore structures and the parts where viscous (Λ) and thermal characteristic length (Λ′) are effective (Szűcs, 2023) ... 13
Figure 2.5. Differential volume of intruded mercury vs. pore diameter for thepaste made of Folwark Roman cement, (a) w/c=0.6, (b) w/c=1 cured at various ages ... 23
Figure 2.6. Differential volume of intruded mercury vs. pore diameter for samples collected from various decorative elements of the Trade Academy in Krakow, Poland ... 24
Figure 2.7. Porosity variation with water/cement ratio ... 25
Figure 2.8. The relation between porosity and water/binder (w/b) ratio in mortars in lime-pozzolan mortar prepared with natural river sand (right) and standard sand (left) ... 25
Figure 2.9. Pore size distribution at 12 months curing time, metakaolin/lime ratios for MK1: 1, MK05: 0.5, MK5: 0.2 and MK2.5: 0.09 ... 26
Figure 3.1. Mineralogical content of hydrated lime powder used in the study ... 41
Figure 3.2. Mineralogical content of siliceous aggregates of 1st sample set ... 43
Figure 3.3. Mineralogical content of siliceous aggregates of 2nd sample set ... 43
Figure 3.4. Mineralogical content of pumice aggregates ... 44
Figure 3.5. Mineralogical content of tuff aggregates ... 44
Figure 3.6. Nomenclature of samples ... 47
Figure 3.7. Sound absorption coefficient measurement system set up ... 56
Figure 3.8. Individual's coding as chromosomes (Lee & Park, 2022) ... 59
Figure 4.1. Carbonated (neutral) and not carbonated (pink color) areas in plaster samples. ... 62

Figure 4.2. Frequency distribution of visually observable pore sizes 65
Figure 4.3. Section image of W-S1-1/1.5-DistB sample 66
Figure 4.4. Section image of W-S1-1/1-DistM sample 67
Figure 4.5. Section image of W-S1-1/0.4-DistS sample 67
Figure 4.6. Section image of W-S1-1/1.5-DistB sample (left) and V-S2-1/0.6-DistSp (right) 69
Figure 4.7. Section image of V-S2-1/0.6-DistSp 69
Figure 4.8. Section image of V-T-1/0.6-DistSp 70
Figure 4.9. Section image of V-P-1/0.6-DistSp 70
Figure 4.10. Sound absorption coefficients of plaster samples 75
Figure 4.11. Measured and predicted sound absorption coefficient for the first six samples of first plaster set 79
Figure 4.12. Measured and predicted sound absorption coefficient of the last three samples of first plaster set and the samples of the second plaster set 80
Figure 5.1. The change in porosity with respect binder to aggregate ratio and aggregate size distribution 81
Figure 5.2. Open porosity of samples in the second plaster set 82
Figure 5.3. Water absorption (%) of different type and size of aggregates used in the second plaster set 83
Figure 5.4. The change in fine porosity (%) with respect binder to aggregate ratio and aggregate size distribution 84
Figure 5.5. Fine porosities (%) in the second plaster set 84
Figure 5.6. The change in effective porosity (%) with respect binder to aggregate ratio and aggregate size distribution 86
Figure 5.7. The effective porosities (%) of second plaster set. 86
Figure 5.8. The frequency of pore sizes for the first plaster sample set 87
Figure 5.9. The frequency of pore sizes for the second plaster sample set 88
Figure 5.10. The tortuosity values for the first plaster set 88
Figure 5.11. The tortuosity values for the second plaster set 89
Figure 5.12. The airflow resistivity values for the first plaster sample set 90

Figure 5.13. The airflow resistivity values for the second plaster sample set 90
Figure 5.14. Viscous characteristic length for the first plaster sample set..... 91
Figure 5.15. Viscous characteristic length for the second plaster sample set..... 91
Figure 5.16. Thermal characteristic length for the first plaster sample set..... 92
Figure 5.17. Thermal characteristic length for the second plaster sample set 92
Figure 5.18. The correlation of open porosity and fine porosity 94
Figure 5.19. The relation between fine to total open porosity (%) and fine porosity (%)..... 95
Figure 5.20. The correlation of effective porosity (%) and open porosity (%)..... 96
Figure 5.21. The relation between tortuosity and viscous characteristic length..... 97
Figure 5.22. The relation between viscous characteristic length and pore size for the first (left) and the second (right) sample set..... 98
Figure 5.23. The relation between characteristic length and pore size for the second sample set..... 99
Figure 5.24. The relation between water vapor resistance factor and open porosity 100
Figure 5.25. The relation between water vapor resistance factor and fine porosity 101
Figure 5.26. The relation between water vapor resistance factor and effective porosity 102
Figure 5.27. Water vapor resistance factor and air flow resistivity 103
Figure 5.28. The relation between water vapor resistance factor and tortuosity .. 103
Figure 5.29. Ultrasonic pulse velocity with respect to open porosity..... 105
Figure 5.30. Ultrasonic pulse velocity with respect to density 105
Figure 5.31. Ultrasonic pulse velocity with respect to fine porosity 106
Figure 5.32. Dynamic modulus of elasticity with respect to open porosity..... 107
Figure 5.33. Dynamic modulus of elasticity with respect to fine porosity 108
Figure 5.34. Dynamic modulus of elasticity with respect to tortuosity 109
Figure 5.35. Average values of parameters related to pore structure for the first plaster set grouped aggregate size distribution 113

Figure 5.36. Average values of parameters related to pore structure for the first plaster set grouped according to binder to aggregate ratio 114

LIST OF ABBREVIATIONS

ABBREVIATIONS

BA Binder to aggregate

JCA Johnson Champoux Allard Model

NRC Noise reduction coefficient

SAA Sound absorption average

UPV Ultrasonic pulse velocity

WVP Water vapor permeability

WVTR Water vapor transmission rate

LIST OF SYMBOLS

SYMBOLS

A	Surface area, m^2
c	Speed of sound, m/s
d	Thickness, m
f	Frequency, Hz
j	Imaginary number ($\sqrt{-1}$)
k_c	Complex wave number or characteristic propagation constant
K_e	Effective bulk modulus
N_p	Prandtl number (≈ 0.71)
p_0	Athmospheric pressure ($\approx$101,320), N/m^2
R	Reflection coefficient
α	Absorption coefficient
α_w	Weighted sound absorption coefficient
α_∞	Tortuosity
s_b	Shape factor
T	Bessel function
Z_c	Characteristic impedance, Pa·m/s
Z_s	Surface impedance, Pa·m/s
Z_n	Normalized impedance, Pa·m/s
Z_0	Characteristic impedance of air, Pa·m/s

γ	Ratio of the specific heat capacity (≈1.4)
ρ	Bulk density, kg/m^3
ρ_e	Effective density, kg/m^3
ρ_0	Specific density of air (≈1.204), kg/m^3
σ	Flow resistivity, N·s/m^4
η	Viscosity of air (≈1.84·10^{-5}), Pa·s
ϕ	Porosity
Λ	Viscous characteristic length, m
Λ'	Thermal characteristic length, m
λ	Wave length, m
ω	Angular frequency, 1/s
M	Mass of the sample
M_{dry}	Dry weight, g
M_{std}	Saturated weight, g
M_{arch}	Weight of the sample in water, g
S_d	Equivalent air layer thickness of water vapor diffusion, m

CHAPTER 1

INTRODUCTION

The porosity characteristics of materials strongly affect the sound absorption performance. Moreover, these characteristics also play a major role in water transport, breathing ability, mechanical strength, durability, and compatibility of building materials (Arenas & Crocker, 2010; Thomson et al., 2007; Bágel' & Živica, 1997; Papayianni & Stefanidou, 2006; Lafhaj et al., 2006; Eve et al., 2007). Knowing the possible relations between porous structure and some performance properties, the formation of pores in materials and the ways to alter its structure with different raw materials, material production and processing techniques are also popular subjects in material characterization research (Neithalath, 2004; H. K. Kim & Lee, 2010b; Losa & Leandri, 2012; Balksten & Steenari, 2010; Lawrence et al., 2007; Mosquera et al., 2006; Sugrañez et al., 2013). Most of the research conducted on materials focuses on highly sound absorptive materials such as foams, metallic foams, fibrous materials, or granular materials having loose bigger size granules/aggregates or consolidated with a minimum amount of binder in which sound absorption can be observed nearly 100% at a broad frequency range. On the other hand, less has been done so far to investigate sound propagation in materials with porosity less than 0.5.

1.1 Argument

Lime plasters were frequently used in the past until the 19th century and the first half of the 20th century (Aggelakopoulou et al., 2011; Lawrence et al., 2007). Many studies have been conducted on the lime plasters employed in historic structures in

recent years (Garofano et al., 2014; Maravelaki-Kalaitzaki et al., 2005; Böke et al., 2006). As underlined in various research, the porosity of lime plasters and mortars is higher than that of cement plasters (Stefanidou & Papayianni, 2005; Lawrence et al., 2007). Due to their porous structure, these plasters absorb sound remarkably higher than contemporary cement plasters (Aydin et al., 2008). On the other hand, the researches on the acoustical characteristics of lime plasters are limited (Aydin, 2008; Bozkurt & Demirkale, 2018, 2019, 2020b) and do not thoroughly investigate the porous structure and link its characteristics to the sound absorption performance. Although the absorption performance of lime plasters was much below that of the materials used as sound absorbers, in its own category, it is worth investigating the porous structure of these materials in detail to reveal the connection between porous structure and acoustical performance. As this investigation will lead to additional knowledge on pore structure of lime plasters besides standard test methods.

1.2 Aim and objectives

The main aim of this research is to identify the parameters related with pore structure that govern the sound propagation within the porous lime plasters though systematic and comprehensive experiments. This PhD research is expected to contribute to the knowledge of material science with the objectives as stated below;

(1) The detailed pore analysis of lime plasters to understand the mechanisms that form the unique pore structure connected to compositional characteristics.

(2) The development of a systematic experimental approach to analyze the effect of different pore structure characteristics on performance properties such as sound absorption, water vapor permeability and dynamic modulus of elasticity,

(3) Investigating the possibility of employing acoustical data for inverse characterisation as a non-destructive method for analyzing plaster pore structure

1.3 Disposition

The thesis has six chapters: (1) introduction, (2) literature survey, (3) materials and method, 4) results, (5) discussion, and (6) conclusion, respectively. In the first Chapter, an introduction to the relevant field is presented. The knowledge gaps in the current material research field are emphasized, focusing on acoustical performance and the necessity of filling those gaps. The main aim and how the objectives fulfill the aim are given in this part. In the second Chapter, the literature review starts with a summary of the theory of sound propagation in porous materials. The Chapter includes the definition and the general compositional characteristics of mortar and plasters, followed by an overview of recent research areas on pore structure with an emphasis on related performance properties. Chapter 3 gives information about the research material and the experimental methods used. In the 4th Chapter, the results of experiments that characterize the plaster samples are presented, accompanied by a comparative discussion in Chapter 5. The last Chapter summarizes the main results and what has been achieved throughout this thesis.

CHAPTER 2

LITERATURE REVIEW

This chapter begins with a section on sound propagation in porous materials. The pore structure parameters related to sound absorption are described first. Afterward, sound propagation models are presented. A brief section on the general description of mortar and plaster and their compositional features is followed by a discussion of research on pore structure and its impact on performance parameters. The last section summarizes the literature on acoustic performance regarding compositional features and pore structure for consolidated granular materials.

2.1 Propagation of sound in porous materials

The acoustical parameters, such as acoustic impedance and sound absorption coefficient, are direct expressions that measure the acoustical performance of a material interacting with sound waves. After a brief explanation of acoustical parameters, the definition of material characteristics (commonly named “non-acoustical" in literature) related to sound absorption is presented in this section. At the end, the sound propagation theories in porous materials are summarized.

2.1.1 Acoustical performance parameters associated with sound absorption

The sound absorption coefficient of a material shows how effectively the material absorbs sound. These coefficients are measured for different frequency bands and express the percentage of absorbed sound energy. It is represented by a number between 0 and 1. The absorption increases as the coefficient changes from “0 - reflective” to “1 - perfect absorber”.

Practical single-number ratings have been used widely to categorize the sound absorption performance of the material. The one used in European countries is "weighted sound absorption." The method to determine this single number rating is described in ISO 11654 (International Standards Organization, 1997). A standard sound absorption coefficient curve is shifted until the differences between the measured data in the 1/1 octave band and data based on the standard curve are below a limit. At the final position of the standard curve, the sound absorption value at 500Hz gives the weighted sound absorption value of the material, which is represented as α_w. Other single-number ratings, namely noise reduction coefficient (NRC) and sound absorption average (SAA), are commonly addressed for describing the performance of sound-absorptive materials (ASTM International, 2023b). For NRC, the measured sound absorption values over 250Hz, 500Hz, 1kHz, and 2kHz frequencies, and for SAA, the measured values in 1/3 octave frequencies between 200Hz to 2500Hz are arithmetically averaged. These ratings are practical for assessing the performance of broad-band sound absorbers. On the other hand, for materials having high performance on specific frequencies, such as granular materials, perforated plates, or metamaterials, the effective performance observed is linearized and minimized.

The sound absorption coefficient, α, is a function of frequency and is defined as

$$\alpha = 1 - |R|^2 \qquad \text{(Equation 2.1)}$$

where R is the sound reflection coefficient. Reflection coefficient R is calculated as

$$R = \frac{Z_s - Z_0}{Z_s + Z_0} \qquad \text{(Equation 2.2)}$$

Where Z_s is the surface impedance (Pa·s/m or kg/m^2·s or rayl) and Z_0 is the characteristic specific impedance of the medium where sound propagates. As the thesis focuses on sound propagation inside air-filled pores, "the air" will be used on

behalf of "the medium" accordingly. The impedance is defined as the resistance of a medium to motion at a given point (Long, 2006). The ratio of the sound pressure to the particle velocity at a point gives the characteristic specific acoustic impedance of the medium.

$$Z_0 = \frac{p_0}{v_0} \qquad \text{(Equation 2.3)}$$

where p_0 is the sound pressure (Pa) and v_0 is the velocity of volume displacement (m/s). For plane waves, this ratio is equals to the product of the density of a medium and the speed of sound in that medium.

$$Z_0 = \rho_0 c_0 \qquad \text{(Equation 2.4)}$$

Where ρ_0 is the density of air (kg/m^3), c_0 is the velocity of sound in air (m/s). In different references, reflection coefficient is also expressed as;

$$R = \frac{Z_n - 1}{Z_n + 1} \qquad \text{(Equation 2.5)}$$

Which Z_n is the called normalized surface impedance where Z_s is normalized with the characteristic impedance of air, Z_0 as shown below.

$$Z_n = \frac{Z_s}{Z_0} \qquad \text{(Equation 2.6)}$$

The surface impedance of material, Z_s is related to the characteristic impedance of the material as indicated below.

$$Z_s = -jZ_c \cot(k_c d) \qquad \text{(Equation 2.7)}$$

Where Z_c is the characteristic impedance (Pa·s/m^3), j is the imaginary number ($\sqrt{-1}$), k_c is the complex wave number or the so called characteristic propagation constant (m^{-1}) and d is the thickness of porous material layer (m).

The attenuation of energy occurs due to viscous and thermal losses as the sound waves propagate within the pores. The basic properties related to this viscous and thermal interaction are the effective/dynamic density, ρ_e, and the effective/dynamic bulk modulus of the medium, K_e. The equations below calculate the characteristic impedance, Z_c, and the characteristic propagation constant, k_c.

$$Z_c = \sqrt{\rho_e K_e} \qquad \text{(Equation 2.8)}$$

$$k_c = \omega \sqrt{\frac{\rho_e}{K_e}} \qquad \text{(Equation 2.9)}$$

Where ρ_e is the effective density (kg/m^3) and K_e is the effective bulk modulus of the medium (Pa).

2.1.2 Material properties related to sound absorption performance

The material properties mentioned in sound propagation theories are porosity, pore size, tortuosity, air flow resistivity, thermal characteristic length, and viscous characteristic length. Further descriptions of these properties are described in detail in this section.

Porosity of a material is a bulk characteristic which gives the volume that is not occupied by the solid part of material (Thomson et al., 2007).

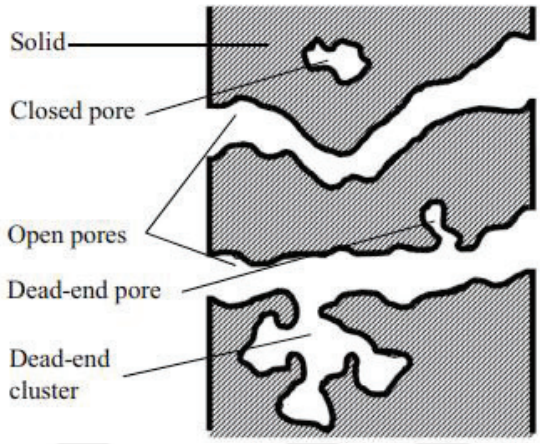


Figure 2.1. Different pore types in porous materials (Mati-Baouche et al., 2016)

The absorption in a porous material is related to the number, size, and types of pores. The structure of the material should allow sound waves to pass through it and be dispersed by internal friction. Figure 2.1 shows the type of pores according to their relation to the surface of materials. Cox and D'Antonio (2009) state that closed pores do not have an effect on the sound absorption capacity of the material, so only the volume of open/interconnected pores should be considered to define the porosity of the material in relation to its sound absorption capacity. Open porosity, also named as effective or acoustic porosity, is the ratio of the volume of interconnected pores to the total volume of that material (Knapen et al., 2003). In Attenborough's definition of open porosity, it is clearly stated that the air path of connected pores inside a material should have been traced to the surface of the material (Attenborough, 1983). The open pores of a material may also be separated as kinematic pores and dead-end pores. The dead-end pores are assumed to be not so effective in sound absorption. Although attempts have been made so far to add a correction factor in sound absorption performance predictions to reflect the situation of dead-end pores (Dupont et al., 2011; Leclaire et al., 2015), there is still a lack of empirical knowledge on this subject.

The influence of pore size, pore aperture/opening size, pore size distribution, and geometry of dominant pores on sound absorption is investigated in detail through a

number of experimental research (Neithalath, 2004; Marolf et al., 2004; Lu et al., 2000; Giese et al., 2011). These factors are also taken into account in sound propagation models in order to associate the pore structure with the absorption of sound (Attenborough, 1983; Champoux & Stinson, 1992). A classification on pore sizes based on International Union of Pure and Applied Chemistry (IUPAC) is given in Figure 2.2 (Thomson et al., 2007).

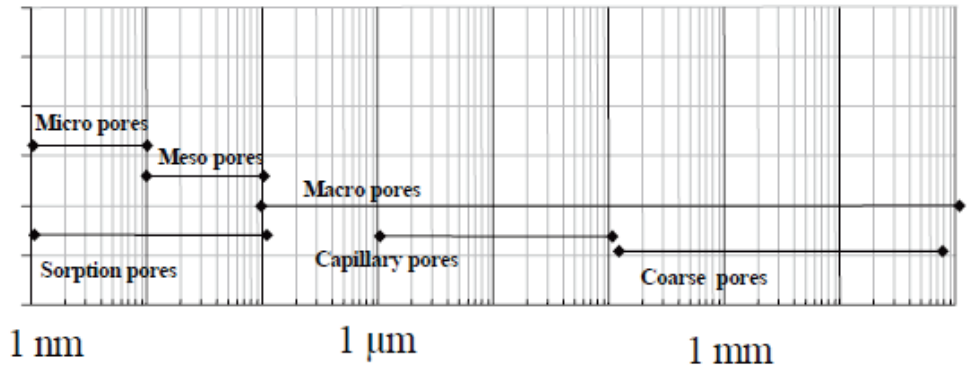


Figure 2.2. Classification of pore sizes and the size range for different type of pores (Thomson et al., 2007)

As mentioned by Thomson et al. (2007), sorption pores that have sizes less than 100nm are observed in hydraulic hydrated phases and are not found in materials containing pure lime. Capillary pores are found in the binder and binder-aggregate interphase. These pores may have been formed by weak adherence of binder to aggregate or possible drying and shrinkage of material during setting. The carbonation process also results in a volume change in molecule size, which triggers the stress and causes fissures within the material. Capillary pores are open pores to the material's surface and play an important role in transport mechanisms for fluids, water vapor, and even sound. Coarse pores mostly occur due to entrapped air while raw materials are mixed in the sample preparation. Entrained air, due to added admixtures that release gas during the chemical reaction, falls into the coarse pore category (Thomson et al., 2007). Shrinkage cracks of coarse pore size due to excess water in preparation can also be observed. The effect of different pore shapes on

sound absorption is studied by researchers (Attenborough, 1983; Stinson & Champoux, 1992) to be used in different sound propagation models, but predictions based on a simplification of shapes do not compare much with experimental results received from naturally occurring complex pore shapes.

There are a number of methods to measure porosity and investigate the pores in detail. The simplest is the water immersion technique, which is going to be also described in Chapter 3rd of the thesis. The others can be listed as image analysis through a microscope, gas adsorption, mercury intrusion porosimetry (MIP), scanning electron microscopy (SEM), nuclear magnetic resonance (NMR) (Da Silva et al., 2023; Maria, 2010; Thomson et al., 2007). The researchers working in the field of acoustics also developed methodologies to measure porosity. Some of these are based on air volume pressure differences (Champoux et al., 1991; Leclaire et al., 2003), while the other depends on ultrasonic measurements that can be done through sophisticated equipment (Fellah et al., 2003).

The flow resistivity of a material is the flow resistance of the material per unit thickness and directly affects the sound absorption performance. Flow resistance is described as a material property that measures the resistance of the material to airflow (Kuczmarski & Johnston, 2011). The equations 2.10 and 2.11 are used to calculate the flow resistance (σ_s) and flow resistivity (σ) respectively (Cox & D'Antonio, 2009).

$$\sigma_s = \frac{\Delta p}{U} \qquad \text{(Equation 2.10)}$$

$$\sigma = \frac{\Delta p}{U d} \qquad \text{(Equation 2.11)}$$

In Equation 2.10 and 2.11, Δp is the pressure difference across the test sample in Pa, U is the mean steady flow velocity in m/s and d is the thickness of the porous test material in m. Standard test method to determine the air flow resistance of a material

is described in the international standard, ISO 9053 (International Standards Organization, 1991).

Tortuosity, another important parameter in the propagation of sound, is related to the pore structure. Seddeq (2009) describes it as “a measure of the elongation of the passageway through the pores, compared to the thickness of the sample” (Figure 2.3). In Fahy’s book (2005), tortuosity is defined as the degree of irregularity and variation of channel direction inside a porous material. Cox and D’Antonio (2009) refer to tortuosity and say that the absorption of sound in a material will increase as the complexity of the sound propagation path in that material increases. It is noted by Seddeq (2009) that “the value of tortuosity determines the high frequency behavior of sound absorbing porous materials”.

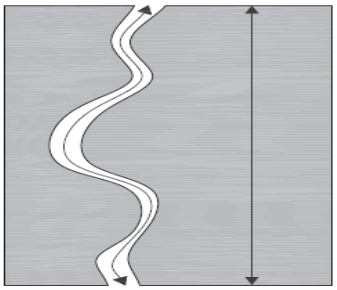


Figure 2.3. Representation of tortuosity (drawn by author, 2023)

Pore shape plays an important role in the propagation of sound through the material and it affects the viscous and thermal events that occur while sound propagates within the pore (Cox & D’Antonio, 2009). The two parameters mostly referred to in literature related to pore shape are viscous characteristic length (Λ) and thermal characteristic length (Λ'). The viscous forces are mostly effective in the narrow parts of the pores while the thermal interaction takes place in the broader part of the pores. A schematic representation of the pore structure and where the two characteristic lengths are related is shown in Figure 2.4 (Szűcs, 2023).

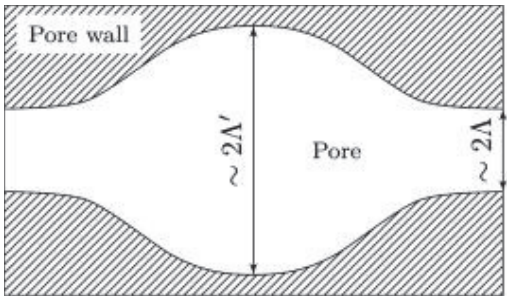


Figure 2.4. A representation of pore structures and the parts where viscous (Λ) and thermal characteristic length (Λ′) are effective (Szűcs, 2023)

Viscous characteristic length is a weighted ratio of the volume of open pores to the surface area of open pores. The weighting is done according to the squared modulus of microscopic velocity evaluated, considering the viscosity effects (Cox & D'Antonio, 2009). Knapen et al. (2004) describe the viscous characteristic length as "the viscous interaction of the stiff frame and the fluid at high frequencies" and they define the term as in the Equation 2.12.

$$\Lambda = \frac{2\int_V |v(r)|^2 dV}{\int_A |v(r_\omega)|^2 dA} \qquad \text{(Equation 2.12)}$$

In Equation 2.12, v(r) is the microscopic flow velocity of a non-viscous fluid in a pore, and $v(r_\omega)$ is the microscopic flow velocity of the same non-viscous fluid against the wall of the pores. In Equation 2.13, a more simplified version of this equation for simple pore shapes is shown (Cox & D'Antonio, 2009).

$$\Lambda = \frac{1}{s}\sqrt{\frac{8\eta k_s}{\varepsilon\sigma}} \qquad \text{(Equation 2.13)}$$

In Equation 2.13, s is a constant which lies between 0.3 and 3 for many porous absorbers, η is the viscosity of the air, k_s is the tortuosity, ε is the porosity, and σ is the flow resistivity of the material.

The thermal characteristic length is defined as the exchange of heat between the fluid and the stiff pore structure at high frequencies (Knapen et al., 2004). Equation 9, which shows the thermal characteristic length formula, is given below.

$$\Lambda' = \frac{2V_p}{S_p} \qquad \text{(Equation 2.14)}$$

In Equation 2.14, V_p is the volume of pores and S_p is the surface area of pores.

These two parameters and tortuosity can be determined through ultrasonic measurements (Allard et al., 1994; Fellah et al., 2003). These measurement methods are still not standardized and open to many errors. As the wavelength of ultrasound approaches the pore size, the waves can be attenuated easily and be diffused due to the heterogeneities of the pore structure (Atalla & Panneton, 2005). Also electrical resistivity measurements where material placed in a conducting fluid (Brown, 1980) can be used to measure tortuosity. This method is found to be destructive to the material structure and not suggested for most material types (Atalla & Panneton, 2005).

2.1.3 Sound propagation theories

Numerous models were developed to characterize the propagation of sound within porous materials. Some of these models were based on empirical data received from measurements. Others can be defined as phenomenological, in which the microstructure of the porous materials was simplified, and the propagation of sound was described on a micro-scale.

There may have three kind of waves propagating through a porous material (Biot, 1956a, 1956b):

1. Longitudinal (compression/dilatational/P-wave) waves in the solid part
2. Transverse (shear/rotational/S-wave) waves in the solid part
3. Longitudinal (compression/dilatational/P-wave) waves in the fluid part

The frame of a material can be categorized as elastic, rigid, or limp, depending on its stiffness and elasticity. In a porous material having an elastic frame, such as foam, all three mechanical wave types are observed when the material is excited by a sound wave. Due to the frame's elastic property, both longitudinal and transverse waves propagate within the frame. Besides the propagation in the frame, the air within the pores (fluid part) is affected, and longitudinal waves penetrate into the material through the pores within the fluid body. In this condition, the viscous and thermal dissipation of energy occurs not solely in solid or fluid parts, but the coupling between these two parts also contributes to the loss of energy.

The rigid frame assumption is valid when the stiffness of the solid part of the material is much greater than the stiffness of the fluid part (air in the pores) (Attenborough, 1983). In this situation, the frame is motionless and non-deformable (Panneton, 2007). Sound propagation only occurs in the fluid part of the porous material. The material is represented as an "equivalent fluid" where only longitudinal waves propagate.

When shear stresses are almost negligible as the sound propagates within the material, but an unconstrained "rigid body motion of the solid phase exists," as Panneton (2007) describes in his work, the porous material can be defined as limp frame. Existing rigid and elastic frame theories underestimate the contribution of this body motion and accordingly give inaccurate results, especially at low frequencies. On the other hand, it should be underlined that the limp frame theory is only suitable for materials under certain conditions. Beranek (1947) suggests limp frame assumption can be used as soon as the ratio of bulk modulus of the fluid phase over bulk modulus of solid phase is over 20. Later on, Doutres et al (2007) offer a metric called "frame stiffness influence (FSI)" to decide whether to use the methods that accept the frame as a "limp" in acoustic characterization.

Table 2.1 Type of waves propagating in rigid, elastic and limp frame materials

	Longitudinal waves in solid	Transverse waves in solid	Longitudinal waves in fluid
Rigid frame	×	×	✓
Elastic frame	✓	✓	✓
Limp frame	✓	×	✓

Many scientists contribute to the existing propagation models by improving their applicability to different materials and expanding the frequency ranges in which models work. According to various approaches, researchers use different acoustic and non-acoustic parameters to describe sound propagation within the porous materials they are dealing with. Phase decoupling frequency should be calculated to assess which frame assumption is suitable for the material of interest (Zwikker & Kosten, 1949). This study's frequency range of interest is between 63Hz and 8000Hz, the audible range for most people. If the calculated phase decoupling frequency is below this range, the coupling between the solid and fluid parts of the material is negligible, and the solid part, the frame, can be regarded as motionless or rigid. The formula for phase decoupling frequency is given below.

$$f_d = \frac{\sigma \phi^2}{2\pi \rho_1} \qquad \text{(Equation 2.15)}$$

Where σ is the flow resistivity (N·s/m^4), ϕ is porosity (-), ρ_1 is the density of material (kg/m^3). Within the framework of this thesis, the acoustical performance of lime plasters is examined, and rigid frame models are explained in more detail in the following parts.

The first theories related to porous materials investigated sound propagation in various sizes of tubes (Zwikker & Kosten, 1949). Tubes are practiced as an analogy of pores in porous media. The viscous and thermal effects are studied to reveal their

relation to the material's effective density and complex bulk modulus. Zwikker and Kosten's work is the one that is mostly referred to in the studies of sound propagation. According to their study, the propagation occurs in several uniform tubes perpendicular to the surface, which can be stated as a simplified model of porous materials (Zwikker & Kosten, 1949). The effective density (ρ_e) and complex bulk modulus (K_e) in their work are given as in Equation 2.16 and Equation 2.17.

$$\rho_e = \frac{\rho_0}{\phi_e} \frac{1}{\left[1 - \frac{2}{\beta\sqrt{-j}} \frac{J_1(\beta\sqrt{-j})}{J_0(\beta\sqrt{-j})}\right]} \quad \text{(Equation 2.16)}$$

$$K_e = \frac{\gamma p_0}{\phi_e} \frac{1}{\left[1 + (\gamma - 1)\frac{2}{\beta N_p\sqrt{-j}} \frac{J_1(\beta\sqrt{-j})}{J_0(\beta\sqrt{-j})}\right]} \quad \text{(Equation 2.17)}$$

In Equation 2.16 and 2.17, the term ρ_0 is the density of air (kg/m^3), ϕ_e is effective porosity, γ is the ratio of specific heat capacity (≈1.4), N_p is the Prandtl number, J1 and J0 are the Bessel functions of the first kind of order 1 and 0. The term β is a dimensionless quantity and can be calculated through the Equation 2.18.

$$\beta = \sqrt{\frac{\omega\rho_0 r^2}{\eta}} \quad \text{(Equation 2.18)}$$

The term ω is the angular frequency, η is the dynamic viscosity of air (Pa·s) and r is the radius of pore.

Biot (1956a, 1956b) derived a phenomenological approach that takes into account the coupling mechanisms between the fluid and solid phases of the material during sound propagation. The frame of material is almost motionless for a range of frequencies in his model. Out of this range, the interaction between air and frame affects the sound propagation, and the frame can be assumed to be elastic. Biot, in his work, accounts for the shape and tortuosity of pores (i.e., not perpendicular to the

surface) as he denoted them as “structural factor” and “sinuosity factor”. The theory is given extensively in the original work; in this thesis, the author refers to the papers published by Biot (Biot, 1956a, 1956b) for further information.

The model derived by Attenborough (1983) improves the previous models of Morse and Ingard and Smith and Greenkorn. Effective resistivity and stiffness, which are related to thermal effects, were associated with frequency. The model includes structure factors in order to consider the effect of increased inertia with the friction of air particles at the pore walls as they propagate and the effect of microstructure which can result in deviations in the pathway of the motion of air. Besides the dynamic shape factor proposed by Smith and Greenkorn, Attenborough also added a static shape factor. The effective density and effective bulk modulus in Attenborough’s work are given in Equation 2.19 and Equation 2.20.

$$\rho_e = \frac{\rho_0}{\phi_e} \frac{1}{\left[1 - \frac{2}{\varepsilon\sqrt{-j}} \frac{J_1\left(\varepsilon\sqrt{-j}\right)}{J_0\left(\varepsilon\sqrt{-j}\right)}\right]} \qquad \text{(Equation 2.19)}$$

$$K_e = \frac{\gamma p_0}{\phi_e} \frac{1}{\left[1 + \frac{2(\gamma - 1)}{\varepsilon\sqrt{N_p}\sqrt{-j}} \frac{J_1\left(\varepsilon\sqrt{-j}\right)}{J_0\left(\varepsilon\sqrt{-j}\right)}\right]} \qquad \text{(Equation 2.20)}$$

In Equation 2.19 and 2.20, ε is the dimensionless quantity as described by the Equation 2.21.

$$\varepsilon = \frac{1}{s_A} \sqrt{\frac{8\rho_0 \alpha_\infty \omega}{\phi_e \sigma}} \qquad \text{(Equation 2.21)}$$

In the Equation 2.21, σ is flow resistivity ($\mathrm{N \cdot s/m^4}$), α_∞ is the tortuosity and s_A is pore shape factor ratio which is a ratio as given in Equation 2.22.

$$s_A = \frac{n}{\sqrt{s}} \qquad \text{(Equation 2.22)}$$

In the Equation 2.22, *n* is the dynamic shape factor and s is the static shape factor.

Johnson et al (1987) came up with a new approach. The work is concentrated on the viscous effects that take place in arbitrarily shaped pores. A new term called "viscous characteristic length" is introduced. Following the work of Johnson et al., Allard and Champoux (1992) extend the theory to define the thermal interactions in arbitrarily shaped pores. A second parameter is introduced with this work called thermal characteristic length. The model with the extended version is mentioned as the Johnson Champoux Allard model (JCA) in literature.

$$\rho_e = \frac{\alpha_\infty \rho_0}{\phi_e}\left[1 + \frac{\sigma\phi_e}{j\omega\alpha_\infty\rho_0}\sqrt{1 + \frac{4j\alpha_\infty^2\eta\omega\rho_0}{{\phi_e}^2\Lambda^2\sigma^2}}\right] \qquad \text{(Equation 2.23)}$$

$$K_e = \frac{\gamma p_0}{\phi_e}\left[\gamma - \frac{\gamma - 1}{1 + \frac{8\eta}{j\Lambda'^2 N_p\omega\rho_0}\sqrt{1 + \frac{j\rho_0\omega N_p\Lambda'^2}{16\eta}}}\right] \qquad \text{(Equation 2.24)}$$

In Equation 2.23 and 2.24, the terms Λ and Λ' are the viscous characteristic length and thermal characteristic length respectively. Later, Lafarge et al. (1997) improved Equation 2.24 to account for the thermal effects more accurately. The modified version of the effective bulk modulus is presented in Equation 2.25.

$$K_e = \frac{\gamma p_0}{\phi_e}\left[\gamma - \frac{\gamma - 1}{1 + \frac{\eta\phi_e}{jk_0' N_p\omega\rho_0}\sqrt{1 + \frac{4jk_0'^2\rho_0\omega N_p}{\eta\Lambda'^2{\phi_e}^2}}}\right] \qquad \text{(Equation 2.25)}$$

There exists a new term, k_0', in Lafarge et al.'s equation called static thermal permeability. Although the improved equation gives a more accurate result, it is hard

to measure static thermal permeability and mostly it is predicted through measured sound absorption values.

After all, due to the lesser number of unknown parameters, which are porosity, static flow resistivity, tortuosity, and the two characteristic lengths, the JCA model is one of the most favored theories as it gives reasonable and converging results to the measured data.

2.2 Mortar and plaster: Definition and compositional characteristics

Mortar is a mixture of aggregate, binder, and water. It serves different purposes in buildings, such as bedding and jointing the building blocks, plastering, and rendering. The term "plaster" is a common name in terminology that refers to the application area, the use of mortar as a coating layer of masonry elements in the interior of a building (Arizzi & Cultrone, 2021). Mortars are called rendering when applied as a coating layer on the exterior surface of masonry elements. Whether used for plastering or rendering, mortars may participate in various roles such as protecting the building core from different weather conditions, forming a fine finish for decorative purposes, serving as a thermal barrier or a sound absorptive coating (Ergenç et al., 2021; Caner, 2003).

The binder is the main ingredient in the mixture to classify the plasters. It serves as a binding medium that transforms chemically to a stable compound as aging that holds the aggregates together (Arizzi & Cultrone, 2021; Ergenç et al., 2021; Rodriguez-Navarro, 2012). From the early ages to the present day, the materials used as binders have varied depending on the source region and the technology. According to their binder, the plaster types can be listed mainly as mud (clay-rich earth) plasters, gypsum plasters, lime plasters, and cement plasters.

The aggregates in the plasters contribute to the volume stability, strength, and durability (Ergenç et al., 2021; Stefanidou & Papayianni, 2005). Natural aggregates used since antiquity originate from quarries, rivers, and seas. These aggregates may

contain silicate minerals, carbonate minerals, or sulfate minerals. In recent practices, researchers explored the capacity of artificial aggregates such as expanded clay, expanded perlite, expanded polystyrene beads, recycled glass, or recycled rubber as a filler. Another popular trend of research is exploring the use of biobased materials as aggregates. The biobased aggregates commonly used are hemp, flax, coconut, rice husk, date palm, wood shelves etc (Amziane & Sonebi, 2016). The main drives behind these attempts are to decrease the weight, improve mechanical properties, increase the thermal insulation capacity and sound absorption performance, and/or reduce the carbon print in the manufacturing process.

Apart from these essential constituents, additives and/or admixtures may have been used to enhance specific characteristics of the plaster mixture.

2.3 Pore structure of mortars and plasters

The manufacturing process of plasters and mortars, in general, results in a unique pore structure that can not be controlled due to naturally occurring physical and chemical bonds. This complex structure is the subject of many studies. Researchers try to understand the pore structure in mortars/plasters and its connection to numerous performance properties.

The effect of raw materials, compositional ratios, and curing conditions are discussed through selected research.

The effect of shape, size and minerological composition of aggregate:

The quarried aggregate may contain sharp edges. The form of a river or sea sand is mostly rounded as abrasion on the surface occurs due to the movement of water. Sharp-edged aggregates are preferred generally as their specific surface area increases the adherence with lime (Çizer, 2004). The use of rounded shape aggregates in plaster and mortars increases the amount of larger pores and decreases the strength (Lanas et al., 2004).

Using fine aggregates below 2mm in size increases the strength of mortars. Coarse aggregates are found to be useful in the development of long-term strength and preserve volume stability (Stefanidou & Papayianni, 2005). The aggregate size used in mixtures can affect the pore formation and size (Neithalath, 2004).

The mineral composition of aggregates is important as some of the minerals in aggregates contribute to chemical reactions during the setting process. Limestone aggregates contribute to the strength as a similarity exists between lime used as a binder and limestone used as aggregates. The quartz minerals are reported as not so effective in the early setting of mortar (Çizer, 2004).

Pore size change during carbonation:

Lawrence et al. (2007) studied the alteration of pore structure during carbonation in non-hydraulic lime mortars. Observations were made on lime mortars prepared with different forms of lime (dry lime hydrate, 4-month-old lime putty, 20-year-old lime putty, dispersed hydrated lime, and hot lime), three different aggregates (crushed bioclastic stone, crushed oolithic stone, and silicate sand) and water. Mercury intrusion porosimetry method, thermogravimetric technique, and scanning electron were used to identify samples' pore alterations and carbonation state. The research showed that the volume of pores with 0.1 μm size increased with calcination. Due to the attachment of calcite crystals to aggregate surface and uncarbonated portlandite crystals, the volume of pores smaller than 0.03 μm size increased. In the research, it was also underlined that the pores under 0.1 μm size kept water outside, and this reduced the carbonation. This phenomenon clarifies why the process of carbonation in air lime mortars goes on for many years.

The effect of compositional ratio and curing on pore structure of mortars:

Researchers have also investigated the effect of the water-to-cement ratio on the pore size distribution of mortars. Klisinska-Kopacz et al. (2010) focused on the pore structure of repair mortars intended to conserve historic buildings. They compared the pore structure of freshly prepared Roman cement mortars with the pore structure

of historical Roman cement mortars collected from various historical buildings that date back to 17th and 18th history. The fresh mortars were produced from Roman cement and quartz sand, which were 0.5-1mm in size and water. The water/cement ratios of the sample mortars ranged between 0.6 and 1, and the aggregate-to-cement ratio was 1:2 by weight. The ratios used to produce mortars were chosen, similar to the ones used to produce Roman cement mortars for casting decorative elements. The results showed that as curing continued, the amount of smaller pores increased in the range of 0.01-0.03 μm. The pore size distribution curve exhibited a different character for the mortars with different water/cement ratios. As shown in Figure 2.1(a), the pore size distribution curve of mortars having a low water/cement ratio is unimodal. On the other hand, for the mortars having a higher water-to-cement ratio, the pore size distribution curve takes a bimodal form, showing two porosity domains (Figure 2.1(b)).

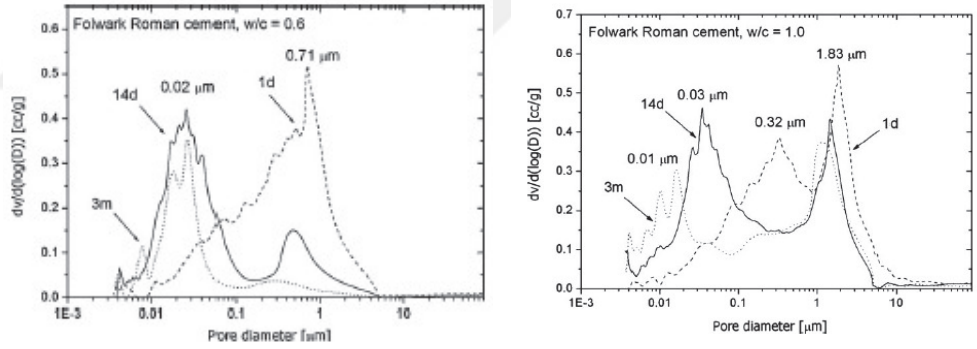


Figure 2.5. Differential volume of intruded mercury vs. pore diameter for thepaste made of Folwark Roman cement, (a) w/c=0.6, (b) w/c=1 cured at various ages

The Roman mortar samples collected from historical buildings had porosity values changing from 20% to 45%. In Figure 2.2, the pore size distribution of Roman cement materials collected from different places of a building is given. As the authors pointed out, the bimodal and multimodal shapes of these distribution curves indicated the coexistence of well-reacted cement and pores formed after the excess water that was not consumed during carbonation evaporated.

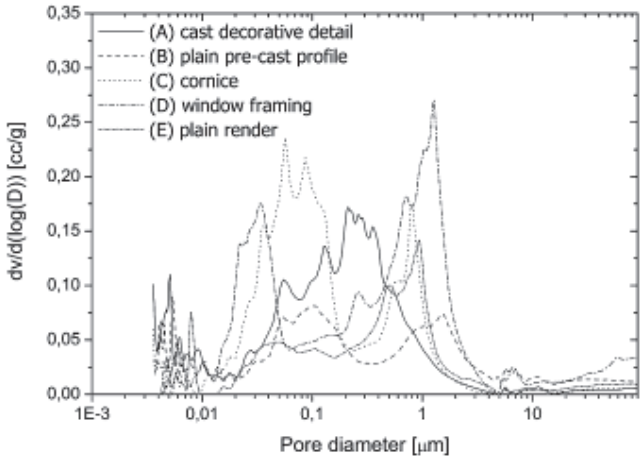


Figure 2.6. Differential volume of intruded mercury vs. pore diameter for samples collected from various decorative elements of the Trade Academy in Krakow, Poland

The ability of old mortars to continue their hydration was also tested in the research of Klisinska-Kopacz et al. (2010), and it was seen that after re-wetting the historic mortar, the pore size distribution changed, and the threshold of the distribution curve was shifted to smaller sizes.

Another similar research was conducted by Lafhaj et al. (2006), which aimed to reveal the correlations between porosity, permeability, and ultrasonic pulse velocity values of mortars produced with variable water/cement ratio. The cement used in experiments was Portland cement, and the water/cement ratios varied between 0.3 and 0.6. Fine sand in 0.16-2 mm size and coarse sand in 0.8-3.15mm were included in cement mixes. Figure 2.3 shows the change of porosity with water/cement ratio. As can be seen, porosity did not change linearly with the increase in the water/cement ratio.

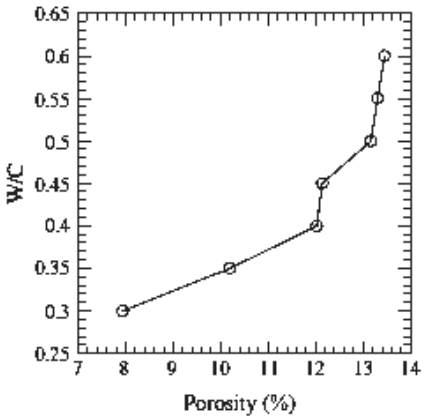


Figure 2.7. Porosity variation with water/cement ratio

In the research of Papayianni & Stefanidou (2006) which investigates the relation between porosity and strength in lime pozzolan mortars, the effect of water/binder content on porosity was investigated. In the production of test samples, hydrated lime, natural pozzolan from Milos Island, and river aggregates in fine and coarse form were mixed with different amounts of water. In some of the samples, standard sand was used in the content instead of river aggregates. The results showed that as the water/binder ratio was increased, generally, the samples got more porous (Figure 2.4).

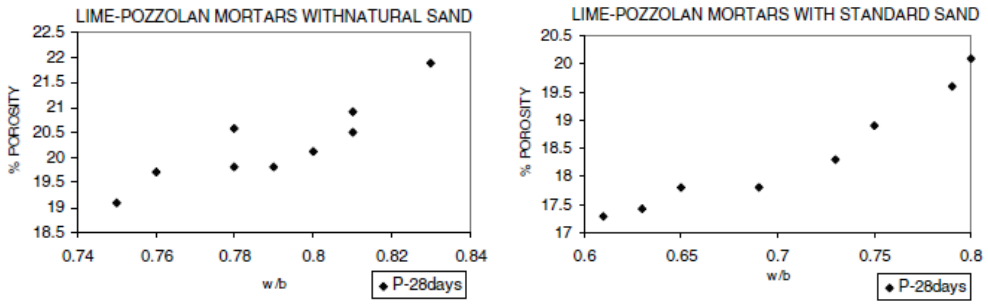
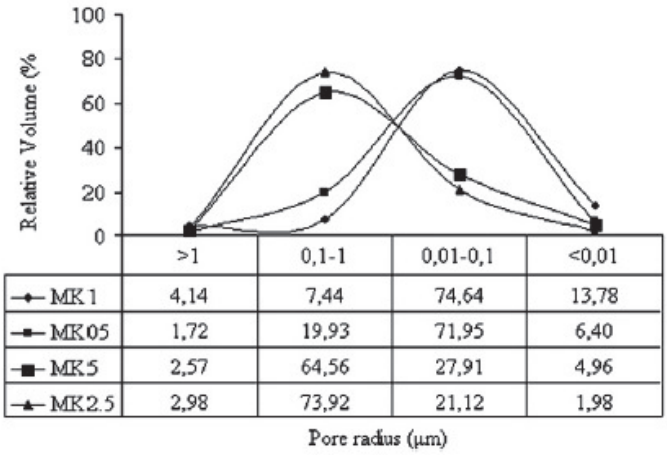


Figure 2.8. The relation between porosity and water/binder (w/b) ratio in mortars in lime-pozzolan mortar prepared with natural river sand (right) and standard sand (left)

Aggelakopoulou et al. (2011) conducted tests to find the chemical and physico-mechanical properties of prepared samples to examine the compatibility of lime mortars prepared with a pozzolan metakaolin to be used to restore historic masonries. Mercury intrusion porosimetry was used to acquire information about the microstructural properties such as cumulative volume, specific surface area, average pore radius, bulk density, and open porosity for samples cured for 1, 3, 6, and 12 months. For the samples with higher metakaolin/lime ratio by mass (1 and 0.5), open porosity and cumulative volume decreased from 1 to 3 months, then increased from 3 to 12 months. The samples with a lower metakaolin/lime ratio (0.2 and 0.09) showed a different behavior. The cumulative volume and open porosity slightly increased with time from 1 to 6 months and then decreased from 6 months to 12 months. The average pore radius of samples did not change during the curing period, regardless of their metakaolin/lime ratio. On the other hand, the average pore radius of samples with 0.2 and 0.09 metakaolin/lime ratio by mass was larger than the pore radius of samples with 0.5 and 1 metakaolin/lime ratio by mass.



	>1	0,1-1	0,01-0,1	<0,01
MK1	4,14	7,44	74,64	13,78
MK05	1,72	19,93	71,95	6,40
MK5	2,57	64,56	27,91	4,96
MK2.5	2,98	73,92	21,12	1,98

Figure 2.9. Pore size distribution at 12 months curing time, metakaolin/lime ratios for MK1: 1, MK05: 0.5, MK5: 0.2 and MK2.5: 0.09

When the pore radius distributions were examined for samples with different metakaolin/lime ratios, it was observed that samples with higher metakaolin/lime ratios of 1 and 0.5 had pores smaller than 0.1 μm radius for their 88% and 78% of

their relative volume (Figure 2.5). The percentages of pores smaller than 0.1 μm radius for mortar samples with lower metakaolin/lime ratios of 0.2 and 0.09 were 67% and 77%, respectively.

2.4 Acoustic performance in relation to pore structure for consolidated granular materials

Arenas & Crocker (2010) classify porous materials according to their structure as cellular, fibrous, and granular. Studies related to the granular category examine sound propagation in unconsolidated loose granular mixes and/or consolidated granule compounds. The materials like mortar and plaster are categorized under consolidated granular materials as their aggregates are compounded together by a binder or an adhesive agent. The sound absorptive properties of porous concrete are a popular subject as this type of material is promising to be used for many applications as an absorptive surface on outdoor noise barriers, on roads, or within the buildings of industrial settlements, sports halls, etc (Carbajo et al., 2015; Horoshenkov et al., 2003; H. K. Kim & Lee, 2010a; Zhang et al., 2020). The aggregate size used in porous concrete materials is mostly above 2mm. The type of aggregates used in the studies can be listed as siliceous sand (Bozkurt & Demirkale, 2020b; H. Kim et al., 2018; Knapen et al., 2004; Leiva et al., 2012; Palomar & Barluenga, 2022), crushed brick (Bozkurt, 2023), crushed limestone (Bozkurt, 2023; Marolf et al., 2004), basalt (Zhang et al., 2020), zeolite (H. Kim et al., 2018), pumice (Bozkurt & Demirkale, 2020b), perlite (Bozkurt & Demirkale, 2020b; Palomar & Barluenga, 2018), expanded glass (Bozkurt, 2023), expanded shale (H. K. Kim & Lee, 2010b), expanded clay (Carbajo et al., 2017; Pereira et al., 2019) and vermiculite (Palomar & Barluenga, 2022). Apart from using cement as a binder, also adhesives or admixtures such as silica fume, fly ash, and plasticizers are utilized to increase the strength and workability of mixtures (H. Kim et al., 2018; H. K. Kim & Lee, 2010b; Marolf et al., 2004; Park et al., 2005; Vasina et al., 2006). There is also research on plasters or composite materials that have aggregates below 2mm in size

and contain hydrated lime or hydraulic lime as a replacement or an alternative to cement used as a binder (Bozkurt & Demirkale, 2019, 2020b; Palomar & Barluenga, 2017). The effect of adding fiber to the mixtures is another topic investigated in studies related to sound absorption. Polypropylene fiber, cellulose fiber, flax fiber, basalt fiber, and glass fiber are the ones used in these studies (Bozkurt, 2023; Bozkurt & Demirkale, 2019, 2020b; H. Kim et al., 2018; Marolf et al., 2004; Palomar & Barluenga, 2022). In recent years, composites from natural materials such as hemp shiv and sunflower stem used as a granular infill combined with clay or natural biopolymers draw interest due to a tendency to use sustainable and eco-friendly materials in the building industry (Degrave-Lemeurs et al., 2018; Glé et al., 2011; Mati-Baouche et al., 2016). Substituting recycled aggregates as rubber crumbs or waste concrete aggregates is another attempt to increase the lifespan of used products to sustain natural resources.

The knowledge gained through these mentioned studies is mainly presented as the effect of raw materials and their compositional ratios on sound absorption performance. The strength of these materials is another issue discussed in most of the published work, as the main intent is to use these material composites as sound absorbers in various applications. Little has been done so far to investigate the microstructural properties of the porous network formed due to chosen raw materials and compositional ratios. The microstructural properties affecting sound absorption are previously described in detail in Chapter 2.1.2 of this thesis. The most common tendency is to comment only on porosity values, as porosity is the most practically measured parameter. On the other hand, the microstructural properties such as pore size, pore shape, tortuosity, flow resistivity, and viscous and thermal characteristic lengths require complex and expensive measurement/analysis setups that are not standardized and/or require extensive user knowledge. For granular consolidated materials, Horoshenkov et al. (2003), Horoshenkov & Swift (2001), Vasina et al. (2006), Knapen et al. (2003), and Carbajo et al. (2015) measure some of the microstructural properties and/or use the theoretical sound propagation models to deduce the unknown properties or use inverse methods based on optimization to

make a prediction depending on measured sound absorption data. Shape-specific models to estimate void ratios (similar to porosity) are utilized in sound absorption characterization research conducted by Kim and Lee (2010a) and Marolf et al. (2004).

The general conclusions on compositional properties gathered from various works on the sound absorption of consolidated granular media are summarized below:

The effect of binder on sound absorption:

Increasing the binder amount in granular mixes decreases porosity. As a result, overall sound absorption performance drops off (Bozkurt, 2023; Bozkurt & Demirkale, 2018; Glé et al., 2011; Zhang et al., 2020). Pereira et al. (2019) noted that in their porous samples prepared with cement and expanded clay aggregates, increasing cement content in the materials moves the peak absorption curve to lower frequencies. Bozkurt & Demirkale (2019) found that using hydrated lime as a binder results in higher sound absorption than using hydraulic lime. Gle et al. (2011) also found a similar result in their study, where they compared the sound absorption curves of different hemp concrete samples prepared with aerated lime, hydraulic lime, pozzolanic lime, and cement. The samples prepared with a cement binder had the lowest sound absorption performance. Overall, the binder prepared mostly with aerated lime shows higher sound absorption performance in a broader frequency range.

The effect of aggregate on sound absorption:

Using aggregates above 2mm enhances the sound absorption performance (Bozkurt, 2023). The size distribution of aggregates is an important aspect of the propagation of sound (Bozkurt, 2023). Samples having a broader aggregate size distribution show higher overall sound absorption performance compared to the alternatives having single-size aggregates (Bozkurt, 2023; Carbajo et al., 2015; Marolf et al., 2004). As the aggregate size decreases in samples, the peak absorption shifts to the lower

frequencies (Carbajo et al., 2015) and decreases (Zhang et al., 2020). The aggregate type also affects the sound absorption of samples. As noted by Bozkurt (2023) and Bozkurt and Demirkale (2020b), samples prepared with lightweight aggregates such as perlite, pumice, and expanded glass have higher sound absorption than samples containing crushed brick, crushed limestone or river sand. Crumbed rubber, as a replacement for perlite aggregate, increases sound absorption at low and high frequencies (Bozkurt & Demirkale, 2020b).

The effect of pozzolanic materials:

Pozzolanic materials in composition react with calcium hydroxide in the presence of moisture to form a solid cementitious body composed of calcium silicates and aluminum (Güney, 2012). Pozzolanic materials are used to increase strength in compositions (Marolf et al., 2004). The addition of pozzolanic materials to porous concrete is a way of improving the strength of the material while targeting the maximum achievable sound absorption. On the other hand, pozzolanic additives increase the material's density, resulting in poorer absorption. This condition is seen in the work of Leiva et al. (2012). The samples prepared with fly ash and bottom ash show a remarkable decrease in sound absorption performance.

On the other hand, when both pozzolanic additives are compared, the samples prepared with bottom ash present better sound absorption performance than those prepared with fly ash. The effect of pozzolanic material on sound absorption is also verified by the work of Bozkurt and Demirkale (2019). They observed that adding pozzolan to hydrated lime or hydraulic lime as a natural pozzolanic material decreases sound absorption compared to the sound absorption of samples prepared by only hydrated lime and aggregates.

The effect of fibers:

The general conclusion from studies including fibers in compositions is that sound absorption is enhanced overall by adding fibers (Bozkurt, 2023; Bozkurt &

Demirkale, 2020b; Palomar & Barluenga, 2022; H. Kim et al., 2018). In some of the research it is seen that as fiber content increases, the maximum sound absorption value increases as well (Neithalath et al., 2004). A similar result was also observed in the work of Bozkurt and Demirkale (2020b). Many different fiber types have been included in the studies, such as polypropylene fiber, cellulose fiber, flax fiber, basalt fiber, and glass fiber. Bozkurt and Demirkale (2020a) found that the addition of flax fiber to the compositions results in greater sound absorption compared to the polypropylene fiber addition.

The results of the investigation on microstructural pore properties of consolidated granular materials can be summarized below:

The effect of porosity:

The measurement techniques of porosity vary a lot, and depending on the chosen technique, different types of pores can be considered, such as open pores, closed pores, or kinematic/effective pores (excluding the dead-end pores). Horoshenkov et al (2003) use image analysis of cross sections to determine the porosity of samples prepared with high alumina cement and aluminous aggregate curing under high temperature and pressure in a moist environment. One of these samples is also water-cured. The porosity determined in this way is similar to the one calculated with densities and gives results of 0.38 and 0.39 for the consolidated two samples in this study. On the other hand, the results of sound absorption measurement show that the sample that is not water-cured has higher sound absorption coefficient values between 500 and 2500 Hz. This can be attributed to pore structure, which may have been particular to the sample, although the porosity, somewhat of a macro property, is similar to the other sample. In the work of Horoshenkov, coauthored with Swift (2001), the porosity values of rubber granules consolidated with a polyurethane binder under determined by the water suction method (Leclaire et al., 1998). The porosity values of consolidated samples changes between 35% and 60%. The authors interpreted the sound absorption measurement results with the compaction ratio and binder concentration. For different grain sizes, no consistent relation is observed

between porosity and the maximum sound absorption. Still, it should be noted that with the decrease of porosity due to the compaction ratio, the peak point of maximum absorption shifts to lower frequencies. Knapen et al. (2003) use the Biot-Allard-Johnson model to interpret the performance of measured sound absorption values of different mixes prepared with sand up to 2mm in size, Portland cement, and polyvinyl acetate. They stated that as porosity increases, the peak point of absorption also increases, but no frequency shift of this peak point was reported in their study. Carbajo et al. (2015) reported a minor reduction of sound absorption as porosity decreased in their samples prepared with perlite and vermiculite aggregates with cement. In a different study, Carbajo et al. (2017) measured the sound absorption performance of two distinct materials composed of dissimilar types of perlite aggregates of various sizes with the same cement-to-aggregate ratio. The porosity values determined with the water saturation method were similar, and only a slight difference was observed at peak absorption values based on close but particular frequencies. Looking at this limited data, the porosity values cannot be directly related to the sound absorption. These findings presented in the mentioned studies show that it is not simple to associate only porosity and sound absorption performance without considering other microstructural pore characteristics.

The effect of flow resistivity:

Vasina et al. (2006) found that the flow resistivity of the samples prepared with 3.5mm size expanded clay aggregates is higher than that of those prepared with bigger aggregates. As the flow resistivity of the sample increases, the maximum sound absorption also increases in their study. On the other hand, in the study of Knapen et al. (2004), the samples prepared with smaller grain sizes (0.8-1.2mm) have higher flow resistivity than those composed of 1.4-2mm size grains. Contrary to what Vasina et al. (2006) found, with the higher values of flow resistivity, the maximum sound absorption decreases for the samples in Knapen et al.'s work (2004). In the study of Carbajo et al. (2015), the increase in sound absorption is also linked to increased flow resistivity in their samples prepared below 4mm size

aggregates. The authors state that a shift in peak absorption towards lower frequencies is associated with increased flow resistivity due to the reduced-sized grains. The results of Swift et al. (1999) agree well with the results of Carbajo et al (2015).

The effect of tortuosity:

Tortuosity is one of the parameters that requires complex measurement setups. Although a method based on electrical resistance exists, some materials can deteriorate due to the use of a saturated solution in the experiment. For the other alternative methods, one must use expensive equipment, which is unavailable for most laboratories. Due to these consequences, in most research, scientists prefer inverse methods based on optimizing the differences between measured and predicted sound absorption data. Horoshenkov and Swift (2001) predict the tortuosity values of samples prepared with rubber granules and polyurethane binder. It has been reported by authors that tortuosity values primarily define the position of maximum and minimum absorption points in the frequency range. The results show that tortuosity values increase as the compaction ratio rises. Also, as binder concentration increases, the tortuosity increases. Vasina et al. (2006) also interpret the data based on predicted tortuosity values for the samples containing Portland cement, expanded clay aggregates, pulverized fuel ash, and plasticizer. The tortuosity, together with the standard deviation in the pore size, cannot be linked to the aggregate size used in the samples. No more information, such as a direct association, is given for tortuosity and sound absorption data, which may depend on a relatively small number of samples. The study of Knapen et al (2003) is another example of how predicted tortuosity values are interpreted. The prediction method enables us to keep the other effecting parameters fixed and observe the change in sound absorption with the shift in tortuosity. The prediction method used in this study is based on a hybrid model of Biot Allard and Johnson. As the value of tortuosity increases, the peak sound absorption value shifts to a lower frequency by decreasing gradually. All in all, it should be noted that this observation stands highly theoretical

since the complex pore structure cannot be altered in naturally occurring materials. As a result, more than one parameter affects the sound absorption curve.

The increase of tortuosity (predicted) is observed using smaller-size arlite aggregates in the samples prepared with Portland cement in the study of Carbajo et al. (2017). In another work of the same authors, tortuosity values are again predicted through optimization for the material samples having arlite and vermiculite aggregates and Portland cement in their compositions. The study shows that the tortuosity values of samples with the same size of aggregates do not change significantly. Still, the authors also point out that these tortuosity values are obtained through prediction, and experimental work should have been done to clarify this argument.

Mahasaranon et al. (2012) conducted different research to understand the change of porous structure through the section of a thick material sample. Their sample is a composite material formed with a polyurethane binder, polyol, and tire shred (a mix of rubber grains and nylon fibers). The sample was measured as a whole and as shredded pieces of equal thickness of 35mm. It has been seen that the upper piece shows remarkably different characteristics in terms of tortuosity, although porosity values stay almost the same for every other piece. The measured tortuosity is around 6 for the upper piece and changes between 2.5 and 1.5 for the rest. The measured sound absorption coefficients are the lowest for this upper piece compared to the other pieces from different depths. The authors interpreted that this difference may result from a polymerization reaction in which the reaction rate changes exponentially along the depth of the material. The difference observed in this study is somewhat expected as the sample's original thickness is 140mm.

The effect of characteristic lengths:

Viscous and thermal characteristic length are the two important pore structure parameters in the sound propagation models. Many have been done to characterize these two lengths for sound absorptive materials such as fibrous materials like fiber wool, glass wool, jute, cellular materials like melamine foam, metallic foam, or loose

granular materials. On the other hand, only a few researchers also try to determine the characteristic lengths of consolidated granular materials (Degrave-Lemeurs et al., 2018; Knapen et al., 2003; Mati-Baouche et al., 2016; Othmani et al., 2017). The common characteristic of these studies is the attempt to use natural wastes such as hemp, sunflower seeds, and sugarcane plants. Only in the study of Knapen et al. (2003) are sand and cement utilized as traditional ingredients of porous cement materials. They observe the effect of characteristic length on sound absorption using a prediction method based on a Biot–Allard–Johnson hybrid model. They conclude that the thermal characteristic length predicted through optimization for different mixes does not alter much for their type of polymer-modified cement mortars. For viscous characteristic length, an increase in the parameter shifts the maximum absorption point to higher frequencies with an increase. The characteristic lengths measured in the other studies only give an idea about the range of these parameters as they are not directly linked to sound absorption coefficients.

Below in Table 2.2 the measured and predicted microstructural pore properties of different materials from various studies are given. Measured and predicted values are followed by M or P, respectively.

Table 2.2 Measured (M) and predicted (P) microstructural pore properties of different granular materials reported in literature

Author	Material	Porosity		Flow Resistivity (Ns/m^4 or $Pa.s/m^2$)		Tortuosity		Viscous characteristic length (μm)		Thermal characteristic length (μm)	
Carbajo et al, 2015	Vermiculite type 2 (V2) ≤1 mm	0.39	M	2230	M	1.7	P	-	-	-	-
Carbajo et al, 2015	Vermiculite type 3 (V3) 0.5–4 mm	0.4	M	1720	M	1.7	P	-	-	-	-
Carbajo et al, 2015	Vermiculite type 2 (V2) >1 mm	0.37	M	1424	M	1.73	P	-	-	-	-
Carbajo et al, 2015	Concrete with arlite agg (<4mm)	0.39	M	2176	M	1.82	P	-	-	-	-

Table 2.2 (continued)

Author	Material	Porosity		Flow Resistivity (Ns/m^4 or $Pa.s/m^2$)		Tortuosity		Viscous characteristic length (μm)		Thermal characteristic length (μm)	
Carbajo et al, 2015	Concrete with arlite agg (>4mm)	0.38	M	1830	M	1.87	P	-	-	-	-
Carbajo et al, 2017	Porous concrete with arlite aggregates (expanded clay) - B	0.35	M	1507	M	1.56	P	-	-	-	-
Carbajo et al, 2017	Porous concrete with arlite aggregates (expanded clay) - A	0.38	M	1839	M	1.86	P	-	-	-	-
Degrave-Lemeurs et al, 2018	Hemp-clay composites	0.5	M	30000	M	1.1	P	22	P	-	-
Degrave-Lemeurs et al, 2018	Hemp-clay composites	0.47	M	185000	M	1.2	P	5.5	P	-	-
Degrave-Lemeurs et al, 2018	Hemp-clay composites	0.61	M	13000	M	1.9	P	150	P	-	-
Degrave-Lemeurs et al, 2018	Hemp-lime composites	0.7	M	4000	M	2.4	P	236	P	-	-
Degrave-Lemeurs et al, 2018	Hemp-lime composites	0.55	M	9400	M	3.8	P	94	P	-	-
Degrave-Lemeurs et al, 2018	Hemp-lime composites	0.26	M	25000	M	4	P	26	P	-	-
Gle et al, 2011	S3-binder B - hemp concrete	0.73	M	19300	M	3	P	23	P	-	-
Gle et al, 2011	S1-binder A - hemp concrete	0.75	M	11000	M	-	-	-	-	-	-
Gle et al, 2011	S1-binder B - hemp concrete	0.75	M	31300	M	-	-	-	-	-	-
Gle et al, 2011	S1-binder C - hemp concrete	0.74	M	33300	M	-	-	-	-	-	-
Gle et al, 2011	S2-binder A - hemp concrete	0.67	M	73000	M	-	-	-	-	-	-
Gle et al, 2011	S2-binder B - hemp concrete	0.68	M	32300	M	-	-	-	-	-	-
Gle et al, 2011	S2-binder C - hemp concrete	0.75	M	55700	M	-	-	-	-	-	-

Table 2.2 (continued)

Author	Material	Porosity		Flow Resistivity (Ns/m^4 or $Pa.s/m^2$)		Tortuosity		Viscous characteristic length (μm)		Thermal characteristic length (μm)	
Gle et al, 2011	S3-binder A - hemp concrete	0.68	M	20300	M	-	-	-	-	-	-
Gle et al, 2011	S3-binder C - hemp concrete	0.72	M	24700	M	-	-	-	-	-	-
Horoshenkov & Swift,2001	Consolidated rubber granulates 0.71-1mm	0.36	M	92200	M	1.68	P	-	-	-	-
Horoshenkov & Swift,2001	Consolidated rubber granulates 1.41-2mm	0.36	M	19800	M	1.68	P	-	-	-	-
Knapen et al, 2003	Polymer modified concrete 11	0.39	M	33500	M	1.6	P	30	P	300	P
Knapen et al, 2003	Polymer modified concrete 4	0.38	M	10700	M	1.9	P	50	P	400	P
Knapen et al, 2003	Polymer modified concrete 26	0.36	M	13500	M	2.2	P	50	P	400	P
Knapen et al, 2003	Polymer modified concrete 10	0.39	M	35800	M	2.3	P	50	P	240	P
Knapen et al, 2003	Polymer modified concrete 8	0.34	M	48300	M	2.3	P	35	P	220	P
Knapen et al, 2003	Polymer modified concrete 3	0.38	M	12300	M	2.4	P	55	P	500	P
Knapen et al, 2003	Polymer modified concrete 23	0.37	M	12300	M	2.5	P	70	P	500	P
Knapen et al, 2003	Polymer modified concrete 31	0.4	M	28700	M	2.5	P	75	P	200	P
Knapen et al, 2003	Polymer modified concrete 7	0.36	M	16100	M	2.5	P	55	P	500	P
Knapen et al, 2003	Polymer modified concrete 6	0.35	M	21900	M	2.7	P	55	P	500	P
Knapen et al, 2003	Polymer modified concrete 30	0.39	M	30000	M	2.8	P	80	P	200	P
Knapen et al, 2003	Polymer modified concrete 29	0.35	M	55200	M	2.9	P	55	P	220	P
Knapen et al, 2003	Polymer modified concrete 9	0.34	M	40300	M	2.9	P	60	P	200	P
Knapen et al, 2003	Polymer modified concrete 21	0.34	M	15900	M	3	P	70	P	500	P
Knapen et al, 2003	Polymer modified concrete 20	0.37	M	9200	M	3.1	P	120	P	300	P
Knapen et al, 2003	Polymer modified concrete 28	0.35	M	41000	M	3.1	P	60	P	240	P

Table 2.2 (continued)

Author	Material	Porosity		Flow Resistivity (Ns/m^4 or $Pa.s/m^2$)		Tortuosity		Viscous characteristic length (μm)		Thermal characteristic length (μm)	
Knapen et al, 2003	Polymer modified concrete 1	0.35	M	17700	M	3.2	P	50	P	500	P
Knapen et al, 2003	Polymer modified concrete 27	0.35	M	15600	M	3.3	P	75	P	500	P
Knapen et al, 2003	Polymer modified concrete 0	0.36	M	12200	M	3.4	P	55	P	500	P
Knapen et al, 2003	Polymer modified concrete 24	0.36	M	17300	M	3.6	P	90	P	400	P
Mahasaranon et al, 2012	PU foam with nylon fibers and rubber grain - layer D	0.94	M	13 813	M	1.56	M	-	-	-	-
Mahasaranon et al, 2012	PU foam with nylon fibers and rubber grain - layer C	0.92	M	32 029	M	2.06	M	-	-	-	-
Mahasaranon et al, 2012	PU foam with nylon fibers and rubber grain - layer B	0.91	M	64 415	M	2.41	M	-	-	-	-
Mahasaranon et al, 2012	PU foam with nylon fibers and rubber grain - layer A	0.91	M	81 729	M	6.27	M	-	-	-	-
Swift et al, 1999	Consolidated rubber granulates >2.0 mm	0.336	M	22000	M	-	-	-	-	-	-
Swift et al, 1999	Consolidated rubber granulates 0.71-1.0 mm	0.317	M	489000	M	-	-	-	-	-	-
Swift et al, 1999	Consolidated rubber granulates 1.0-1.4 mm	0.34	M	80500	M	-	-	-	-	-	-
Swift et al, 1999	Consolidated rubber granulates 1.4-2.0 mm	0.3	M	62100	M	-	-	-	-	-	-
Minimum		0.26		1424		1.1		5.5		200	
Maximum		0.94		489000		6.27		236		500	
Average		0.48		38190		2		67		366	
Median		0.38		20050		2.4		55		400	

CHAPTER 3

MATERIALS AND METHODS

This chapter describes the raw materials and plaster sample preparation techniques throughout this study. Experimental procedures to define basic material properties and performance properties are presented together with the inverse characterization technique used for predicting the unknown characteristics related to pore structure.

3.1 Raw materials used in plaster sample preparation

The raw materials used as binder and aggregates in the study are described in this section. It is known that lime is one of the oldest binding materials used in plasters. Its history dates back to 4000 B.C. when it was used as plastering material in the pyramids of Eygpt (Boynton, 1966). Lime is a term widely used for the burned form of limestone. The main mineral found in limestones is calcium carbonate ($CaCO_3$). The other minerals or the so-called impurities within the limestone determine the type of lime. The calcination process in kilns relieves carbon dioxide (CO_2) from the limestone and forms calcium oxide (CaO), also known as quick lime. The quicklime formed after the burning process should be slaked for use. The slaking procedure is an exothermic process. The end product is called as hydrated lime or slaked lime ($Ca(OH)_2$). The reactions taking place are given below:

$$\underset{\text{limestone}}{CaCO_3} \xrightarrow{900^{\circ}C} \underset{\text{quicklime}}{CaO + CO_2} \qquad \text{(Reaction 3.1)}$$

$$\underset{\text{quicklime}}{CaO + H_2O} \longrightarrow \underset{\text{slaked lime}}{Ca(OH)_2} + \text{Heat} \qquad \text{(Reaction 3.2)}$$

Lime is classified according to its setting environment. Hardening of lime can take place either in the air or underwater. The ones that harden under water are called hydraulic lime. Other sets in the air are called non-hydraulic lime. Nonhydraulic limes contain a high amount of calcium carbonate. Hydraulic limes contain active clay materials, giving the property of setting under water. Hydraulic limes can be produced either from limestones that naturally contain clay or from or by mixing clays with pure limestones (Çizer, 2004).

According to TS EN 459-1 (Türk Standardları Enstitüsü, 2015) standard, the limes used in buildings are classified into categories according to their content and purities. Table 3.1 gives the lime types and notations used for classification.

Table 3.1 Types of building limes and their classification

Type of building lime	**Classification**
Calcium Lime	CL90, CL80, CL70
Dolomitic Lime	DL85, DL80
Natural Hydraulic Lime	NHL2, NHL3.5, NHL5
Hydraulic Lime	HL2, HL3.5, HL5

The calcium limes are classified according to the amount of CaO and MgO in their content as shown in Table 3.2.

Table 3.2 Classification of calcium lime and the minimum amount of CaO+MgO required for classification

Classification of calcium lime	**Minimum amount of CaO+MgO**
CL 90	90 %
CL 80	80 %
CL 70	70 %

The type of lime used in the initial material preparation is calcium lime, CL90 (hydrated lime). Hydrated lime is chosen for two reasons:

- Open porosity of plasters prepared with hydrated lime is up to 60%. Higher open porosity is a favorable characteristic for sound absorption. The detailed analyses in

the literature state that with an increase in open porosity, the sound absorption in the mid-frequency range increased (Knapen et al., 2003; Neithalath, 2004).

- The material is easier to work with when compared to calcite and un-hydrated lime, and it is commercially available in different purities.

Hydrated lime powder of class CL90 is used as the binding material (Türk Standardları Enstitüsü, 2015). The information for the XRD analysis was gathered from DIFFRACT.SUITE software is shown below in Figure 1. The lime powder was mixed with distilled water in a 1:1 mixing ratio by weight and kept in a closed container for at least two days prior to plaster making.

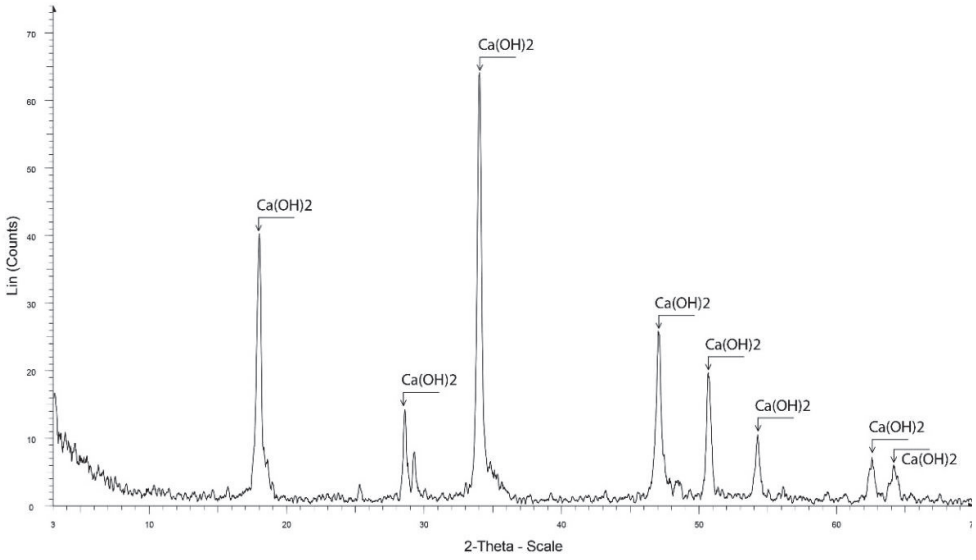


Figure 3.1. Mineralogical content of hydrated lime powder used in the study

Three different kinds of aggregates are used in sample preparation. Only siliceous aggregates are included in the first set of samples to observe the effect of aggregate size distribution on the plaster samples' performance. In the second set, observations are based on aggregate type, so besides siliceous aggregates, aggregates fall into the lightweight category and are also used in the sample preparation. Table 3.3 shows the origin of aggregates and the form they are procured before sample preparation.

Table 3.3 The origin, procurement form and size of aggregates used in samples

Type of aggregate	Procurement form and size	Origin
Siliceous - 1	0-4mm size aggregates	Ankara
Siliceous - 2	0-4mm size aggregates	Ankara
Pumice	0-4mm size aggregates	Nevşehir
Tuff	Rock fragments	Kayseri

Mineralogical compositions of aggregates are determined by X-ray diffraction (XRD) analyses performed by Bruker D8 Advance Model X-ray Diffractometer. X-ray diffraction (XRD) is an analytical technique based on X-ray scattering from crystalline materials. Each material produces a unique X-ray "fingerprint" of X-ray intensity versus scattering angle characteristic of its crystalline atomic structure (Hong Kong Polytechnic University, 2001). The aggregates are pounded in powder form beforehand, and the intensity-theta angle (incident ray angle) graph is gathered for each sample with X-ray diffraction. Using the database in DIFFRACT.SUITE software, mineral peaks observed in the graphs are traced. The mineralogical content of aggregates is given in Figures 2.2, 2.3, 2.4, and 2.5.

Both siliceous aggregates used in different sample sets have andesine (An), albite (Al), and potassium gallium silicate (Po) minerals in common. The siliceous aggregates of the first set also contain sanidine (Sn) ve barium bismuth telluride (Ba) minerals. The other siliceous aggregates in the second set contain nontronite (No) minerals as well. Orthoclase (Or), andesine (An), albite (Al), sanidine (Sn), and quartz (Q) minerals are observed in pumice aggregates. Traces of felspar (F), albite (Al), tridymite (T), quartz (Q), and sanidine (Sn) minerals are observed in tuff aggregates.

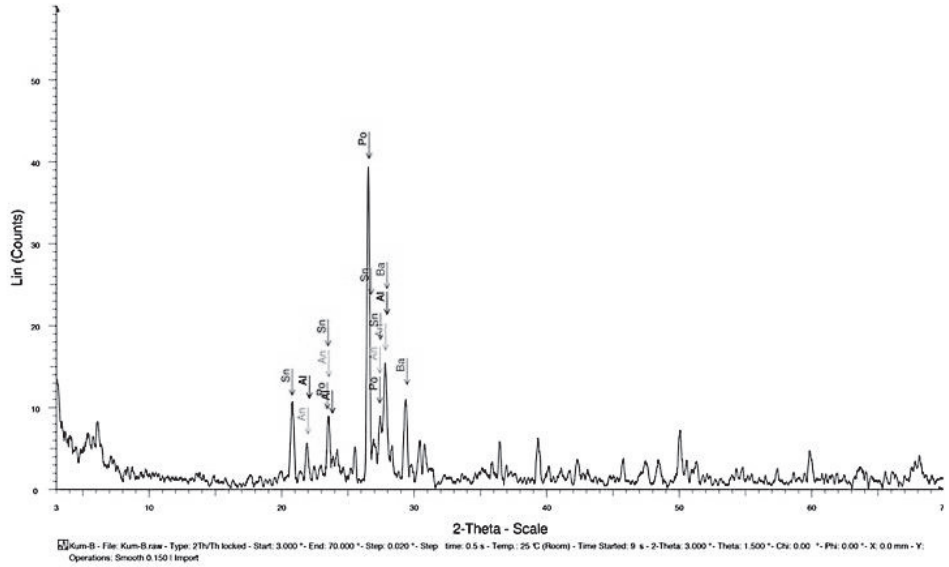


Figure 3.2. Mineralogical content of siliceous aggregates of 1st sample set

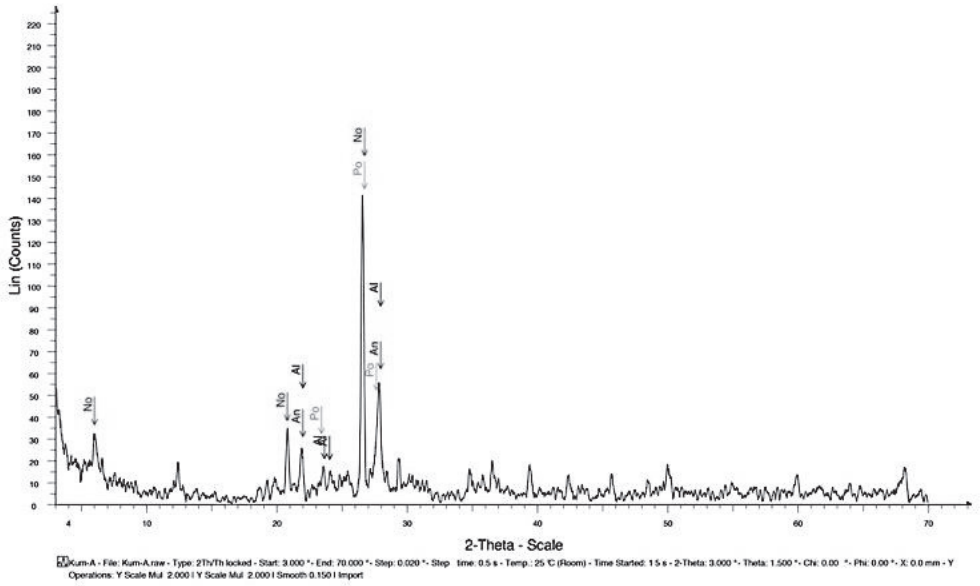


Figure 3.3. Mineralogical content of siliceous aggregates of 2nd sample set

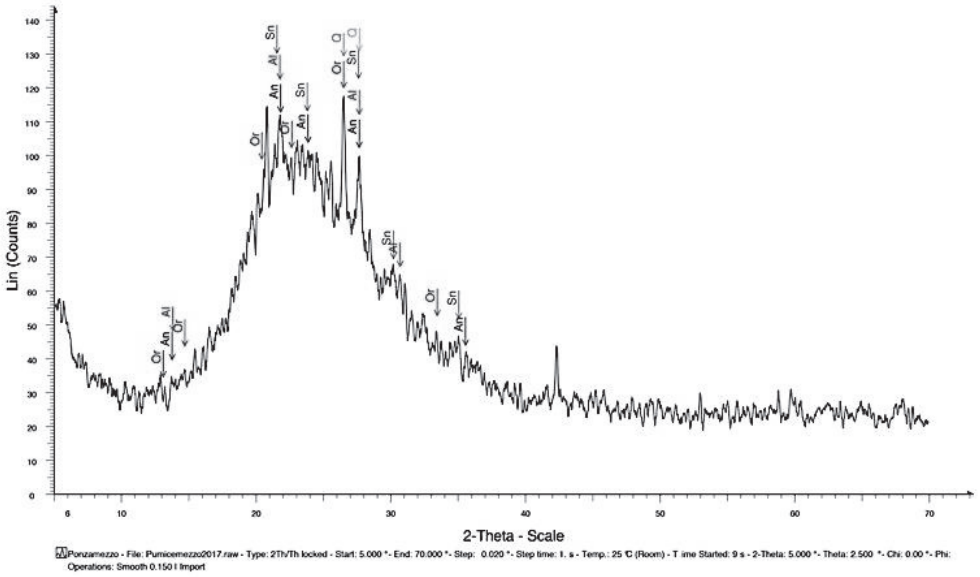


Figure 3.4. Mineralogical content of pumice aggregates

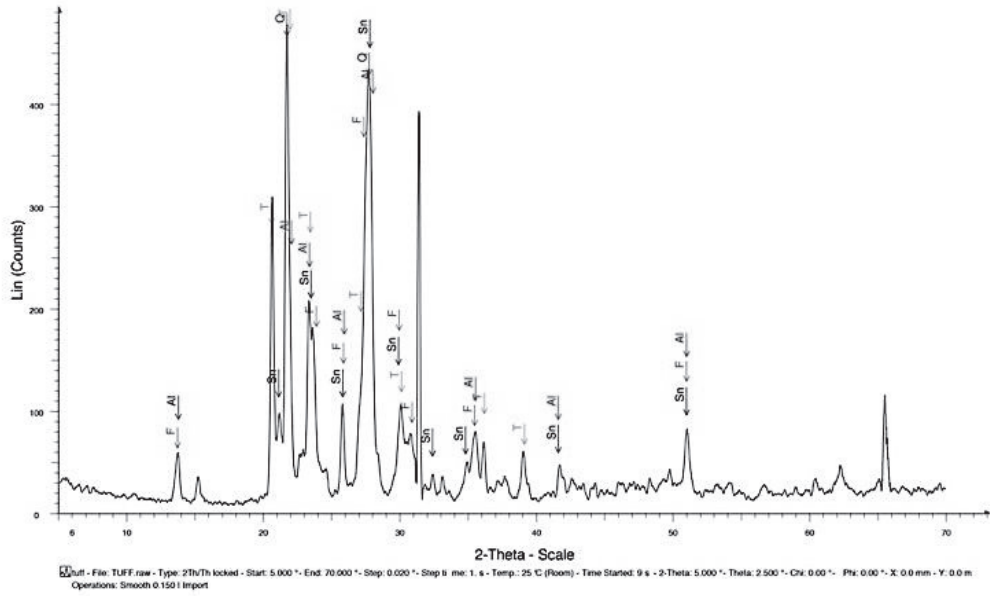


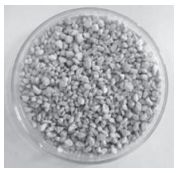
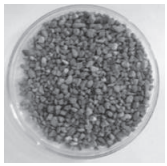
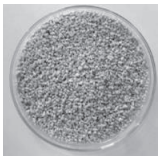
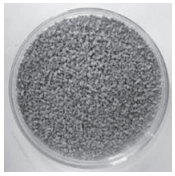
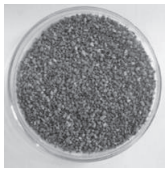
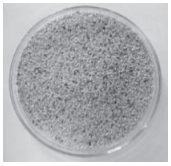
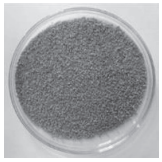
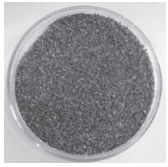
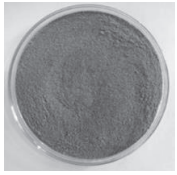
Figure 3.5. Mineralogical content of tuff aggregates

In order to investigate the effect of different types of aggregates, two sets of samples are prepared. The first set contains only siliceous aggregates separated into size

groups by sieves of 1mm, 0.5mm, 0.25mm, and 0.125mm. The aggregates above 2mm in size are small in amount and not included in the mixtures.

The second set contains samples with tuff aggregates, pumice aggregates, and siliceous aggregates. The siliceous aggregates in the second set are marked with "2" as the amount of aggregates left from the first set is insufficient to prepare the samples in the second group. Tuff fragments were crushed in a jaw crusher to have 0-4mm aggregates. All materials were graded using 0.5mm, 1mm, 2mm, and 4.75mm sieves. The aggregates above 4.75 are not used since plasters commonly do not contain aggregates above this size. The sieved aggregates are shown in Figure 1. Small size particles that cling to bigger aggregates and the frame of sieves are observed in pumice and tuff aggregates. To do a thorough separation, materials finer than 75μm are separated by washing sieved aggregates (ASTM International, 2013).

Table 3.4 Sieved and washed aggregates from second set of samples

Aggregate Size	PUMICE AGGREGATES	TUFF AGGREGATES	SILICEOUS AGGREGATES
4,75-2mm			
2-1mm			
1-0.5mm			
0.5mm>			

Aggregates are classified as lightweight if the dry loose bulk density of lightweight aggregate is below 1120 kg/m^3 in ASTM C330/C330M (ASTM International, 2014) standard for fine aggregates below 4.75mm size (ASTM International, 2015). The measured water absorption(%), relative density of saturated surface dry (SSD) aggregate (g/cm3), dry bulk density (g/cm3), and saturated surface dry bulk density (g/cm3) of aggregates are given in Table XX measured according to ASTM C128-15 (ASTM International, 2015) and ASTM C29/29M (ASTM International, 2023a).

Table 3.5 Water absorption, relative density of SSD aggregates, bulk density of dry aggregates and bulk density of SSD aggregates used in sample preparation

Aggregate type and size	Absorption, %	Relative density of saturated surface dry aggregate	Bulk density of dry aggregate (Dry (g/cm3)	Bulk density of saturated surface dry aggregate (g/cm3)
Siliceous aggregate-2 (2-4.75mm)	3.4	2.59	1.49	1.54
Tuff aggregate (2-4.75mm)	24.0	1.91	0.85	1.06
Pumice aggregate (2-4.75mm)	48.5	1.21	0.50	0.74
Siliceous aggregate-2 (1-2mm)	2.4	2.38	1.49	1.52
Tuff aggregate (1-2mm)	25.3	1.91	0.82	1.02
Pumice aggregate (1-2mm)	42.2	1.53	0.57	0.81
Siliceous aggregate-2 (0,5-1mm)	1.2	2.68	1.49	1.51
Tuff aggregate (0.5-1mm)	15.7	1.95	0.93	1.07
Pumice aggregate (0.5-1mm)	26.9	1.77	0.67	0.85

Due to the use of lightweight aggregates in combination with siliceous aggregates that fall into the non-lightweight category, the binder-to-aggregate ratio and aggregate size distributions are defined based on the volumetric amount of saturated

surface dry state to ensure accurate comparisons. The compositional ratios are given in detail in the next section.

3.2 Sample preparation

In the study, 12 different types of plaster samples were prepared. Before giving information about the sample preparation process, the nomenclature used to identify these plasters is given in the Figure below.

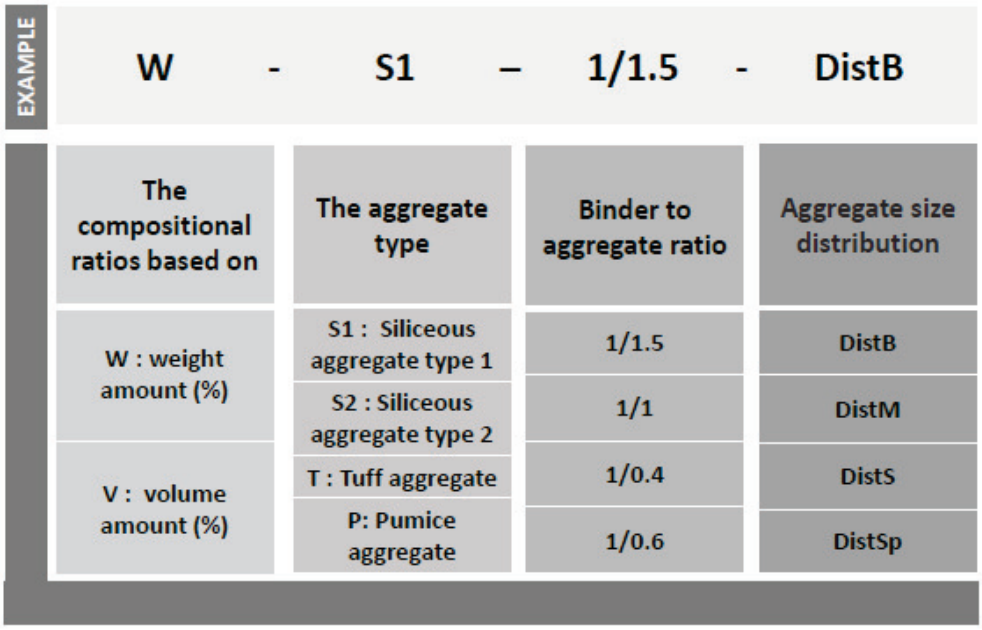


Figure 3.6. Nomenclature of samples

In the first set of samples prepared with only siliceous aggregates, the compositional ratios in terms of binder to aggregate amount ratio and aggregate size distributions are identified according to the previous studies on lime plasters taken from historical buildings (Caner, 2003; Esen et al., 2004; Uğurlu, 2005). The compositional ratios based on weight amounts are given in Table 3.6.

Table 3.6 Compositional ratios of first set of samples

Sample Code	Binder to aggregate ratio based on weight amount	Aggregate Size Distribution Group	Aggregate size distribution (by weight, %)				
			1mm ≤ X < 2mm	0.5mm ≤ X < 1mm	0.25mm ≤ X < 0.5mm	0.125mm ≤ X < 0.25mm	< 0.125mm
W-S1-1/1.5-DistB	1/1.5	A	35	25	20	10	10
W-S1-1/1.1-DistB	1/1	A	35	25	20	10	10
W-S1-1/0.4-DistB	1/0.4	A	35	25	20	10	10
W-S1-1/1.5-DistM	1/1.5	B	25	35	20	10	10
W-S1-1/1.1-DistM	1/1	B	25	35	20	10	10
W-S1-1/0.4-DistM	1/0.4	B	25	35	20	10	10
W-S1-1/1.5-DistS	1/1.5	C	10	25	35	20	10
W-S1-1/1.1-DistS	1/1	C	10	25	35	20	10
W-S1-1/0.4-DistS	1/0.4	C	10	25	35	20	10

Hydrated lime powder is mixed with distilled water in a 1:1 weight amount and kept in a closed container for at least 2 days before blending all the components. The conversion of dry hydrated lime into putty form results in a bimodal pore size distribution in which bigger size pores (>1 μm) can be formed at the binder-aggregate interface (interfacial transition zone) due to drying and paste shrinkage (Aggelakopoulou et al., 2019).

The lime putty and the aggregates are mixed with additional water until a workable consistency with a spread of approximately 180mm is achieved, as measured by the flow table test(ASTM International, 2020). The samples are then kept in a climate chamber at a temperature of 20°C ±2 and a relative humidity of 70% ±5 for their setting. Two sets of 20mm-thick cylindrical samples with diameters of 100mm and 28mm and one set of cubic samples in 40 x 40 x 40mm are prepared. Three parallel samples are molded for each set of samples.

In the second set of samples, as the purpose is to investigate the performance variation due to using different types of aggregates, the same aggregate size distribution is utilized. Due to the differences in relative density and porosity between pumice, tuff, and siliceous aggregates, binder-to-aggregate amount ratio and aggregate size distribution are not defined based on the weight of raw materials. The compositional ratios are set by volume. The ratios depend on the aggregates in their saturated surface dry state (SSD), mainly due to the differences in open porosity between different aggregates. Bulk volume in the SSD state will give the envelope volume of aggregates, especially for lightweight aggregates such as tuff and pumice. For the aggregates not classified as lightweight, the SSD state was achieved when the aggregates were soaked in water for 24h.

On the other hand, the lightweight aggregates are immersed in water for about 72 hours to achieve a saturated surface dry state (ASTM C128-15, 2015). The lime putty and the aggregates in the SSD state are mixed with water to ensure a fixed flow spread of 220mm (ASTM International, 2020) for all compositions of the second set. The compositional ratios of the second set of samples are given in Table 3.6. As the first set of samples proceeded, three parallel samples from each composition were molded and kept in a climate chamber at 20°C ±2 with a relative humidity of 70% ± The samples were de-molded after setting and left in the chamber for about 40 days.

Table 3.7 Compositional ratios of second set of samples

Sample Code	Binder to aggregate ratio based on volume amount	Aggregate Size Distribution Group	Aggregate size distribution (by volume, %)		
			4-2mm	2-1mm	1-0.5mm
V-S2-1/0.6-DistSp	1/0.6	50	25	50	25
V-T-1/0.6-DistSp	1/0.6	50	25	50	25
V-P-1/0.6-DistSp	1/0.6	50	25	50	25

In the setting process, $Ca(OH)_2$ reacts with CO_2 in the high relative humidity conditions to form $CaCO_3$. The reaction is formalized in Reaction 3.1 below. Heat is also released as a product of this reaction.

$Ca(OH)_2 + CO_2 \longrightarrow CaCO_3 + Heat\ (74kJ)$ (Reaction 3.3)

3.3 Experimental procedures for direct characterization

Procedues for determining the physical, physico-mechanical, and performance properties of tested material samples are given in detail in the following sections. These procedures are named direct methods in the terminology of sound propagation studies, as there are also indirect and inverse methods based on theoretical assumptions.

3.3.1 Determination of bulk density, porosity and fine porosity

Bulk density and porosity measurements were carried out according to the testing procedures described in the RILEM test recommendation (RILEM, 1980). Three samples from each plaster composition were dried at 60ºC till they reached a constant weight (M_{dry}). The samples were placed in a vacuum chamber within open beakers to release the air entrapped within the pores. Then, the beakers were filled with water until the samples were totally immersed. The samples were left under water for a period, as stated in the RILEM method. Later, the samples were first weighed in water (M_{arch}), taken out from the water, and weighed right after excessive water on their surface was wiped out. The last recording represents the weights in saturated condition (M_{sat}). Bulk density (ρ_M) is calculated according to Equation 3.1.

$$\rho_M = \frac{M_{dry}}{(M_{sat} - M_{arch})} \quad \text{(Equation 3.1)}$$

The porosity of samples (ϕ) are calculated as in the Equation 3.2.

$$\phi = \frac{M_{sat} - M_{dry}}{(M_{sat} - M_{arch})} \quad \text{(Equation 3.2)}$$

The volumetric percent of pores under 0.5μm size can be estimated by keeping the sample in an environment of high humidity (above 85%) until the sample reaches to a constant weight (De Castro, 1979). To proceed with this measurement, an enviroment with a relative humidity level of 90% is ensured by placing a saturated potassium nitrate (KNO_3) solution in a closed vessel. The dry samples were kept within the vessel until their weight became steady. Porosity related to pores under 0.5μm size is estimated according to Equation 3.3.

$$\phi_{0.5\mu m} = \frac{M_{90\%} - M_{dry}}{M_{sat} - M_{arch}} \quad \text{(Equation 3.3)}$$

The ratio of porosity under 0.5 μm size to total porosity is calculated by the Equation 3.4

$$\phi_{0.5\mu m} = \frac{M_{90\%} - M_{dry}}{M_{sat} - M_{dry}} \quad \text{(Equation 3.4)}$$

3.3.2 Determination of pore size and pore morphology by microscopy

Pore size and pore morphology analysis through microscopy are commonly used in characterization studies (Elsen, 2006). Porosity can be determined through image analysis of cross-sections or thin sections.

Preparations for microscopic observations began with embedding plaster sample fragments in blue-dyed epoxy resin (AKA Resin + Hardener). The epoxy-covered samples were put in the vacuum chamber for about 1 hour to remove any entrapped air inaccessible pores while the resin had not hardened yet and was less viscous. Molds were removed after the epoxy was set.

Prepared samples were cut into thick slices of 2mm by using a low-speed cutter (Buehler IsoMet Low-Speed Saw). At least eight slices were taken out to observe the elongation of pores more in detail and increase the sampling area.

Images of thick sections, captured using stereomicroscope (Leica Z16 APO A model) were processed with Adobe Photoshop CC 2014. Various filters were used to distinguish the pores within the materials..

3.3.3 Determination of water vapor permeability

Water vapor permeability of materials is closely related to the porous network within the material. In order to determine the water vapor permeability of a material, two methods for measuring this property are given in EN ISO 12572 (British Standards Institute, 2016) and ASTM E96/E96M (ASTM International, 2022) standards. Methods are briefly based on measuring vapor transmission through a material from a more humid environment to a lesser one. When mass change becomes stabilized in steady state conditions, water vapor transmission rate (kg/m^2.s and expressed as WVTR or g) is calculated as in Equation 3.3.

$$WVTR = \frac{G}{A} \qquad \text{(Equation 3.3)}$$

Where G is the mass change rate per second (kg/s), A is the area of the specimen face exposed to vapour transmission (m^2). Water vapor permeance of the material (kg/m^2.s.Pa and expressed as WVP or W) is found as given in equation 3.4.

$$WVP = \frac{WVTR}{\Delta p} \qquad \text{(Equation 3.4)}$$

The Δp in equation 3.4 is the pressure difference (Pa) at the reciprocal sides of the material. The equation 3.4 can also be expressed as shown in Equation 3.5.

$$WVP = \frac{WVTR}{p_s(R_1 - R_2)} \quad \text{(Equation 3.5)}$$

The pressure difference is found by multiplying the saturation vapor pressure at the test temperature (p_s) with relative humidity (R expressed as a fraction) difference observed at the two sides of the material, the one in the chamber and the other in the cup filled with dessicant or distilled water. The water vapor permeability (δ) is calculated as in Equation 3.6.

$$\delta = WVP.d \quad \text{(Equation 3.6)}$$

The d in Equation 3.6 is the thickness of the material (m). The water vapor resistance factor (μ), which is another basic property used to define the water vapor transmission characteristics, is a ratio of the water vapor permeability of air (δ_{air}) to the water vapor permeability of material (δ) as shown in Equation 3.7.

$$\mu = \frac{\delta_{air}}{\delta} \quad \text{(Equation 3.7)}$$

The water vapour diffusion-equivalent air layer thickness (m and expressed as S_d) is then calculated as in Equation 3.8.

$$S_d = \mu.\mathrm{d} \quad \text{(Equation 3.8)}$$

EN ISO 12572 states that when the calculated S_d value is below 0.2m, the water vapor permeance of material shall be calculated as in Equation 3.9.

$$WVP_c = \frac{1}{\frac{A.\Delta P}{G} - \frac{d_{air}}{\delta_{air}}} \quad \text{(Equation 3.9)}$$

In Equation 3.9, d_{air} is the thickness of the air zone beneath the sample. The corrected water vapor diffusion-equivalent air layer thickness ($S_{d,cor}$) value is obtained by Equation 3.10 for the high permeable materials.

$$S_{d,cor} = \frac{\delta_{air}.p_s.(R_1 - R_2).A}{G} - d_{air} \qquad \text{(Equation 3.10)}$$

The water vapor permeability properties of plaster samples can be classified according to the S_d and WVTR values according to BS EN ISO 7783-2:1999 (British Standards Institute, 1999) and BS EN 1062-1:2004 (British Standards Institute, 2004). Table 3.8 shows the classification.

Table 3.8 Water vapor permeability classification

Permeability Class	According to S_d (m)	According to WVTR ($g/m^2.d$)
high water vapor permeability	<0.14	>150
medium water vapor permeability	0.14 to 1.4	15 to 150
low water vapor permeability	>1.4	<15

3.3.4 Determination of dynamic modulus of elasticity by ultrasonic pulse velocity

Ultrasonic pulse velocity (UPV) measurement is used to diagnose the inner structure of the selected samples as a non-destructive method calculated by the use of the velocity of ultrasonic waves passing through the samples. The dynamic modulus of the elasticity of samples can be interpreted by using ultrasonic velocity, bulk density, and the Poisson ratio of the samples (RILEM, 1980).

The UPV measurement system consists of pulse-generating test equipment, PUNDIT plus, transmitter, and receiver probes of 220 kHz. At least ten readings on

the signal's transit time from one probe to another and at different reciprocating points on the parallel surfaces are recorded and averaged. Afterward, the ultrasonic velocity is calculated by using the formula below.

$$u_{upv} = \frac{d}{t} \qquad \text{(Equation 3.11)}$$

Where u_{upv} is the ultrasonic velocity (m/s), d is the thickness of material (m) and t is the transit time (s). Dynamic modulus of elasticity (E_{mod}) of samples are calculated as in the Equation 3.12.

$$E_{mod} = \frac{\rho u_{upv}{}^2 (1+\nu)(1-2\nu)}{(1-\nu)} \qquad \text{(Equation 3.12)}$$

Where ρ is the density of material and ν is the poisson's ratio. As it is impossible to measure the Poisson's ratio of plaster samples due to the absence of a required measurement system, an assumption of Poisson's ratio based on related literature was used to calculate the dynamic modulus of elasticity. According to the literature, the Poisson's ratio of similar materials is between 0.1 to 0.3 (Almeida et al., 2023; Apostolopoulou et al., 2021; Diaz & Menéndez, 2020; Palomar et al., 2015; Palomar & Barluenga, 2017). The Poisson's ratio was set to 0.18 in the experiments.

3.3.5 Measurement of sound absorption coefficient

The sound absorption coefficients of the samples were measured by an impedance tube (S.C.S.9020B) after a minimum of 40 days of curing, according to the ISO 10534-2 standard (International Standards Organization, 1998). The sound absorption characteristics of the samples were examined in terms of the characteristic curve showing the sound absorption coefficients (α) at 1/3 octave bands. Two different impedance tubes were utilized in the measurement, the tube with 100mm diameter measures sound absorption coefficients between 50Hz to 1394Hz and the

tube with 28mm diameter measures between 800Hz to 4994Hz. A loudspeaker exists at one end of the tube, and a rigid termination is found on the other side where the material sample is placed. The sample is mounted with or without air space, depending on the application method that will be tested. The rigid termination can be adjusted according to the thickness of the sample, as the distance between the surface of the material facing the loudspeaker and the microphones should be fixed. A signal generator with an amplifier connected to the loudspeaker generates plane waves within the tube. The complex acoustic transfer functions of the signals detected by the two microphones are sent to a data acquisition system connected to the software. Sound absorption coefficients at 1/3 octave band frequencies are determined according to the collected data. The software also gives surface impedance values (Z_s) of the test sample.

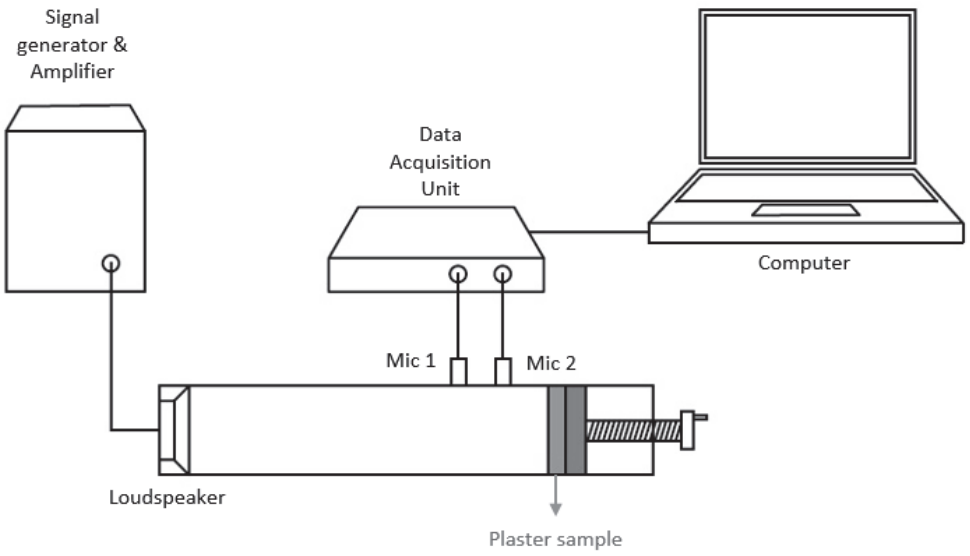


Figure 3.7. Sound absorption coefficient measurement system set up

Before measurements are made, the microphones and the measurement system are calibrated. In mounting the test sample to the tube, care should be given not to leave an air gap between the tube surface and the periphery of the material sample. During this study, lime plaster samples went through shrinkage as they matured.

Approximately 2-3mm shrinkage occurred at the circumference of our samples. To eliminate the effect of gaps and fit the samples to 100mm and 28mm diameter tubes, a 1mm thick tape was wrapped around the samples. Similar methods were advised to be used in the literature (Stanley, 2012).

3.4 Non acoustical parameters estimation using inverse characterization

The direct measurement of parameters such as tortuosity, viscous, and thermal characteristic length is not standardized yet. The equipment used in these types of measurements is not found in most of the laboratories. It is hard to achieve consistent results in measurements as it is previously tried in an interlaboratory test, especially for highly resistive, rigid frame granular materials (Pompoli et al., 2017).

A common approach in research is estimating these intrinsic properties related to porous networks through optimization using existing sound propagation models. With this method, the difference between measured and predicted sound absorption is aimed to be minimized. In order to use the correct sound propagation model, it is important to know whether the material of interest falls into the rigid, elastic, or limp frame category. If the phase decoupling frequency of the material is below the frequency range of interest, rigid frame theories can be used in optimizations. The phase decoupling frequency is calculated using the density, porosity, and flow resistivity data. The density and porosity of the prepared samples were defined by the experimental methods described in previous parts. The samples' flow resistivity can be determined through standardized measurements or indirect measurement techniques based on surface impedance. The results of various research show that for similar materials having granules/aggregates and binder/consolidant, flow resistivity values range between 1490N·s/m^4 to 490000N·s/m^4 (Carbajo et al., 2015, 2017; Degrave-Lemeurs et al., 2018; Glé et al., 2011; Horoshenkov & Swift, 2001; Swift et al., 1999). Considering the measured porosity and density values together with flow resistivity values presented in various research on similar materials, the

phase decoupling frequency is expected to be below 14Hz, which is away from the audible range of frequency.

Optimization is a widely used method for parameter estimation in engineering, statistics, machine learning, economics, and material science. Experimental techniques may not be so feasible when cost and time constrictions exist. Especially in acoustical characterization, the prediction of unknown parameters through optimization gives reasonable outcomes compared to the results of not fully standardized experiments (Atalla & Panneton, 2005; Pompoli et al., 2017).

n optimization, the accuracy of predictions improves using an appropriate propagation model for the search material and a convenient optimization algorithm. Johnson Champoux Allard Model is used in this study. Johnson Champoux Allard model is utilized in many studies for different types of materials and mostly gives approximate results with the measured sound absorption data (Atalla & Panneton, 2005; Bansod & Mohanty, 2016; Chu et al., 2009; Cobo & Simón, 2016; Mosanenzadeh et al., 2013). A detailed description of the model is given in Chapter 2.1.3. There are five parameters to be predicted in the JCA model. In most studies, the number of unknown parameters is less because porosity and flow resistivity can be measured with standard methods and equipment. As more parameters are known in predictions, estimating the unknown yields more straightforward and reliable results.

Optimization is a technique used to find the best solution set to achieve an objective function. In sound-absorbing materials characterization, the objective function mainly tries to find the optimum solutions for a set of parameters to achieve a convergent match between the predicted and measured sound absorption or surface impedance data. Many optimization algorithms based on different principles have been found. Nelder Mead, Differential Evolution, Simulated Annealing, Particle Swarm Optimisation, and Genetic Algorithms are the most commonly used for optimization studies in acoustics. All algorithms mentioned here are derivative-free algorithms, do not depend on derivative information, and search for optimal

solutions in the whole points of parameter space. Each algorithm has its strengths and weaknesses. In order to overcome the disadvantages, the working principles and settings have to be known to avoid possible local minima in the solution set (Bonfiglio & Pompoli, 2007).

In this study, the genetic algorithm is employed for optimization. The algorithm is inspired by genetics and mimics the rules of natural selection to reach the optimal solution. The solutions generated by randomly selected variables are called individuals. These individuals are coded as the representatives of chromosomes in DNA and are evaluated according to their fitness for the objective function (Akin & Demiral, 1998). Figure 3.7 given below from the study of Lee & Park (2022) is a descriptive example of how the information regarding the chromosomes are gathered.

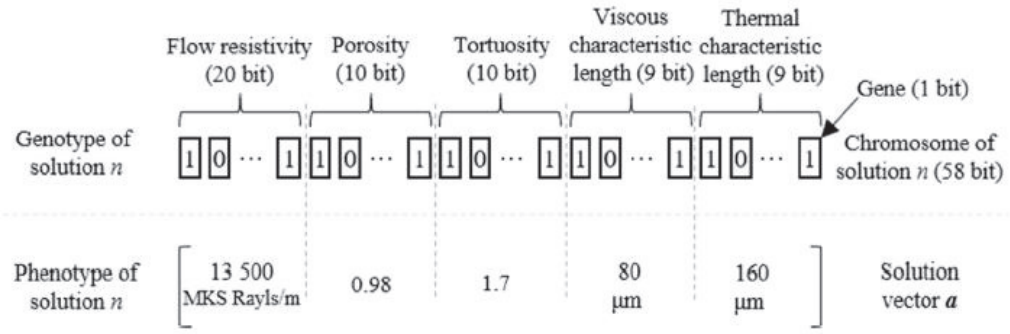


Figure 3.8. Individual's coding as chromosomes (Lee & Park, 2022)

The best-fit individuals are selected for offspring generation by operators such as fitness proportionate, tournament selection, and ranking selection. The offspring generation process produces new individuals by crossover and mutation operators. These new individuals become the new population and a new iteration starts over. This loop is called generation in the genetic algorithm (Akin & Demiral, 1998). The loop continues until a predefined number of generation criteria or a convergence to a successful solution has been met.

The fitness function, mostly called the objective function of the optimization, is chosen as in Equation 3.18. The optimization algorithm tries to minimize the function $f(\alpha)$.

$$f(\alpha) = \sum_{i=1}^{N} (\alpha_{mea} - \alpha_{mod})^2 \qquad \text{(Equation 3.18)}$$

In Equation 3.18, N is the total number of frequencies, α_{mea} is the measured sound absorption coefficients, and α_{mod} is the predicted sound absorption coefficients through optimization based on chosen sound propagation model.

Additionally, a few configurations must be completed before conducting an optimization study with the genetic algorithm. It is necessary to provide the algorithm with unknown parameters' lower and upper boundaries. In addition, the population's size, the number of individuals who will be handed down to the following generation, and the maximum number of generations should also be provided.

CHAPTER 4

RESULTS

In this chapter the results of experiments and inverse characterization are presented in the next sections. Beforehand, it is important to note that the level of carbonation within the binder affects the porous structure of materials. As carbonation occurs, the calcium hydroxide minerals in the binder transform to calcium carbonate, increasing their volume, which decreases the pore volume (Pavlík et al., 2012). On the other hand, the volume changes sometimes cause internal stress that result in new pores in the form of cracks. Carbonation is a slow process and only takes place in high relative humidity environments. Besides, temperature affects the solubility of carbon dioxide (Cultrone et al., 2005). All the samples were kept in a chamber with controlled humidity and temperature during the setting period. Afterward, the samples were kept in standard laboratory conditions, and their carbonation status was expected to be stable. To define the carbonation state of samples, a qualitative test using a saturated phenolphthalein ethyl alcohol solution was chosen (Rodriguez-Navarro et al., 2002). Phenolphthalein reacts with alkaline materials, and this reaction's result is a magenta color. As calcium hydroxide ($CaOH_2$) is alkaline, the expected color change is observed in the areas where carbonation is not finished.

On the other hand, the outcome of carbonation is that calcium carbonate ($CaCO_3$) has a lower pH and remains neutral in color. The samples were chosen from cylindrical specimens. In order to observe the condition within the material, specimens were broken into pieces to prevent any material transfer from different areas by sectioning through standard equipment such as a saw. Phenolphthalein is applied to freshly broken pieces. The photographs of samples after the phenolphthalein test are shown in Figure 4.1.

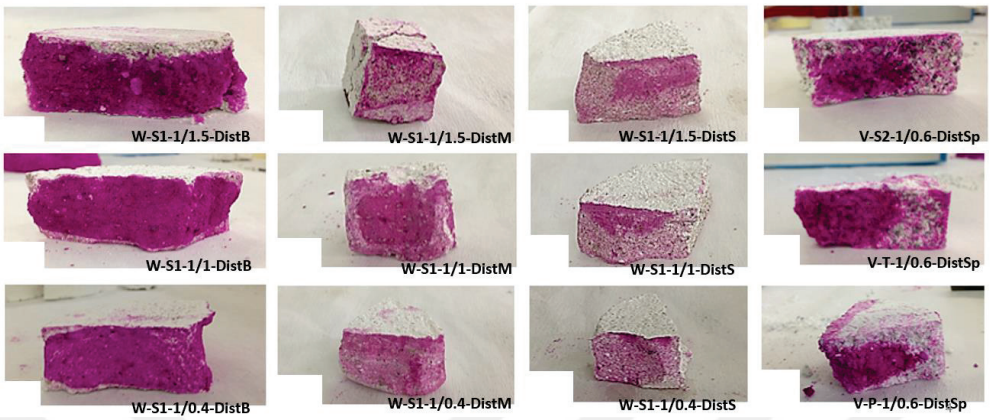


Figure 4.1. Carbonated (neutral) and not carbonated (pink color) areas in plaster samples.

A thin layer of the carbonated area close to the surface is observed in the section of the first set of samples that have aggregates of bigger sizes in higher amounts. A similar appearance but a thicker carbonated area is seen on the sections of the second set of samples containing different aggregate types of above 1mm size. In the samples having siliceous aggregates of 1-0.5 mm or 0.5-0.25mm size in higher weight amounts, the carbonated and uncarbonated areas do not show a sharp transition except sample W-S1-1/1-DistM.

4.1 Density, porosity and fine porosity of plaster samples

The density values of all plaster samples, including open porosity, fine porosity, and fine to total porosity in percentages, are given in Table 6. The density values range between 1063kg/m^3 to 1446kg/m^3 for the first set of samples and between 1031kg/m^3 and 1521kg/m^3 for the second set. The minimum porosity observed in the first group is 35%, and the maximum porosity is 43%. The second set of samples with different types and bigger sizes of aggregates have porosities in the range of 42% and 53%.

Table 4.1 Density, porosity (%), fine porosity (%) and fine to total porosity (%)

Sample Code	Density (kg/m^3)	ϕ Porosity (%)	$\phi_{0.5\mu m}$ Fine porosity (%)	Fine porosity/ Total porosity (%)
W-S1-1/1.5-DistB	1446 ± 0.01	37 ± 0.23	2.1 ± 0.23	5.69
W-S1-1/1-DistB	1406 ± 0.01	38 ± 0.63	2.2 ± 0.04	5.88
W-S1-1/0.4-DistB	1194 ± 0.06	40 ± 1.02	3.8 ± 0.31	9.45
W-S1-1/1.5-DistM	1298 ± 0.02	35 ± 0.77	3.1 ± 0.17	9.07
W-S1-1/1-DistM	1285 ± 0.01	37 ± 0.18	2.4 ± 0.13	6.36
W-S1-1/0.4-DistM	1070 ± 0.02	41 ± 0.61	2.8 ± 0.31	7.01
W-S1-1/1.5-DistS	1331 ± 0.00	35 ± 0.77	3.0 ± 0.50	8.58
W-S1-1/1-DistS	1211 ± 0.00	37 ± 0.41	3.4 ± 0.27	9.30
W-S1-1/0.4-DistS	1063 ± 0.01	43 ± 0.83	4.0 ± 0.14	9.23
V-S2-1/0.6-DistSp	1521 ± 0.01	42 ± 1.47	3.9 ± 0.22	9.26
V-T-1/0.6-DistSp	1161 ± 0.00	53 ± 0.22	2.3 ± 0.21	4.27
V-P-1/0.6-DistSp	1031 ± 0.01	50 ± 0.23	2.9 ± 0.13	5.92

In the first set of samples, the density of samples increases inversely as porosity values decrease. When the binder is used in higher amounts, the density of samples increases as well, while porosity decreases. On the other hand, the changes in aggregate size distribution do not affect the total open porosity noticeably.

The fine porosity characterized by pores of size below 0.5 μm changed from 2.1% to 3.9% in the first set of samples. In the second set prepared with different types of aggregates, fine porosity values range from 2.3% to 3.9%. No pattern exists in fine to total porosity (%) values, which compositional ratios may define.

4.2 Pore size and morphology of plaster samples

Pore size distribution and pore morphology were determined through microscopy. The epoxy impregnation was not successful in all of the samples. The list of impregnation success is given in Table 4.2.

Table 4.2 Impregnation status of material samples

Sample code	Impregnation status
W-S1-1/1.5-DistB	Successful
W-S1-1/1.1-DistB	Failed
W-S1-1/0.4-DistB	Partially
W-S1-1/1.5-DistM	Failed
W-S1-1/1.1-DistM	Successful
W-S1-1/0.4-DistM	Failed
W-S1-1/1.5-DistS	Partially
W-S1-1/1.1-DistS	Failed
W-S1-1/0.4-DistS	Successful
V-S2-1/0.6-DistSp	Successful
V-T-1/0.6-DistSp	Successful
V-P-1/0.6-DistSp	Successful

For a fair comparison, pore size distributions were gathered from the cross sections of fully impregnated samples. In order to increase the sampling and enable representative information about each material sample, the following procedure was followed. The data was collected by recording the width of 10 randomly chosen pores in the form of channels. The number of pores that data collected was a

minimum of 90 and a maximum of 121 for every distinct sample. For frequency graphics, the unit size for the observation range is taken as 0.01mm. The number of pores at different unit sizes recorded for each sample is projected in the frequency graphics given in Figure 4.2.

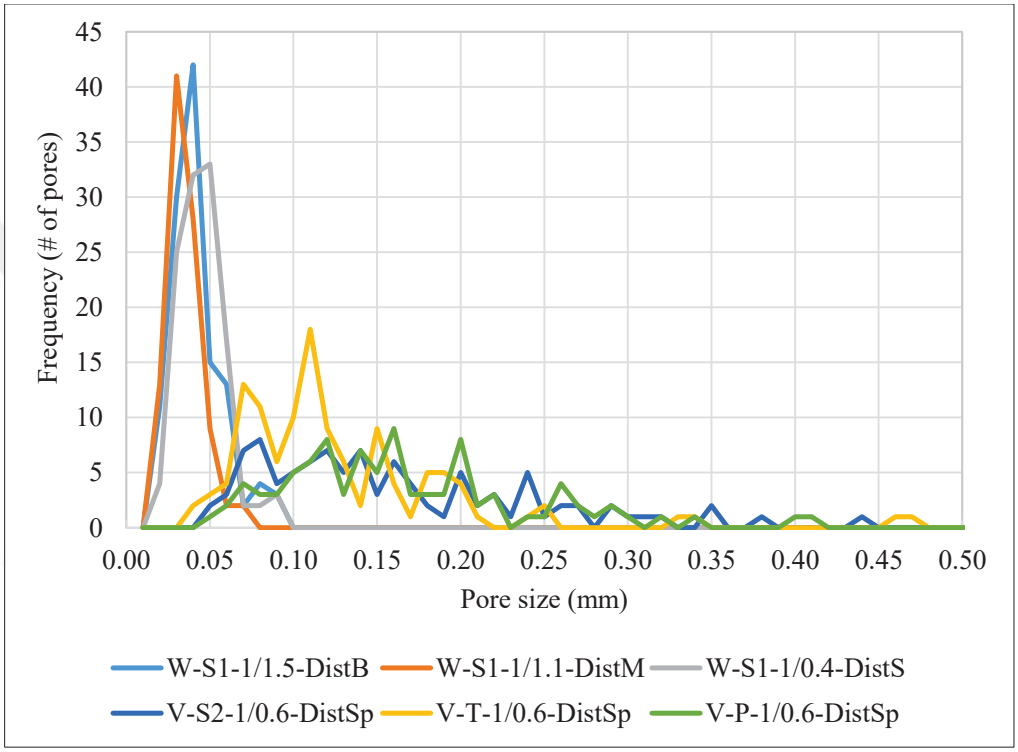


Figure 4.2. Frequency distribution of visually observable pore sizes

In Figure 4.2, the widths of visually observable pores are between 0.0025mm and 0.06mm for the first set of samples. The dominant pore size in W-S1-1/1.5-DistB, W-S1-1/1-DistM, and W-S1-1/0.4-DistS samples are 0.04mm, 0.03mm, and 0.05mm, respectively. The dominant pore size and its frequency in W-S1-1/0.4-DistS are dissimilar to the other samples of the first group. The binder amount compared to the aggregate amount (by weight %) is higher in this plaster sample than in the first group. Also, small-size aggregates are found in higher weight amounts other than the two samples in the first plaster group. In order to comment, the visuals

of samples are given in Figures 4.3, 4.4, and 4.5 to understand if the difference is related to the pore morphology.

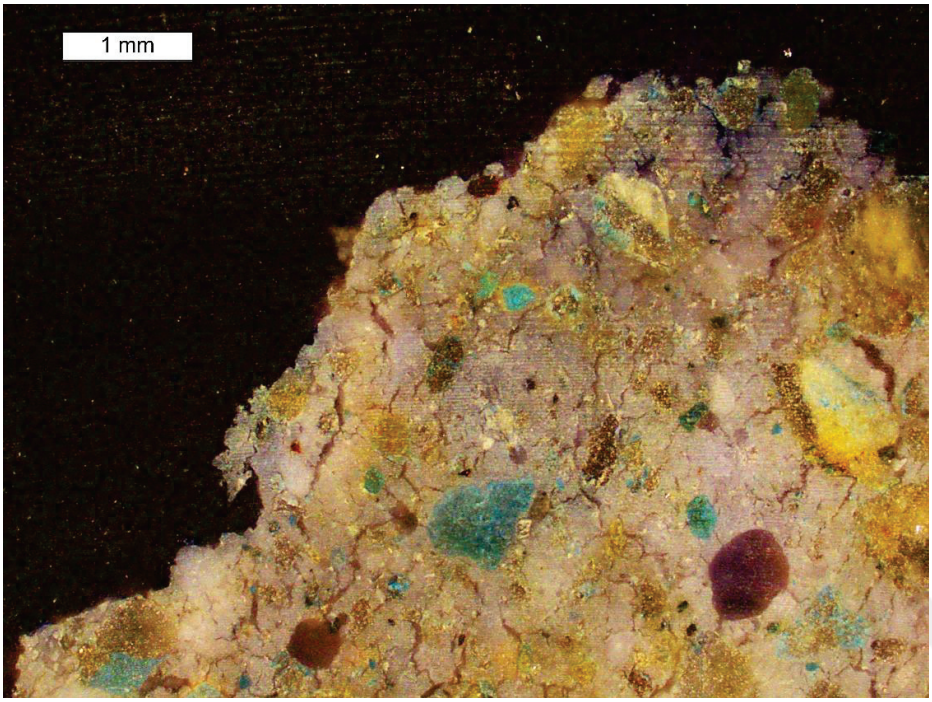


Figure 4.3. Section image of W-S1-1/1.5-DistB sample

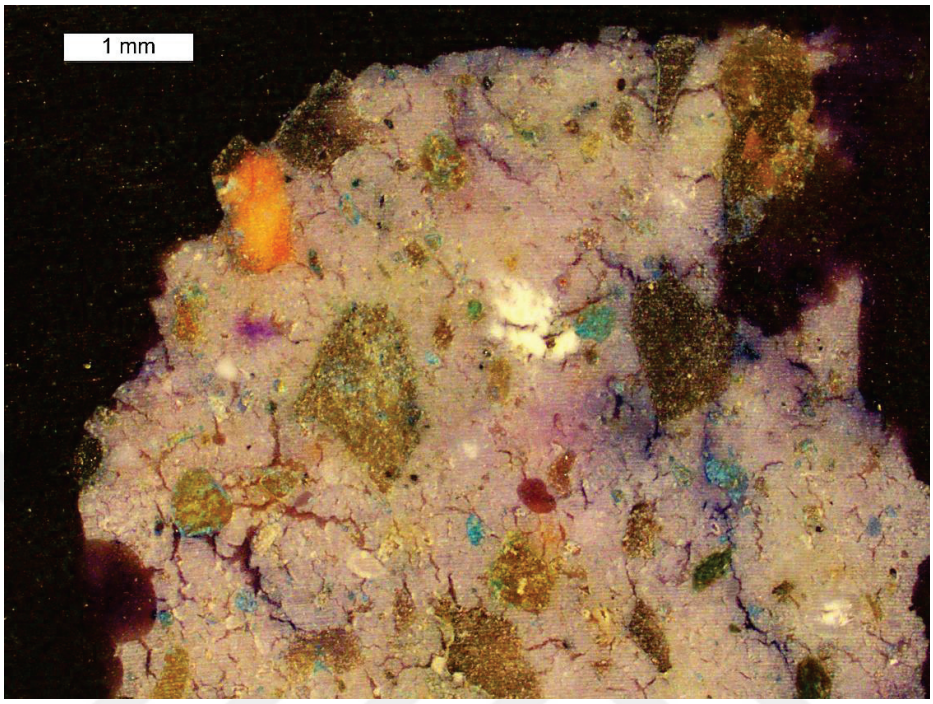


Figure 4.4. Section image of W-S1-1/1-DistM sample

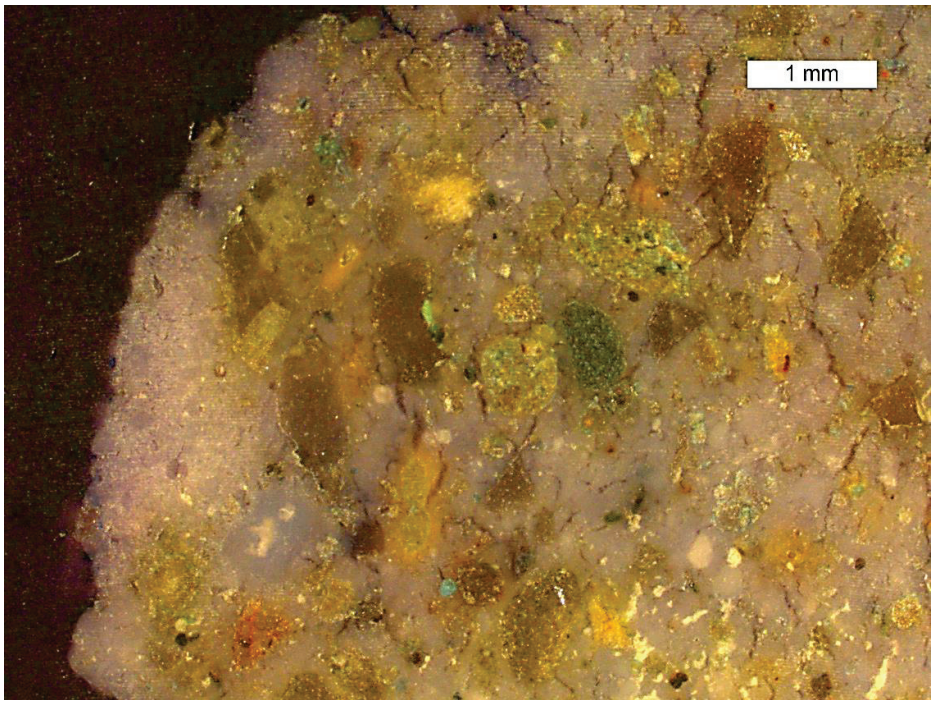
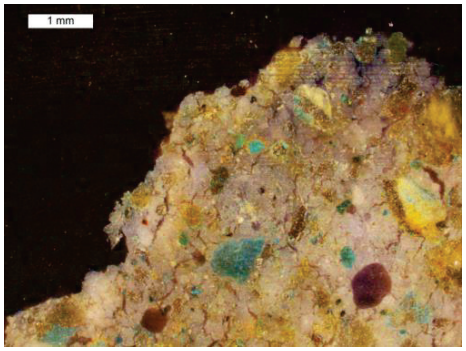


Figure 4.5. Section image of W-S1-1/0.4-DistS sample

The images show that in W-S1-1/1.5-DistB and W-S1-1/1-DistM, pores within the binder matrix are more disseminated than in the W-S1-1/0.4-DistS sample. In sample W-S1-1/0.4-DistS, the smaller size aggregates and binder amount are higher than W-S1-1/1.5-DistB and W-S1-1/1-DistM, the binder between the smaller aggregates occupy more area than the first two samples. This leads to shortly elongated smaller-sized pores of even appearance. As given in section 4.1.1, the measured porosity of sample W-S1-1/0.4 is higher than the other samples of the first group. These results show that the smaller size pores in the form of cracks observed in the sample with a higher binder aggregate ratio (1/0.4) and smaller size aggregates in higher amounts constitute more area than the pores of other samples having lower binder aggregate ratio and high amount of bigger size aggregates.

According to Figure 4.1, in the second set of samples, the widths of visually observable pores are between 0.05mm and 0.60mm, different from the pore size range observed in the first set of plasters. The absence of aggregates smaller than 0.5mm in the second set of samples seems to result in pores with larger sizes. This argument can be supported through a comparison of section images because the sample from the first group, W-S1-1/1.5-DistB, and the sample, V-S2-1/0.6-DistSp, in the second group, do have the same binder to aggregate ratio depending on the weight amount, also have the siliceous type of aggregates. Figure 4.6 shows the two samples together. The larger pore sizes in the binder matrix in sample V-S2-1/0.6-DistSp in the absence of aggregates are obviously seen as the result of bigger size aggregates smaller than 0.5mm.



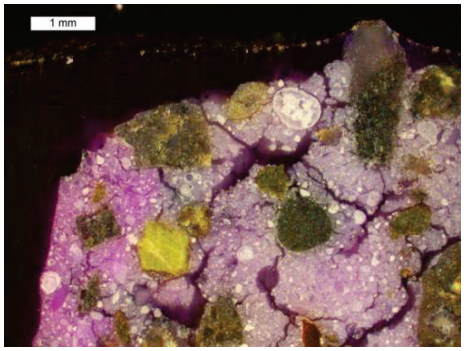


Figure 4.6. Section image of W-S1-1/1.5-DistB sample (left) and V-S2-1/0.6-DistSp (right)

The dominant pore sizes in the V-S2-1/0.6-DistSp sample, V-T-1/0.6-DistSp sample, and V-P-1/0.6-DistSp sample are 0.15mm, 0.1mm, and 0.2mm, respectively. In this second sample group, only for V-T-1/0.6-DistSp, a dominant pore size is observed. The other samples' frequency trends are widely distributed over all sizes and decrease gradually as pore size increases.

The images in Figures 4.6, 4.7, and 4.8 belong to V-S2-1/0.6-DistSp, V-T-1/0.6-DistSp, and V-P-1/0.6-DistSp samples.

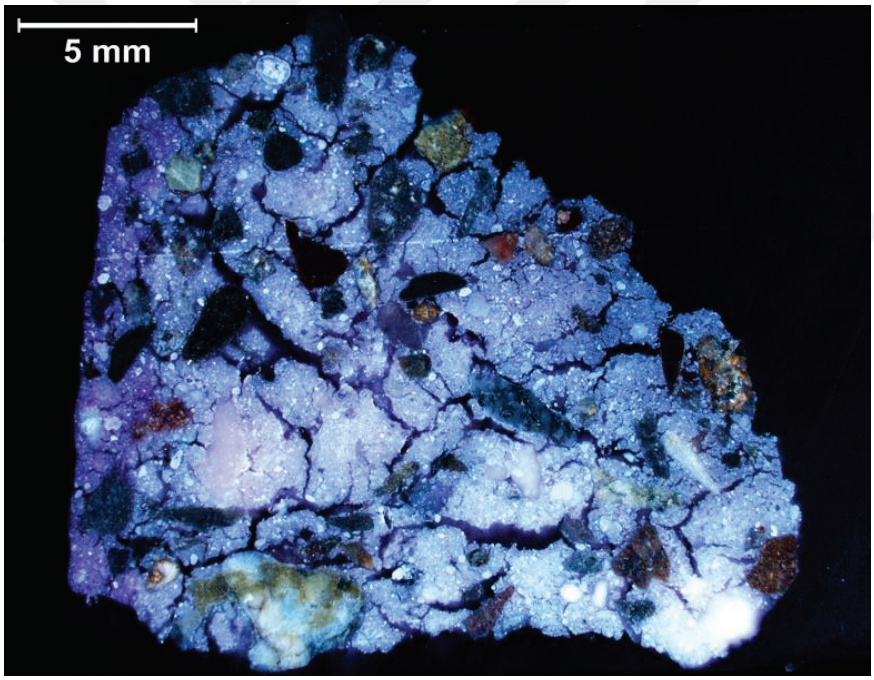


Figure 4.7. Section image of V-S2-1/0.6-DistSp

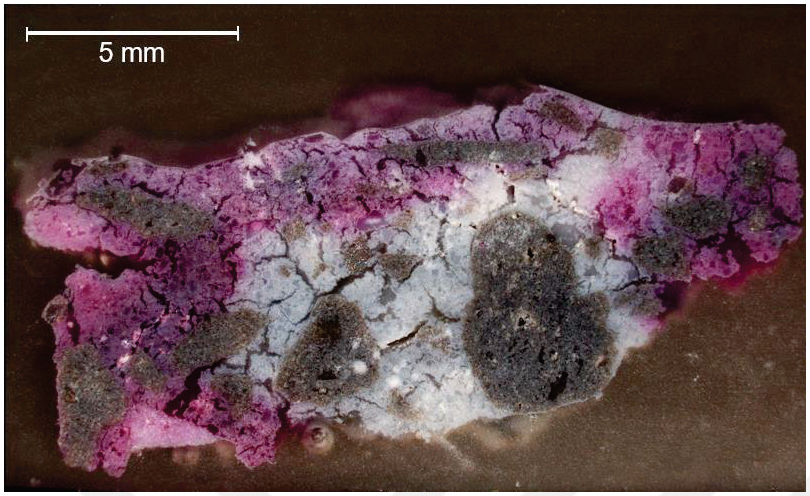


Figure 4.8. Section image of V-T-1/0.6-DistSp

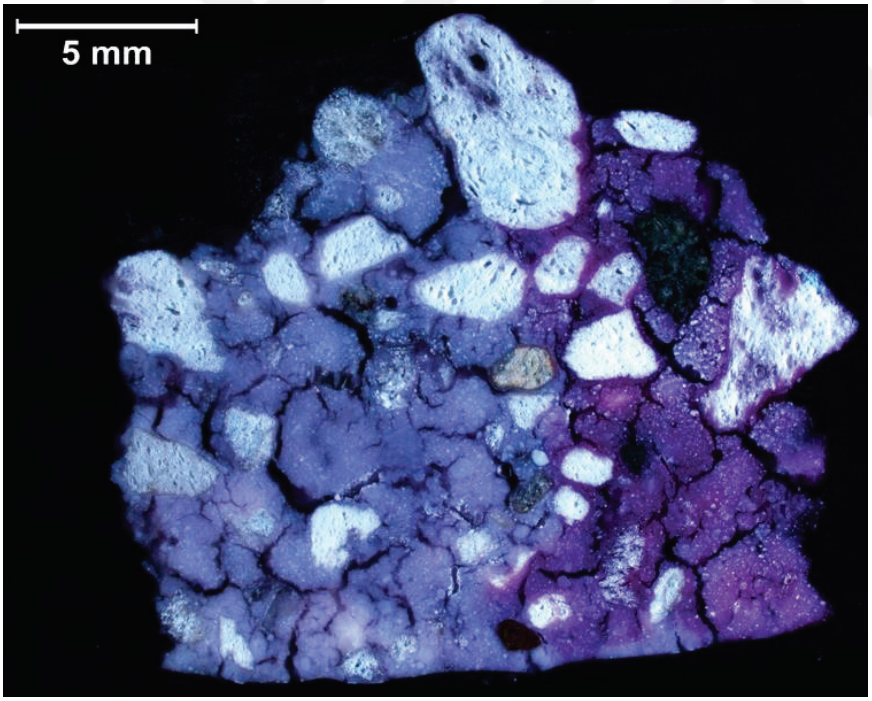


Figure 4.9. Section image of V-P-1/0.6-DistSp

In the second set of samples, the biggest pores in the form of cracks mostly elongate from aggregate to aggregate and continue in the outer zone of aggregates but not in the binder-aggregate interface. While the samples are kept in the chamber for setting,

surface dry saturated lightweight aggregates of porous nature may have released water gradually to the binder matrix, and this process seems to reduce the shrinkage cracks elongated between binder and aggregate. The adherence problem between binder and siliceous aggregates results in fissures in the binder-aggregate interface zone.

The average, median, minimum, and maximum pore sizes observed through the microscope on the sections of W-S1-1/1.5-DistB, W-S1-1/1-DistM, W-S1-1/0.4-DistS, V-S2-1/0.6-DistSp, V-T-1/0.6-DistSp, and V-P-1/0.6-DistSp samples are listed in Table 4.3.

Table 4.3 Average, median, minimum and maximum pore sizes observed visually through microscopy.

Pore Size (mm) Information	W-S1-1/1.5-DistB	W-S1-1/1.1-DistM	W-S1-1/0.4-DistS	V-S2-1/0.6-DistSp	V-T-1/0.6-DistSp	V-P-1/0.6-DistSp
Average size	0.037	0.030	0.040	0.154	0.162	0.122
Median size	0.035	0.027	0.040	0.135	0.151	0.106
Minimum size	0.013	0.012	0.019	0.048	0.040	0.035
Maximum size	0.089	0.069	0.083	0.432	0.408	0.462

The average pore size for the first set of samples, which had aggregates below 2mm, was around 0.03 and 0.04mm. The average and median pore sizes are almost similar in these samples. The minimum pore size observed in the samples of this group has a value of 0.012mm at the lowest. The maximum pore sizes are between 0.069mm and 0.083mm. In the second set of samples, the minimum size of pores visually observed is larger than the ones in the first group. Likely, due to the use of bigger aggregates, the median pore sizes are significantly lower than the average pore sizes

of the first plaster group. The minimum pore size visually observed in the second samples are in between 0.035 and 0.048mm. The maximum pore size of the same group is around 0.408 to 0.462 mm.

4.3 Water vapor permeability of plaster samples

The results of water vapor permeability experiment are listed in Table 4.4.

Table 4.4 Water vapour diffusion-equivalent air layer thickness (S_d) and water vapour resistance factor (μ)

Sample code	Water vapour diffusion-equivalent air layer thickness **S_d (m)**	water vapour resistance factor **μ**
W-S1-1/1.5-DistB	0.122 ± 0.01	6.08 ± 0.44
W-S1-1/1.1-DistB	0.127 ± 0.01	6.34 ± 0.48
W-S1-1/0.4-DistB	0.130 ± 0.01	6.51 ± 0.26
W-S1-1/1.5-DistM	0.086 ± 0.00	4.28 ± 0.22
W-S1-1/1.1-DistM	0.109 ± 0.01	5.18 ± 0.65
W-S1-1/0.4-DistM	0.100 ± 0.01	5.01 ± 0.51
W-S1-1/1.5-DistS	0.151 ± 0.01	6.88 ± 0.30
W-S1-1/1.1-DistS	0.143 ± 0.00	6.80 ± 0.03
W-S1-1/0.4-DistS	0.159 ± 0.02	7.59 ± 0.79
V-S2-1/0.6-DistSp	0.062 ± 0.00	2.77 ± 0.03
V-T-1/0.6-DistSp	0.056 ± 0.00	2.49 ± 0.05
V-P-1/0.6-DistSp	0.055 ± 0.00	2.45 ± 0.08

The water vapor resistance of plaster samples, μ, changes from 2.45 to 7.59. The highest μ is observed for the W-S1-1/0.4-DistS sample of the first set. This sample has the highest binder amount by weight and contains the lowest size of aggregates

in higher weight amounts. The second set of samples have μ values below 2.77, which is lower when compared to the μ values of the first set. This feature is associated with the use of bigger-size aggregates. The data can be grouped according to the aggregate size distribution. It is clearly seen that in the first set of samples, the group that has 0.5-1 mm size aggregates in higher amounts has lower water vapor resistance than other aggregate size distribution groups.

The results show that the samples having aggregates of size below 0.5mm in higher amounts fall into the medium water vapor permeability class depending on their SD value and permeability class given in Table 4.4. The other samples of the first group and second group are all categorized under the high vapor permeability class.

4.4 UPV and modulus of elasticity of plaster samples

Measured ultrasonic pulse velocity (UPV) and the dynamic modulus of elasticity (Emod) calculated from measured pulse velocities are presented in Table 4.5.

Table 4.5 Measured UPV (m/s) and E_{mod} (MPa) values of samples

Sample Code	UPV (m/s)	Emod (MPa)
W-S1-1/1.5-DistB	1127 ± 44	1692
W-S1-1/1.1-DistB	1090 ± 20	1538
W-S1-1/0.4-DistB	1263 ± 21	1756
W-S1-1/1.5-DistM	1143 ± 35	1563
W-S1-1/1.1-DistM	1142 ± 17	1543
W-S1-1/0.4-DistM	1216 ± 28	1458
W-S1-1/1.5-DistS	1201 ± 44	1767
W-S1-1/1.1-DistS	1236 ± 42	1703
W-S1-1/0.4-DistS	1252 ± 45	1534
V-S2-1/0.6-DistSp	1253 ± 34	2227
V-T-1/0.6-DistSp	1147 ± 76	1441
V-P-1/0.6-DistSp	1144 ± 92	1266

Ultrasonic pulse velocity ranges between 1090 to 1263 m/s for the whole sample set. The highest and the lowest UPV values are observed for W-S1-1/0.4-DistB and W-

S1-1/1.1-DistB, respectively. These two samples have the same aggregate size distribution. The main difference between these highest and lowest values is the binder-to-aggregate ratio used in their compositions. The solid matrix in sample S1-1/1.1-DistB should have been interrupted by pores transverse to the elongation route of the pulse, which resulted in the lowest UPV values. The extreme difference may be explained by the heterogeneity of sample W-S1-1/1.1-DistB only or the heterogeneity of both samples. In the second set of samples prepared with different aggregates, the result of sample V-S2-1/0.6-DistSp is reasonable as the other two samples in the group are lightweight aggregates and have pores in their own structure.

Dynamic modulus of elasticity values are between 1266Mpa and 1767MPa. The highest value was observed in the sample containing bigger siliceous aggregates from the second plaster set. The other two of this group show lower values of Emod. The dynamic modulus of elasticity values of the first set are in between the lowest and highest of the whole sample set.

4.5 Sound absorption coefficients of plaster samples

The mean measured sound absorption coefficients of plaster samples are given in Figure 4.10 below. The overlapping sound absorption data at 1000Hz, 1250Hz, and 1600Hz received from both small and large impedance tubes are averaged using the technique described in the ISO 10534-2 standard (International Standards Organization, 1998, pp. 10534–2).

The absorption coefficients of the first plaster sample group are below 0.15. There exist generally two absorption peak groups in observed frequencies, one group is around 500Hz to 8000Hz, the other group is around 2500Hz and 3150Hz. The sound absorption curve of sample W-S1-1/1-DistB does not have a similar peak in the curve as the samples in the same group.

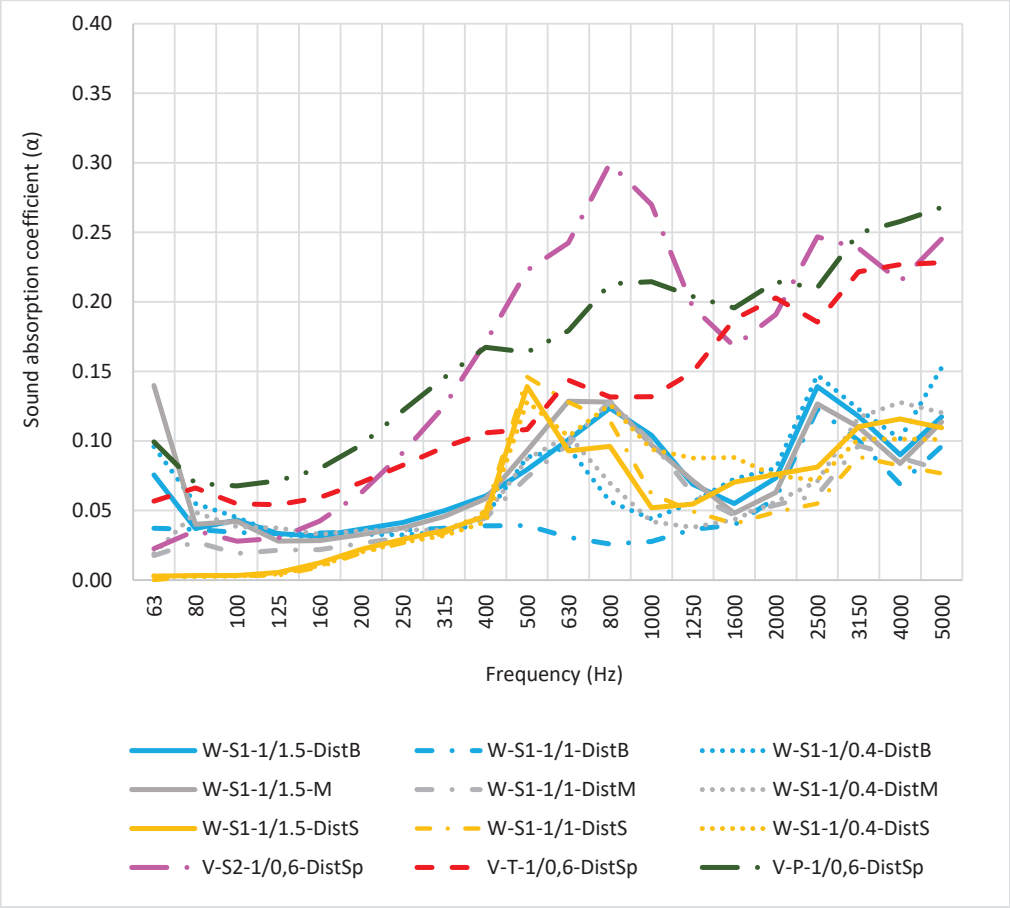


Figure 4.10. Sound absorption coefficients of plaster samples

In the second sample group, due to the use of bigger-sized aggregates in their mixture, the sound absorption coefficients are higher than the absorption coefficients of the first group. The maximum absorption is observed at 800Hz for the sample that has siliceous aggregates of bigger sizes in higher amounts. The sound absorption coefficients of sample W-T-1/0.6-DistSp that have tuff aggregates in its composition are generally lower than those of samples with siliceous and pumice aggregates above 250Hz. The sample is also distinguished from the other two with its frequency of visually observed pore size data given in Figure 4.2.

4.6 Inverse characterization

Inverse characterization was performed through optimization by the JCA model and Genetics Algorithm. The upper and lower bounds defined in the algorithm are given below:

Tortousity = [LB: 1, UB:4]
Airflow Resistivity = [LB: 1000, UB: 500000]
Viscous characteristicLength = [LB: 1, UB:6/17]
Thermal Characteristic Length = [LB: 1, UB:100/230]
Porosity = [LB:0, UB:1]

The frequency range chosen for optimization is between 63Hz and 1600Hz, which includes sound absorption coefficients of all samples measured in the large impedance tube with 100mm diameter. Given that the selected JCA model has a limited capacity to replicate the low-frequency behavior of porous materials, the fitness of the predicted sound absorption values is assessed through the value of objective function calculated considering the frequencies between 500Hz and 1600Hz. A similar approach was utilized in the study of Atalla & Panneton (2005). They pointed out the possible errors that may occur at low frequencies due to the measurement setup, which is associated with the restricted microphone spacing in relation to the wavelengths at these frequencies. All in all, the value of the objective function, which is calculated for the whole measurement frequency range between 63Hz and 1600Hz, is included with the value of the objective function calculated for the frequency range where the JCA model works best, between 500Hz and 1600Hz are presented. Estimated unknown material properties by inverse characterization are given in Table 4.6.

Table 4.6 Results of inverse characterization

Sample Code	Fval (63Hz - 1600Hz)	Fval (500Hz - 1600Hz)	Tortuosity α_∞ (-)	Airflow Resistivity σ (Pa.s/m^2)	Viscous Charac. Length Λ (μm)	Thermal Charac. Length Λ' (μm)	Effective Porosity Φ (%)
W-S1-1/1.5-DistB	0.121	0.00038	1.01	378823	4	5	10
W-S1-1/1.1-DistB	0.053	0.00002	1.20	69117	2	39	5
W-S1-1/0.4-DistB	0.136	0.00101	2.43	88129	6	33	8
W-S1-1/1.5-DistM	0.127	0.00011	1.19	314976	4	11	11
W-S1-1/1.1-DistM	0.050	0.00064	1.49	84170	6	12	9
W-S1-1/0.4-DistM	0.097	0.00139	2.38	133143	6	7	8
W-S1-1/1.5-DistS	0.026	0.00271	2.80	168050	7	12	9
W-S1-1/1.1-DistS	0.024	0.00257	2.84	147759	9	11	11
W-S1-1/0.4-DistS	0.020	0.00148	1.47	94053	5	10	12
V-S2-1/0.6-DistSp	0.052	0.00169	2.22	318620	7	190	37
V-T-1/0.6-DistSp	0.274	0.00136	1.22	91731	4	133	15
V-P-1/0.6-DistSp	0.683	0.00304	1.25	407954	6	127	20

The results indicate that the fitness function, the sum of the squared differences between the measured and predicted values, is less than 0.68 for frequencies between 63Hz and 1600Hz and less than 0.003 for frequencies ranging from 500Hz to 1600Hz. The tortuosity is between 1.01 and 2.8 for the samples of the first group. The highest tortuosity value is estimated for the sample with 0.50-0.25 mm-sized aggregates in higher weight amounts and a BA ratio of 1/1.1 in its composition. The second set of plasters composed of 1-4mm size aggregates of different types has tortuosity values that change from 1.2 to 2.2. The highest tortuosity is observed in the sample containing silica aggregates. The lowest tortuosity belongs to the sample with tuff aggregate.

The estimated airflow resistivities of the first group of samples are between 91731 N·s/m^4 to 378823 N·s/m^4. In the second plaster set composed of different types of aggregates type, the flow resistivity values change from 91731 N·s/m^4 to 407954 N·s/m^4. Predicted viscous characteristic lengths change from 2μm to 9μm for all samples. The thermal characteristic lengths are estimated between 5μm and 190μm. The porosity values for the first sample group determined by the water immersion

approach are much higher than those expected via optimization. While the water immersion method yielded the lowest porosity value of 0.35, predicted values range from 5% to 12%. The kind of pores is responsible for this outcome. The effective porosity is lower than the measured ones because dead-end pores do not contribute as much to sound absorption as open pores do. This disparity should be attributed to aggregates smaller than 2 mm. The effective porosity values of the second set of samples, which have larger aggregates and showed higher sound absorption performance, were higher than those of the first group. Particularly, the samples made with silica aggregates in the second set have an effective porosity similar to those obtained from the water immersion test. This implies that compared to the samples from the first group, these samples have fewer dead-end pores. Contrarily, the samples with lightweight aggregates have lower effective porosity values than those with silica aggregates. The mean effective porosity value of plaster samples with tuff aggregates is almost 70% lower than the measured open porosity value. This variance is observed as 60% for the samples with pumice aggregates. Somehow, dead-end pores are more dominant in the pore structure of the samples with lightweight aggregates rather than through connected pores.

The measured and predicted sound absorption coefficients are shown in the figures below. A good fit is achieved at the maximum absorption for some of the plaster samples. The low-frequency approximation of the JCA model is not sufficient, as stated by other researchers. This is also observed for the sound absorption coefficient predictions in this study.

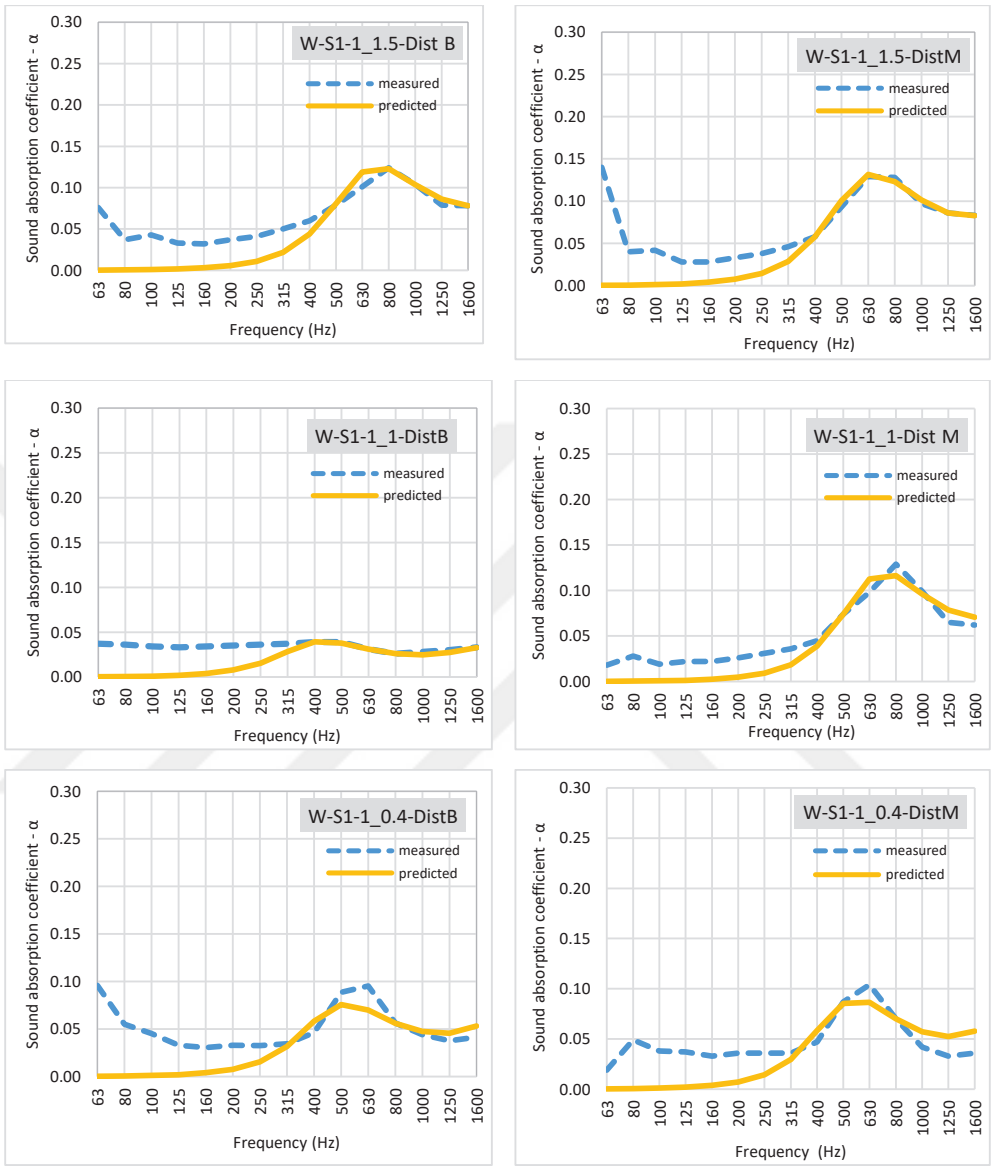


Figure 4.11. Measured and predicted sound absorption coefficient for the first six samples of first plaster set

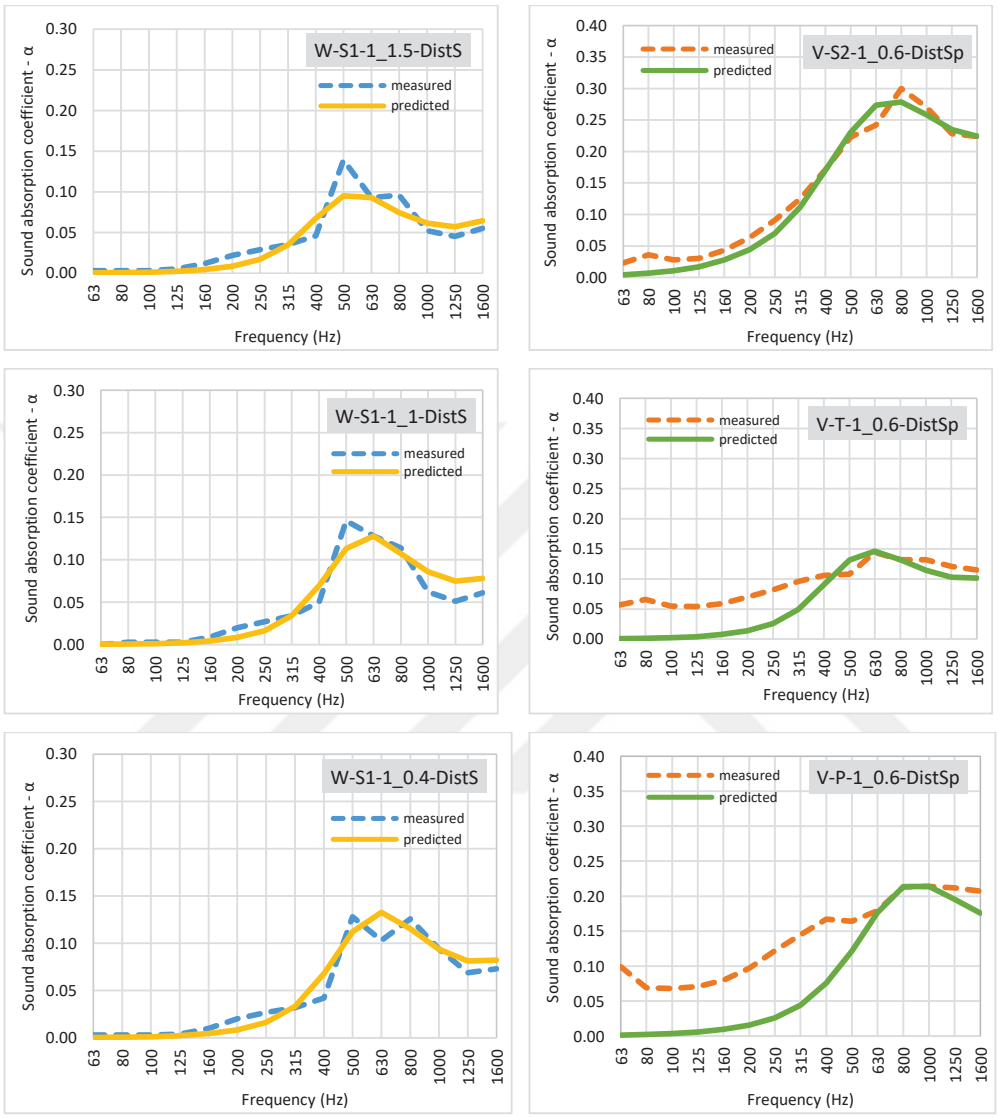


Figure 4.12. Measured and predicted sound absorption coefficient of the last three samples of first plaster set and the samples of the second plaster set

CHAPTER 5

DISCUSSION

5.1 Assessing the effect of compositional properties on the pore structure

The pore structure, which is uniquely composed by the variation of aggregate size distribution, aggregate type, and binder to aggregate ratio, is going to be defined in this section in terms of open porosity, fine porosity, kinematic porosity, pore size distribution, pore morphology, tortuosity, air flow resistivity, viscous and thermal characteristic length.

The first plaster sample set investigates the effect of aggregate size distribution and binder-to-aggregate ratio on open porosity. Figure 5.1 shows the porosity variation depending on the binder-to-aggregate ratio and aggregate size distribution..

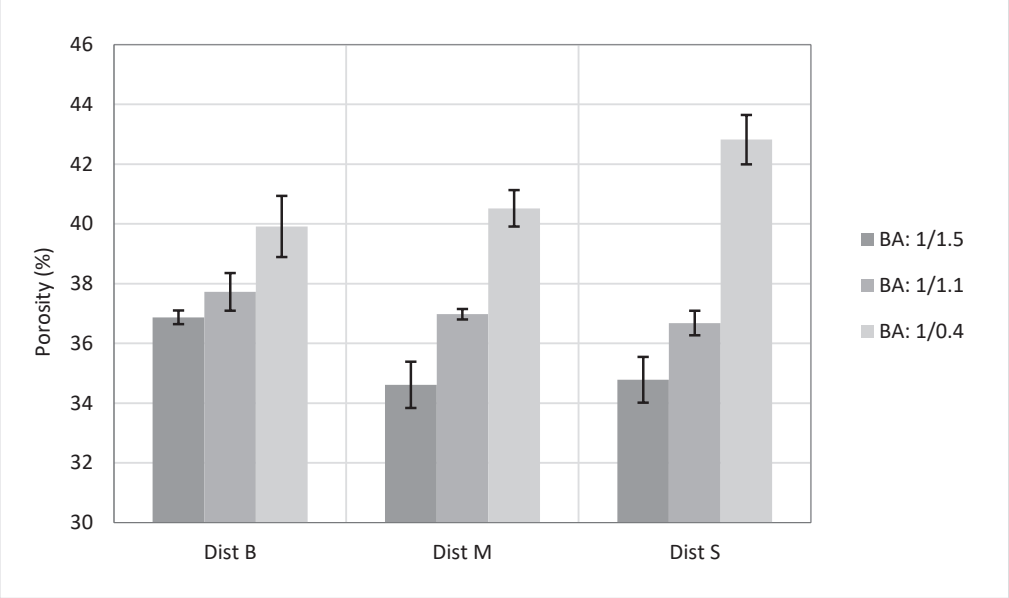


Figure 5.1. The change in porosity with respect binder to aggregate ratio and aggregate size distribution

For the same binder-to-aggregate (BA) ratios, porosity does not change similarly according to the different aggregate size distribution groups. When the BA ratio is 1/0.4, porosity increases by 2% with the change of the weight percentage of small-size aggregates (0.5-0.25mm size) from 20% to 35% in plaster composition. The other porosity values are very close to each other. In the group with a 1/1 BA ratio, the change in porosity is so small that it will be deceptive to comment on the effect of aggregate size. In the third group, where the BA ratio is 1/1.5, a 2% change in porosity occurs when the weight of bigger size aggregates (1-2mm) increases to 35%.

When the changes in porosity are examined depending on the BA ratio, it is seen that for all aggregate size distribution groups, the porosity of samples increases as the binder amount increases in samples. The rate of change in porosity with BA ratio for samples with larger size aggregates in higher amounts is not as sharp as the other two samples belonging to different size distribution groups.

Figure 5.2 displays the porosity values for the second batch of plasters produced using larger-sized aggregates of various kinds. The porosity values for these plasters are close to the highest porosity (42.3%) observed for the first sample group that is prepared with smaller-size siliceous aggregates.

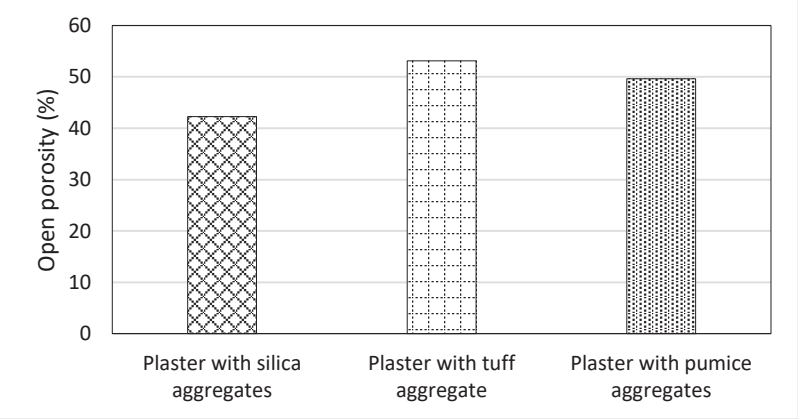


Figure 5.2. Open porosity of samples in the second plaster set

As the main focus in these samples is to observe the impact of different aggregate types in the resulting pore structure, the two lightweight aggregate types, tuff, and pumice, are expected to play an essential role in the differentiation of pore structure compared to siliceous aggregates, which are not in the lightweight aggregate category. The porosity values of samples with lightweight aggregates are higher than those containing siliceous aggregates. The values are predictable as the porous nature of these aggregates contributes to the formation of pores within the binder mix in a distinct way. To assess this contribution, water absorption percentages of aggregates are shown in Figure 5.3. This figure shows that the water absorption of silica aggregates is much lower than that of lightweight aggregates. As expected, when the aggregate size increases, silica and pumice aggregates' water absorption capacity decreases.

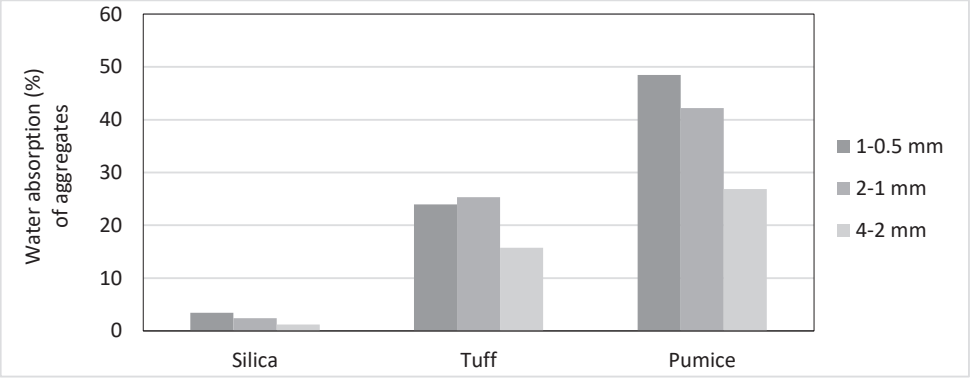


Figure 5.3. Water absorption (%) of different type and size of aggregates used in the second plaster set

On the other hand, for tuff aggregates, the water absorption of 0.5-1mm sized aggregates is slightly higher than 1-2mm sized tuff aggregates. Interestingly, although the water absorption percentages of pumice aggregates are higher than the tuff aggregates, the plaster samples prepared with tuff aggregates have the highest porosity. This result shows that apart from the water absorption capacity of aggregates, other factors related to composition, such as aggregate shape, may have

contributed to the resultant pore structure. In contrast, the cross-section images reveal no clear indication of a variation in pore structure attributable to the pore shape of pumice or tuff aggregate.

The volume of fine pores under 0.5µm to the total volume of samples are examined through fine porosity. The variance of fine porosity values is given in Figure 5.4.

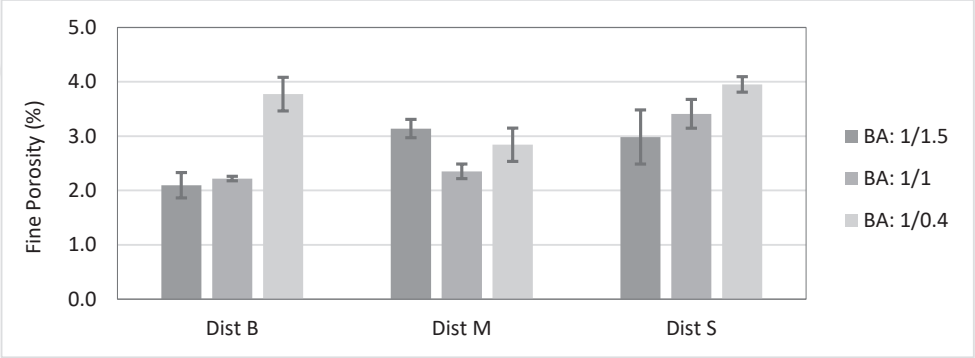


Figure 5.4. The change in fine porosity (%) with respect binder to aggregate ratio and aggregate size distribution

It is seen that the variation of fine porosity is not associated directly with BA ratios or different aggregate size distribution groups. The fine porosity values for the samples of the second plaster set where different types of larger size aggregates used in the compositions are shown in Figure 5.5.

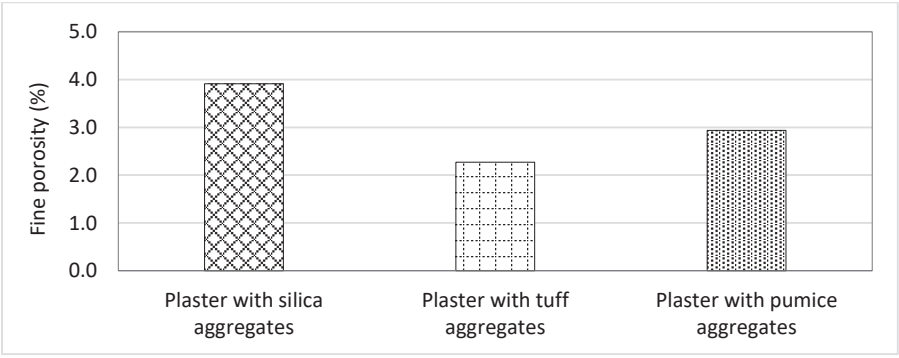


Figure 5.5. Fine porosities (%) in the second plaster set

The fine porosity values of the second set of samples are similar to the ones in the first plaster set. The use of larger-size aggregates does not substantially affect the fine porosity percentage. The fine porosity of samples prepared with tuff and pumice aggregates is slightly lower than that of samples with silica aggregates.

Porosity and fine porosity measurements incorporate the saturation of material with water and water vapor. The saturation occurs in the pores open to the surface that terminate by dead ends or continue throughout the material section. On the other hand, the effect of dead-end pores in sound propagation remains an ongoing discussion for researchers. The most widely used sound propagation models consider only the porosity that is active in sound propagation as kinematic/effective porosity, ignoring the porosity of dead-end pores.

Prediction through inverse characterization using the Johnson-Champoux-Allard model shows that effective porosity for the first sample group where the effect of BA ratio and aggregate size distribution are examined around 8% to 12% (see Figure 5.6) except for the sample that contains larger size aggregates in higher amount and has a BA ratio of 1/1. The difference can be related to a failure in the specimen of this type of plaster used in the sound absorption measurements. Except for this sample, the general tendency in the groups having large size (2-1mm) and medium size aggregates(1-0.5mm) in dominant weight amount is the decrease in fine porosity as BA ratio increases. It is worth saying that these two sample groups have the same amount of aggregates with sizes equal to and below 0.5mm (40%). For the samples where smaller size (0.5mm ≥) aggregates are dominant by 65%, as the BA ratio increases, the effective porosity increases as well.

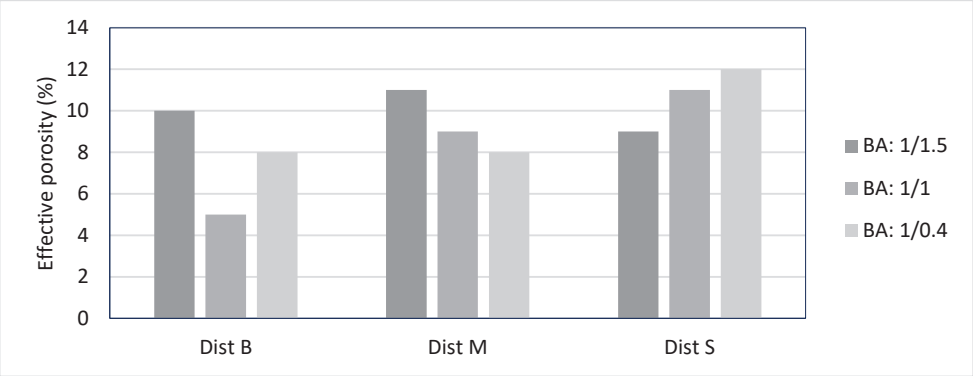


Figure 5.6. The change in effective porosity (%) with respect binder to aggregate ratio and aggregate size distribution

The effective porosities of the second sample set are given in Figure 5.7. The predicted values for plaster samples with silica and tuff aggregates are alike, around 15-20%. Samples containing silica aggregates have an effective porosity of 17% higher than samples containing pumice aggregates and 22% higher than samples containing tuff aggregates. The samples with silica aggregates have longer elongated pores in the form of cracks, as seen in the cross-section image in Figure 4.6. Moreover, the pores do not divaricate much as they are in the samples with pumice or tuff aggregates. The unique way of pore formation in the samples with silica aggregates must result in a more thorough pore structure that constitutes most of its pore volume.

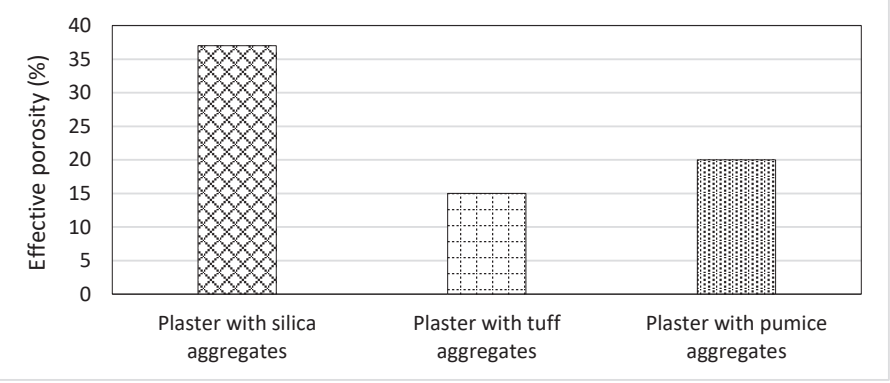


Figure 5.7. The effective porosities (%) of second plaster set.

The pore size distribution data gathered from images of cross sections only give a general idea about the change in pore size depending on compositional choices, as it was not possible to get images from all types of samples in the first plaster group. Figure 5.8 shows the frequency of pore sizes in these examples.

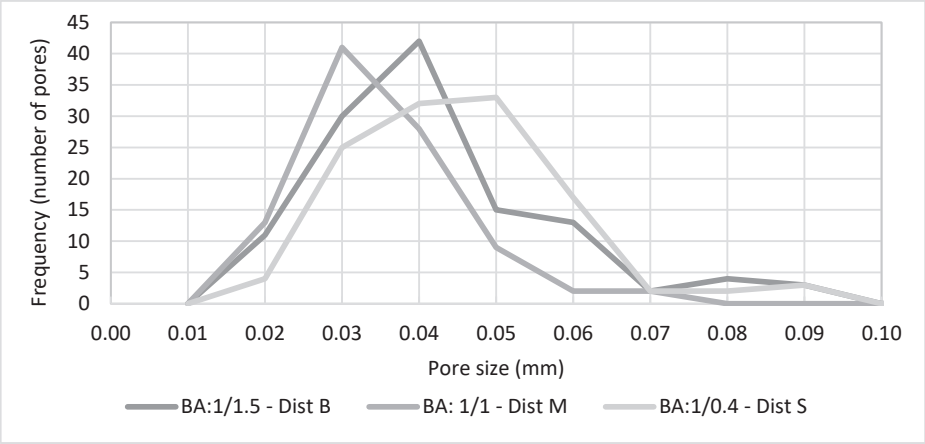


Figure 5.8. The frequency of pore sizes for the first plaster sample set

The samples with 1/1.5 and 1/1 BA ratios and aggregates of 1-2mm and 0.5-1mm in higher weight amounts have dominant pore sizes of 0.04 and 0.03mm, respectively. On the other hand, the frequency curve of the sample containing the lowest aggregate amount in its content and small size aggregates (0.25-0.5mm) in higher weight amounts is distributed along a range of pore sizes between 0.03 and 0.05mm. The pores observed from the cross-section images of this sample (Figure 4.4 in Section 4.2) are distributed evenly within the material, identical in size, and shortly elongated compared to the other samples representing different BA ratios and aggregate size distributions (Figure 4.3 and 4.4 in Section 4.2).

The pore size distribution of the second plaster set is given in Figure 5.9. The pore size ranges show similarity. Pore sizes show a wide distribution in samples containing silica or pumice aggregates. On the other hand, in samples containing tuff, pores with sizes of 0.07 mm and 0.11 mm are dominant in number. This may indicate a homogeneity in the structure that results in an identical size pore layout.

Also, from the cross-section images of these samples given in Figures 4.6, 4.7, and 4.8, pores in the form of cracks are shortly elongated in the plaster sample prepared with tuff aggregates.

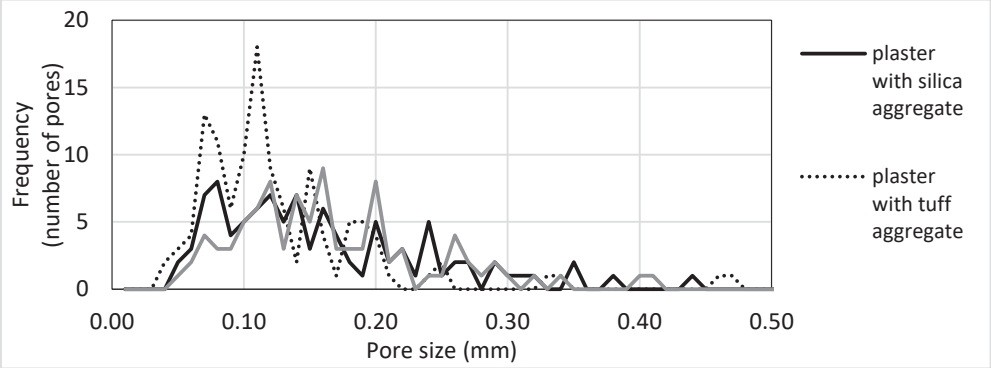


Figure 5.9. The frequency of pore sizes for the second plaster sample set

The tortuosity of pores within the material is an essential parameter in sound propagation. When tortuosity values are assessed in terms of compositional properties, it is seen in Figure 5.10 that tortuosity value for aggregate distribution groups where larger size (2-1mm) or medium size (1-0.5mm) aggregates dominate by weight amount increases as a binder to aggregate ratio increases. On the other hand, samples with small-size aggregates found in greater weight amounts do not show this sort of relationship. Only sample groups with a BA ratio of 1/1.5 and 1.1 saw increased tortuosity due to decreased aggregate size.

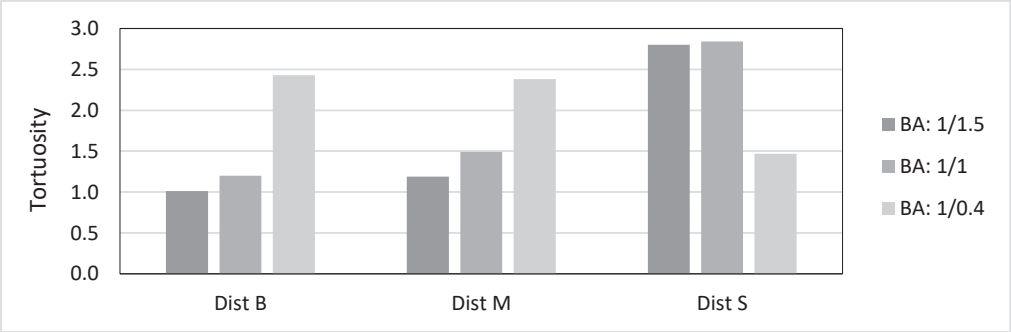


Figure 5.10. The tortuosity values for the first plaster set

Predicted tortuosity values of the second plaster set are shown in Figure 5.11. Tortuosity is close to 1 for the plaster samples containing lightweight aggregates. This indicates a direct propagation path alongside the section of the sample. On the other hand, tortuosity increases in the plaster samples prepared with silica aggregates.

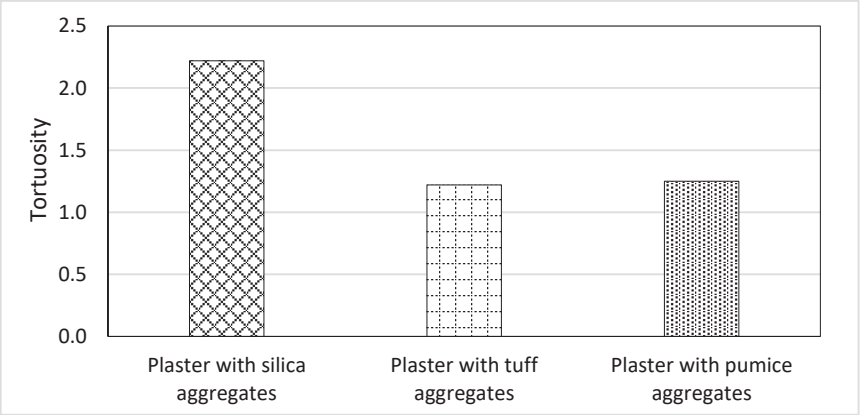


Figure 5.11. The tortuosity values for the second plaster set

The change of airflow resistivity values derived by inverse characterization depending on aggregate size distribution and BA ratio is shown in Figure 5.12. The results show that contrary to what is commonly reported in the literature (see section 2.4), the airflow resistivity values of samples do not increase as the weight of smaller size aggregates (0.25-0.5mm) increases in composition. This observational mismatch may be attributed to the aggregate sizes used in this study. Most of the work, as mentioned earlier, uses bigger particles in compositions above 0.5 mm and up to 12 mm; unlike this study, the gradation of various aggregate sizes is not based on a bell-shaped curve. Mostly, the aggregates used in the related studies are mono-sized.

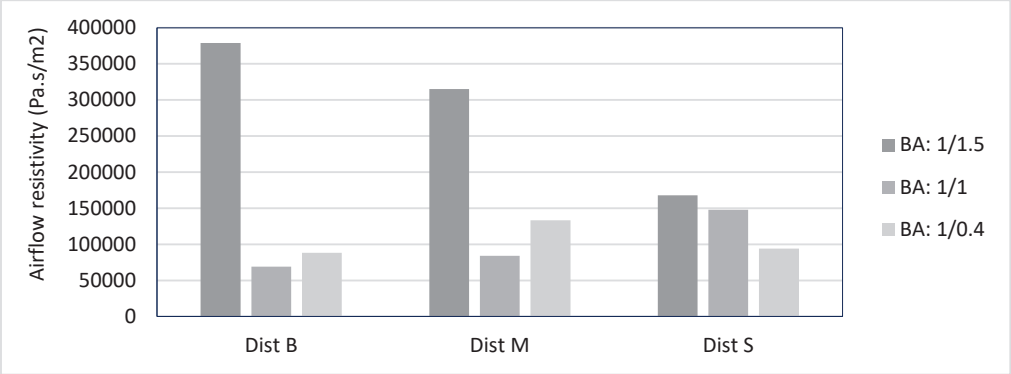


Figure 5.12. The airflow resistivity values for the first plaster sample set

The airflow resistivity decreases with the increase of the BA ratio for the sample group prepared with an aggregate size distribution where smaller-size aggregates (0.5 mm - 0.25 mm) dominate (see Figure 5.12). On the other hand, airflow resistivity values are much greater for the samples with a BA ratio of 1/1.5 than those with a BA ratio of 1/1 and 1/0.4 in samples where larger or medium-size aggregates are dominant in size distribution.

Predicted airflow resistivity values of the second plaster set are presented in Figure 5.13. The airflow resistivity values of plaster samples prepared with tuff aggregates are lower than the resistivity values of the samples containing silica aggregates or pumice aggregates. The samples containing pumice aggregates have the highest airflow resistivity, reaching 407954 Pa.s/m2. It isn't easy to attribute sample differences to the usage of lightweight aggregates or the aggregate size.

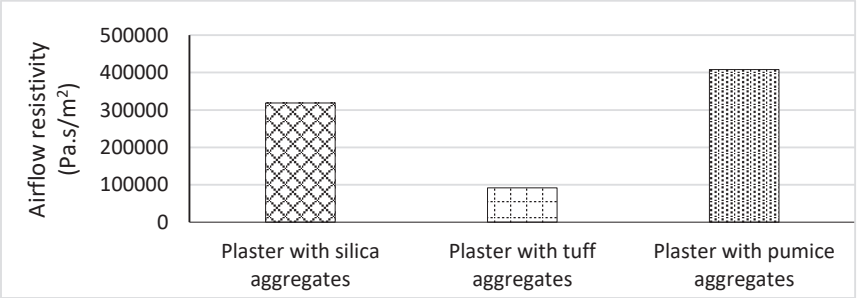


Figure 5.13. The airflow resistivity values for the second plaster sample set

Viscous characteristic length derived using the JCA model and optimization are given in Figure 5.14. There is no consistent change in viscous characteristic length with the increase of the BA ratio. Furthermore, no apparent connection is seen between the dominating aggregate sizes in compositions and viscous characteristic length values.

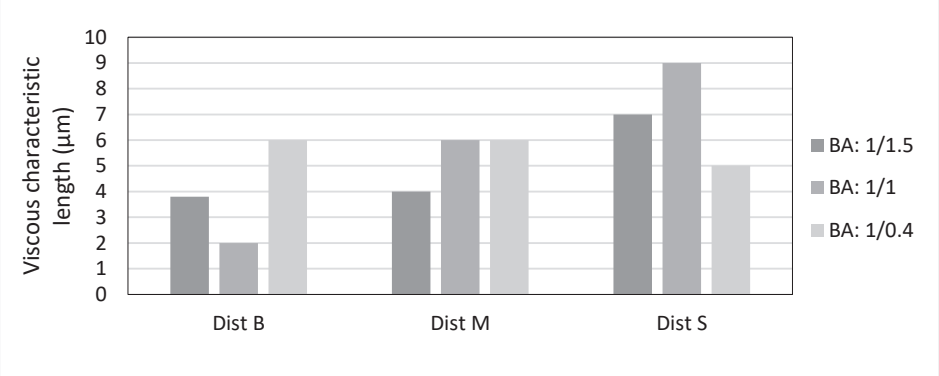


Figure 5.14. Viscous characteristic length for the first plaster sample set

The viscous characteristic length of the second plaster sample set is given in Figure 5.15. This group's lowest viscous characteristic length belongs to the plaster sample with tuff aggregates. Although samples with lightweight aggregates have displayed lower viscous characteristic lengths than those with silica aggregates, the differences are not noticeable.

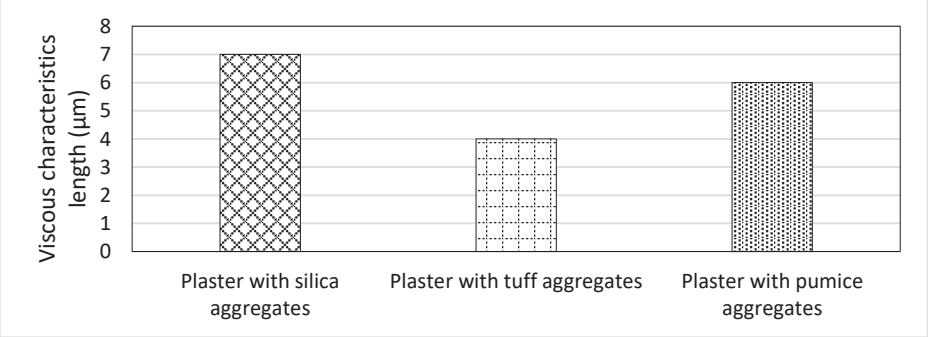


Figure 5.15. Viscous characteristic length for the second plaster sample set

Predicted thermal characteristic lengths are given in Figure 5.16. There is no consistent iterative relation between thermal characteristic length and BA ratio. Again, a discrepancy is observed for the sample containing 2mm -1mm size aggregates in higher amounts (Dist B). Although predicted values are above average for the samples with BA ratios of 1/1 and 1/0.4 in this size distribution group, the thermal characteristics length of the sample with a BA ratio of 1/1.5 is the lowest of all samples. Moreover, thermal characteristic length is also not associated with aggregate size distributions.

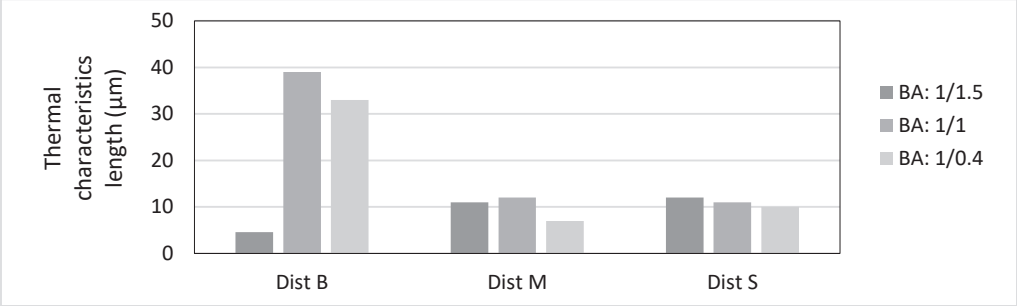


Figure 5.16. Thermal characteristic length for the first plaster sample set

Predicted thermal characteristic lengths for the second set of plaster samples are given in Figure 5.17. The figure shows that the thermal characteristic lengths for the plaster samples with tuff and pumice aggregates are lesser than those of the plaster samples with silica aggregates.

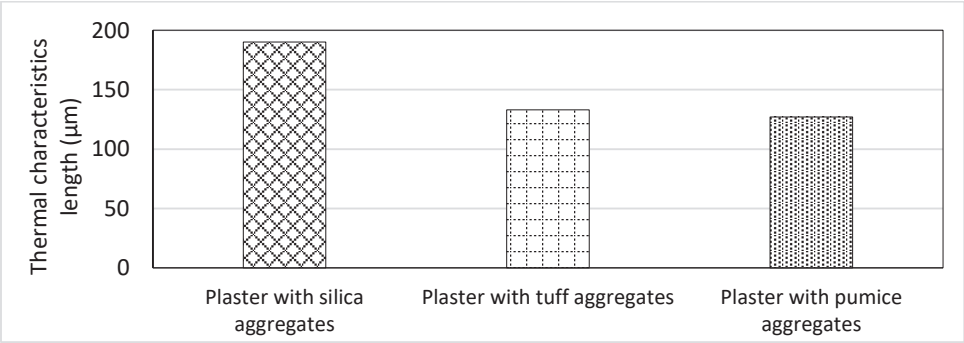


Figure 5.17. Thermal characteristic length for the second plaster sample set

5.2 Discussion on the interrelations between parameters defining pore structure

This section examines the interrelations of the properties associated directly with pore structure. Porosity is a macro property that gives information on the body of the pore structure. The volume occupied by different pore types, such as open-through pores, dead-end pores, closed pores, or different pore sizes, is directly associated with various performance properties such as vapor permeability, water absorption, thermal diffusivity, and sound absorption. This section's primary subjects of discussion are the relationships between the measured parameters and how they relate to the associated pore structure parameters predicted by the JCA model through optimization.

The correlation between open porosity and fine porosity in the plaster samples is shown in Figure 5.18 below. As it is seen, the most robust relation between open porosity and fine porosity is observed in the samples prepared with different types and bigger aggregates of 1-4mm sizes (see Figure 5.18, right side). Although the porosity values of samples prepared with lightweight aggregates are higher than those prepared with silica aggregates, their fine porosity values are lower than those of samples with silica aggregates. The open porosity decreases transversely with the volume increase of fine pores under 0.5µm.

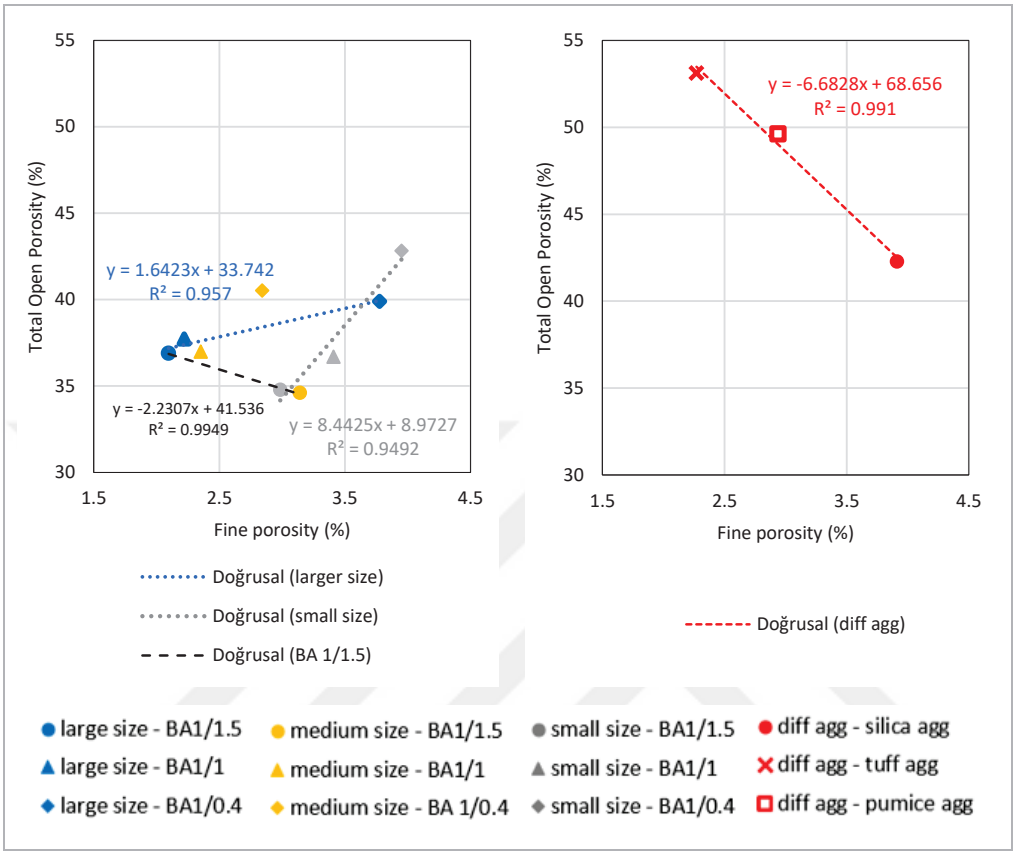


Figure 5.18. The correlation of open porosity and fine porosity

In the first plaster set, for the samples with a BA ratio of 1/1.5, the porosity value decreases independently from the dominant aggregate size as fine porosity increases (see Figure 5.18, left side). No significant relation exists for the sample groups with a BA ratio of 1/1 or 1/0.4. For plaster samples where small-size aggregates (0.5-0.25mm) are dominant, open porosity increases significantly with an increase in fine porosity. In samples containing large-size aggregates (2-1mm) in higher weight amounts, there is also a direct relation between porosity and fine porosity. Still, the slope of change is low when compared to the plaster sample group, where smaller aggregates dominate. The data is dispersed for the samples with medium-size (0.5-1mm) size aggregates in higher quantities and does not allow for a noteworthy conclusion to be drawn.

Another graphic that shows the change between fine porosity (%) and fine to total open porosity (%) is given in Figure 5.19. In this relation, the fine to total porosity keeps increasing as fine porosity increases for both the first and second groups of plasters. This trend is well observed when the data is examined under different BA ratio groups in the first plaster batch (See Figure 5.19, left side). The relation between fine to total porosity and fine porosity is also significant when the results are grouped according to aggregate size distribution.

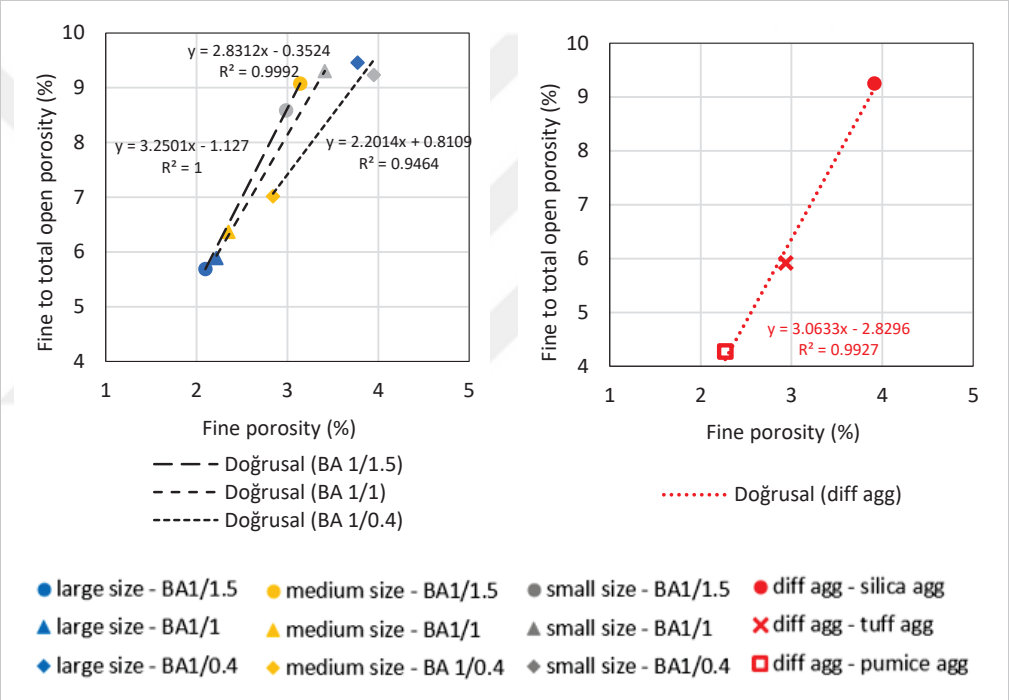


Figure 5.19. The relation between fine to total open porosity (%) and fine porosity (%)

The other interrelation investigated is between the total open porosity (%) and the effective porosity (%). As observed from the iterations realized during optimization, effective porosity is the main parameter that defines the frequency where maximum absorption is located. In the first plaster set, the effective porosity of samples determined through inverse estimation does not change significantly as open porosity (see Figure 5.19) for the plaster samples in the groups based on either the

dominant aggregate size or the BA ratio. In the second group, where aggregate type varies but a standard aggregate size distribution where larger aggregates (4-0.5mm) are used, the total open porosity of samples decreases as the effective porosity increases. Effective porosity gets closer to the total open porosity for the sample with silica aggregates in this second plaster set, which indicates that pores are more connected and continue throughout the sample section.

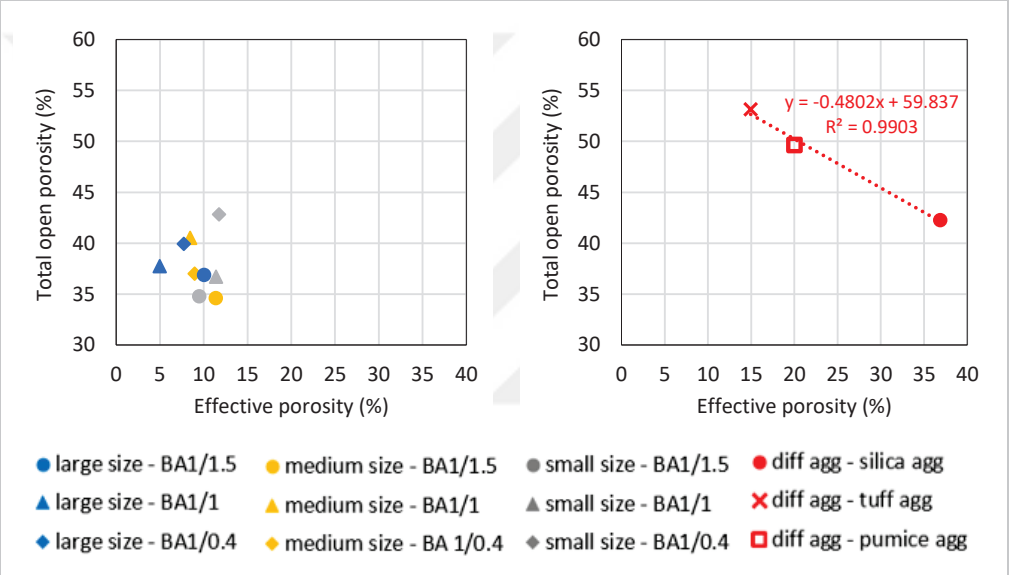


Figure 5.20. The correlation of effective porosity (%) and open porosity (%)

It is known that the low-frequency behavior of sound propagation can not be sufficiently reflected by the JCA model. Both airflow resistivity and thermal characteristic length are the characteristics mostly associated with low frequencies. Consequently, only the relationship between tortuosity and viscous characteristic length is studied with respect to the parameters obtained by optimization. Figure 5.21 shows the viscous characteristics lengths and the tortuosity values together for the whole sample sets. The figures show a direct relation between tortuosity and viscous characteristic length. An increase in tortuosity is followed by an increase in viscous characteristic length.

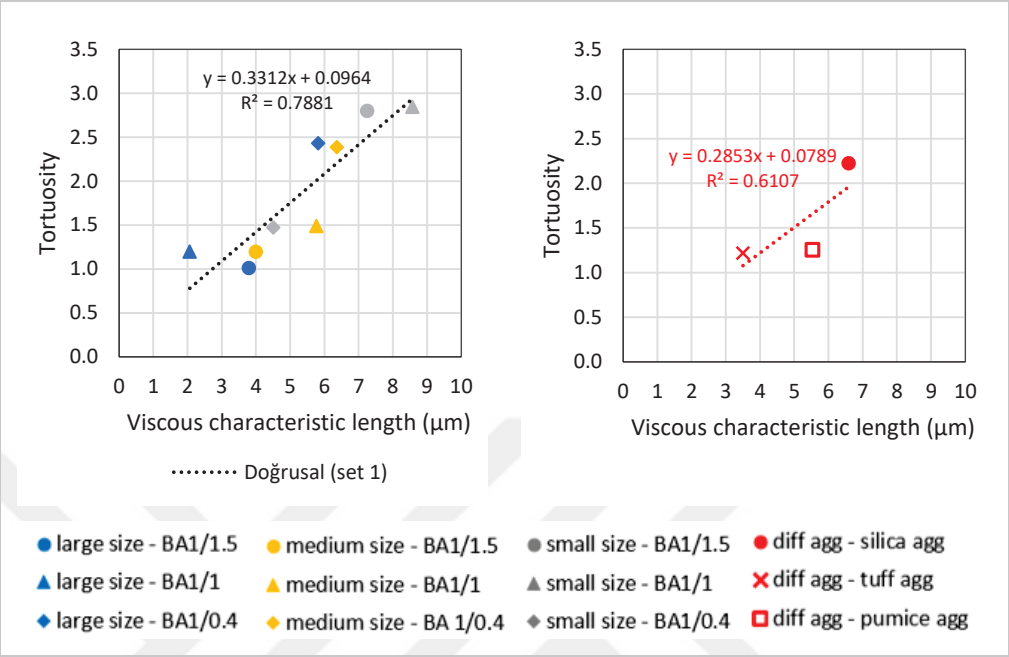


Figure 5.21. The relation between tortuosity and viscous characteristic length

Another assessment is conducted to see the relation between predicted viscous and thermal characteristic length with the observed minimum and maximum pore sizes through cross-sections. Viscous losses are associated with the pores where pore size minimizes, and thermal losses are associated with the pores where pore size maximizes and is proportional to the half-width of the pores. Therefore, the half-width of the maximum and minimum pore size is compared to the viscous and thermal characteristic length. Figure 5.22 shows this relation for the first plaster set.

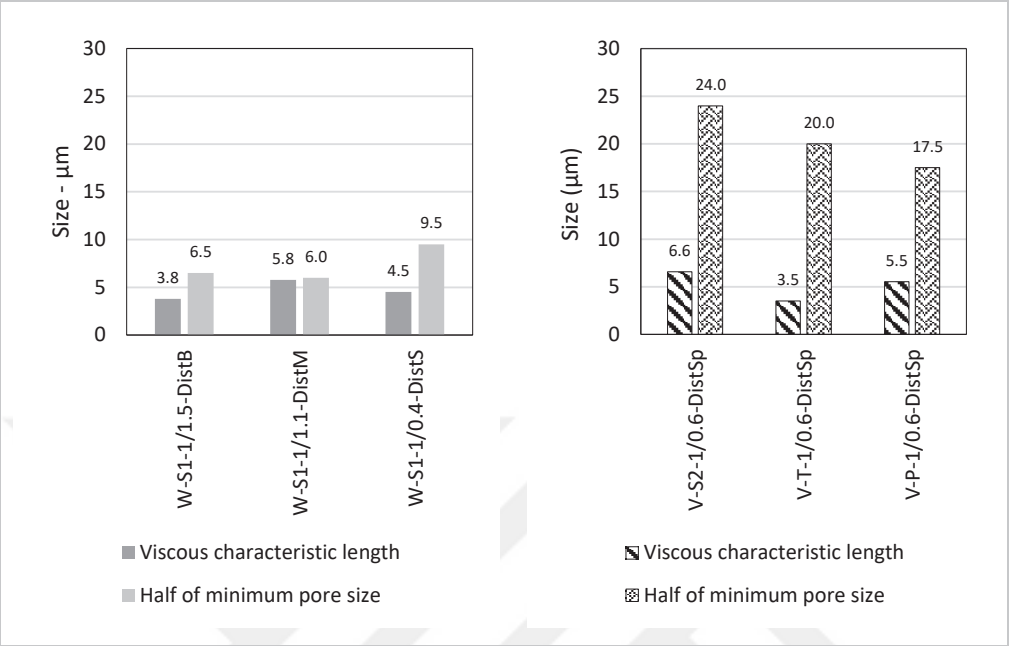


Figure 5.22. The relation between viscous characteristic length and pore size for the first (left) and the second (right) sample set.

The predicted viscous characteristic length is almost 50% lower than half of the minimum pore size for the first group of samples in which larger (2-1mm) or smaller aggregates(0.5-0.25mm) dominate. The viscous interaction zone of the sample having medium size (1-0.5mm) aggregates in higher amounts almost covers the entire pore width in the minimum-sized pores observed from cross sections. For the samples of the second set prepared with lightweight aggregates, the predicted viscous characteristic length is much lower than half of the minimum pore size. Although minimum pore sizes observed through cross sections are more than the ones observed for the first plaster set, the viscous characteristic length values in the second set of plasters align with the predicted values of the first plaster set.

Figure 5.23 shows the thermal characteristic length and half of the maximum pore sizes. For the first plaster set, the difference between thermal characteristic length and half of the maximum pore size is the highest in the plaster sample with larger size (2-1mm) aggregates dominantly. In the second plaster set prepared with

different types of aggregates and fixed aggregate size distribution, the ones containing lightweight aggregates have almost 50% lower thermal characteristic length than half of the maximum pore size. However, for the sample in this group containing silica aggregates, the predicted thermal characteristic length is nearly half the maximum pore size.

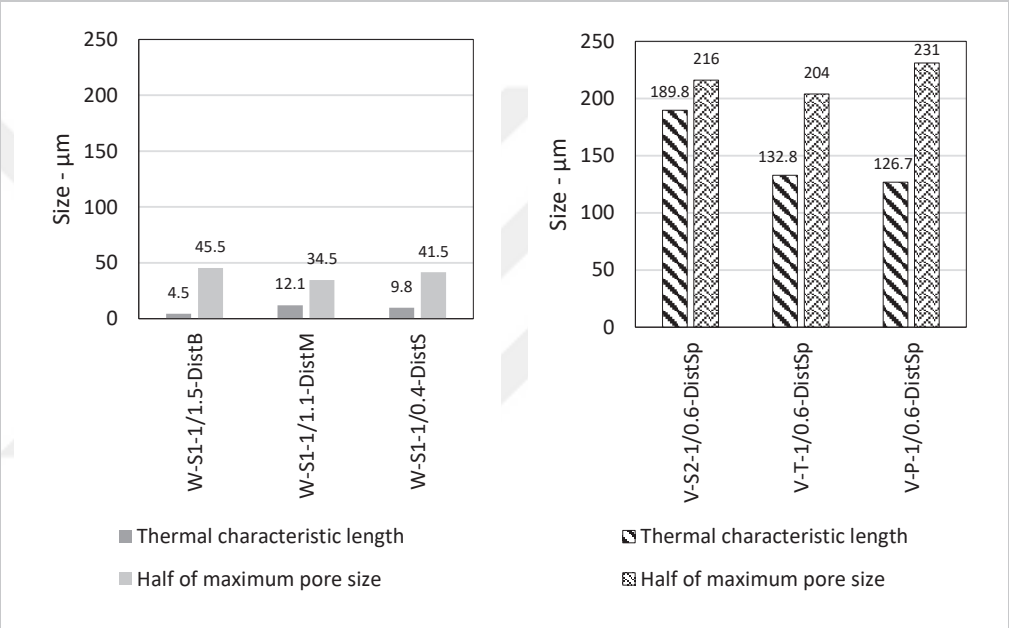


Figure 5.23. The relation between characteristic length and pore size for the second sample set.

It is determined that investigating the relationship between airflow resistivity and other pore structural parameters is not reasonable since the airflow resistivity values predicted by optimization are unevenly distributed across a broader range.

5.3 Performance properties in relation to pore structure and compositional properties

The performance properties are also affected by these plasters' unique pore structure. Before discussing the sound absorption performance; water vapor permeability and

elastic modulus performance concerning measured ultrasonic pulse velocity are analyzed.

5.3.1 Discussion on water vapor permeability and pore structure of plasters

Water vapor permeability information is discussed in terms of open porosity, fine porosity, fine to total porosity, and some of the selected pore structure parameters estimated through inverse characterization, which are effective porosity and airflow resistivity.

The water vapor resistance factor with respect to open porosity is given in Figure 5.24. For the first plaster set, the water vapor resistance factor slightly increases with the increase in total open porosity, which is contrary to what has been reported in other studies (Giosuè et al., 2019). In the second plaster set, the water vapor resistance factor decreases with the increase in total open porosity (see Figure 5.24, right side). However, the changes observed are minimal, so it is unreliable to make inferences.

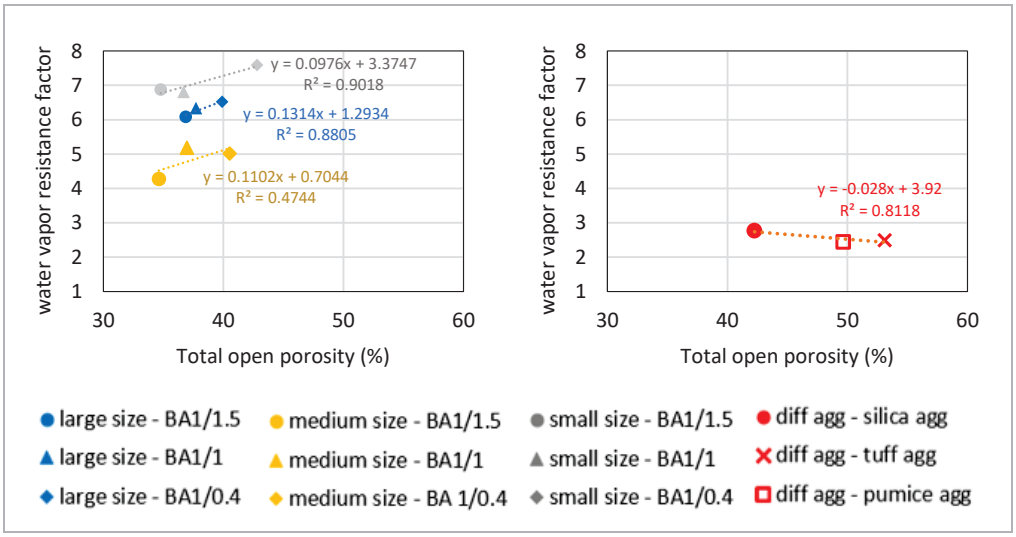


Figure 5.24. The relation between water vapor resistance factor and open porosity

The relation between the water vapor resistance factor and fine porosity is shown in Figure 5.25. Fine porosity variation does not distinctly affect the water vapor resistance factor in the second sample set, where different aggregates are used. For the first sample group, the change in the water vapor resistance factor is minimal with the increase of fine porosity. The relation between the water vapor resistance factor and fine porosity is inverse for the samples in which medium-size (1-0.5mm) aggregates dominate.

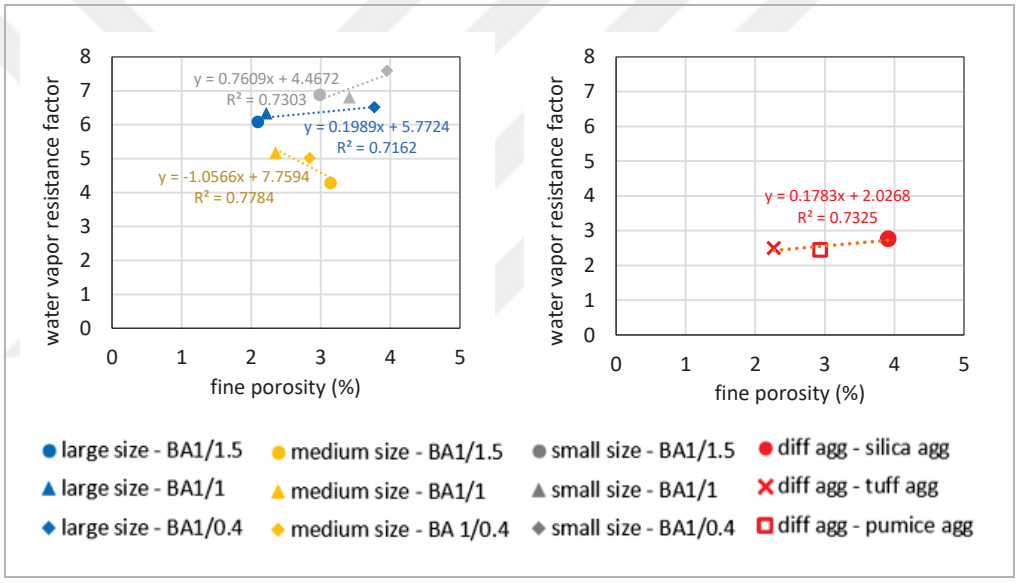


Figure 5.25. The relation between water vapor resistance factor and fine porosity

The water vapor resistance factor with respect to effective porosity values determined through inverse characterization is shown in Figure 5.26.

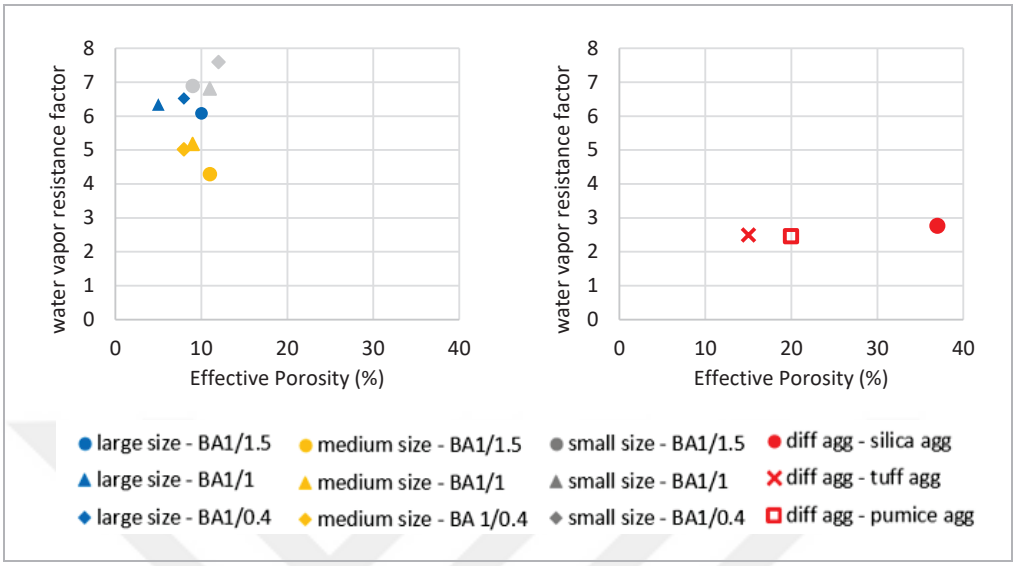


Figure 5.26. The relation between water vapor resistance factor and effective porosity

For the second set of plasters, using different aggregate types does not affect the water vapor resistance factor values. Furthermore, the effective porosity values found in the first sample set are so similar that it is impossible to establish a meaningful relationship between tortuosity and effective porosity.

The water vapor resistance factor and airflow resistivity estimated through the inverse method are shown in Figure 5.27. There is an inverse relationship between the water vapor resistance factor and airflow resistivity; changes in airflow resistivity only cause slight adjustments in the water vapor resistance factor. The water vapor resistance factor in the second set of plasters remains relatively unaffected by the change in airflow resistivity.

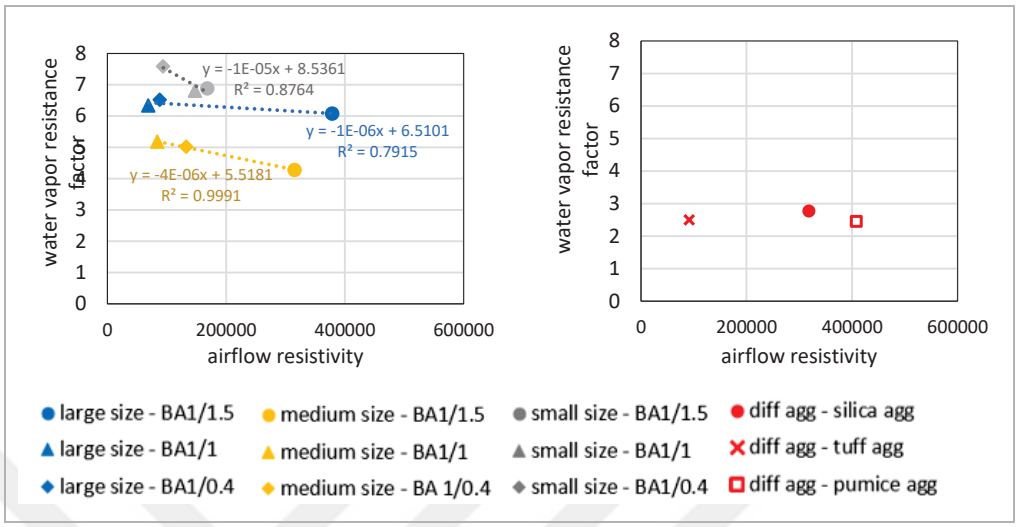


Figure 5.27. Water vapor resistance factor and air flow resistivity

Figure 5.28 displays the tortuosity values and water vapor resistance factor. Given the various BA ratios and aggregate size distributions in the first sample set, it is impossible to correlate the water vapor resistance factor with tortuosity. Since employing different types of aggregates has no influence on the water vapor resistance factor either, there is no link found between tortuosity and water vapor resistance factor for the second batch of plasters.

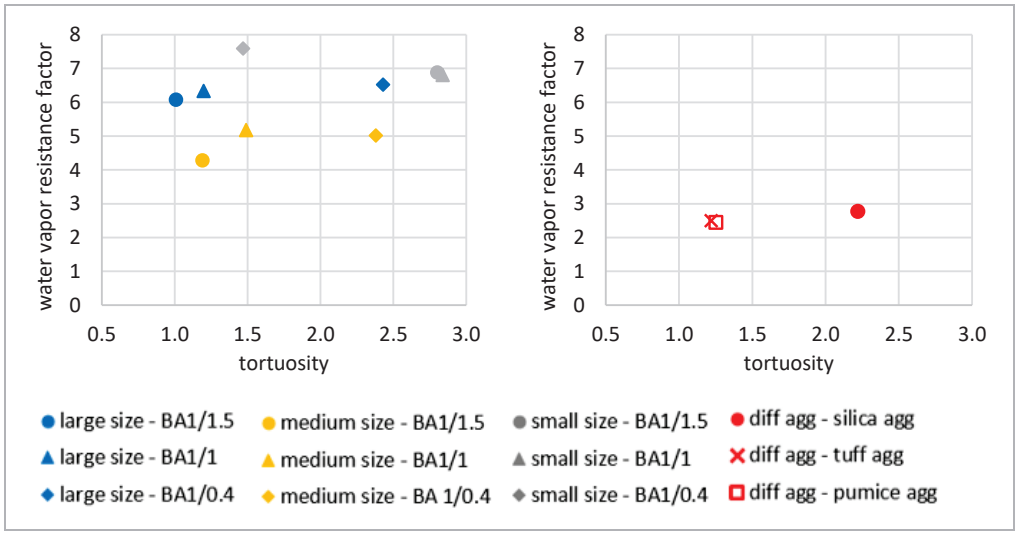


Figure 5.28. The relation between water vapor resistance factor and tortuosity

5.3.2 Discussion on dynamic modulus of elasticity and pore structure of plasters

The dynamic modulus of elasticity is estimated by ultrasonic pulse velocity and density of samples. Ultrasonic pulse velocity (UPV) is a measure that describes the velocity of sound that propagates in the solid part of a porous material. The required time for an ultrasonic wave cross from one probe to another is affected by the heterogeneity and density of the solid matrix. Also, the pores on the propagation path result in an attenuation and/or scattering of the sound signal, decreasing the UPV values. Before discussing the dynamic modulus of elasticity, some parameters related to pore structure, such as open porosity, density, and fine porosity, are examined in relation to UPV values measured for the samples.

The ultrasonic pulse velocity with respect to open porosity is shown in Figure 5.29. The data is dispersed for the first plaster set. No relationship appears to exist between open porosity and ultrasonic pulse velocity, especially for the samples containing large-size or medium-size aggregates dominantly. On the other hand, for the samples prepared heavily by smaller-sized aggregates (0.5-0.25mm), the ultrasonic pulse velocity increases as total open porosity increases. This is somewhat controversial to what is reported in the literature as the studies commonly found an inverse relation between ultrasonic pulse velocity and porosity (Goueygou et al., 2009; Panzera et al., 2011). However, it should be noted that in most studies, the binder-to-aggregate ratio is kept constant. In this case, although the porosity increases by 8% with the rise of binder content, the decrease of aggregates within the matrix must result in a more homogenous unobstructed path for the ultrasound to travel faster in the solid part. In the second plaster set, ultrasonic pulse velocity values of samples prepared with lightweight 1-4mm size aggregates are lower than the UPV of the sample prepared with silica aggregates. Considering the velocities and open porosity, the relation is inversely proportional for the second set of plasters.

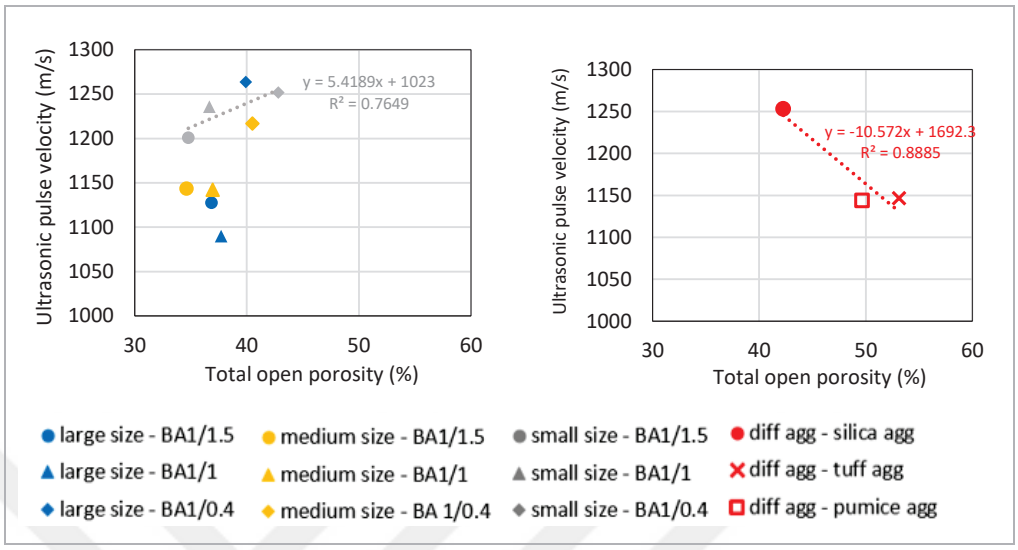


Figure 5.29. Ultrasonic pulse velocity with respect to open porosity

Ultrasonic pulse velocities of samples are also assessed with density values. In Figure 5.30, in the first sample set, there exists an inverse relation between UPV and density, which is not expected since the denser the structure, the UPV should be higher.

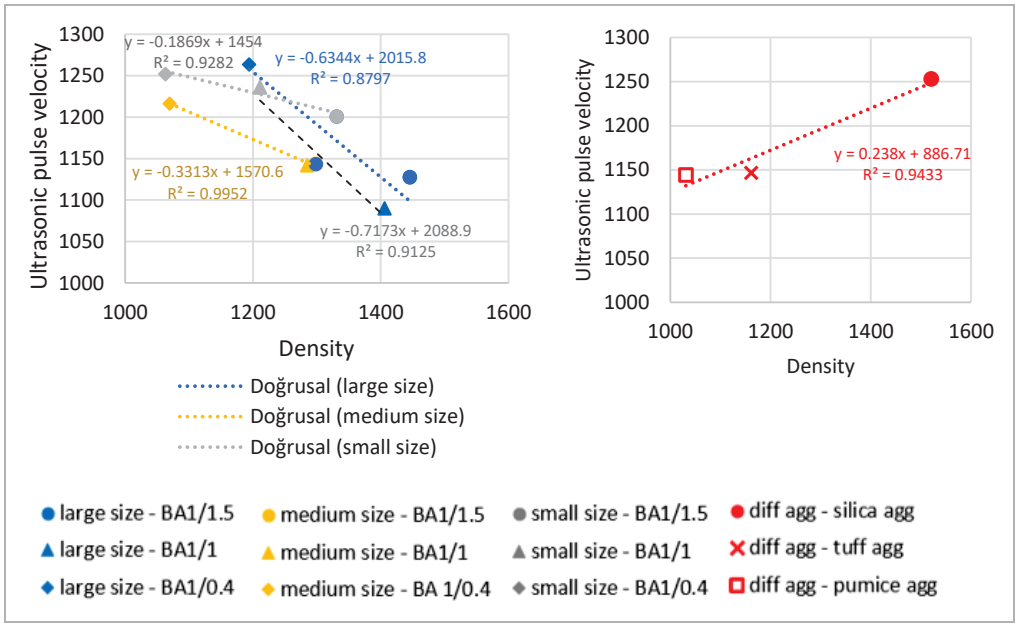


Figure 5.30. Ultrasonic pulse velocity with respect to density

On the other hand, the density of the samples increases with the use of larger size aggregates in higher weight amounts. In this context, the decrease of ultrasonic pulse velocity can be found acceptable since the mass distribution throughout the section becomes diversified, and bigger aggregates create an impedance on the propagation path, possibly slowing down the wave transfer. For the second plaster set, the ultrasonic pulse velocity increases as density increases. This conclusion is also reasonable and expected as the binder-to-aggregate ratio and aggregate size distributions of the second plaster set are the same for all the members of the group.

The relation of UPV to fine porosity is shown in Figure 5.31. Considering all the data sets, there is an overall increase in UPV values with the increase of fine porosity. For the same BA ratio of 1/1.5 and 1/1, when the dominant aggregate size decreases, the ultrasonic pulse velocity of samples increases with increasing fine porosity.

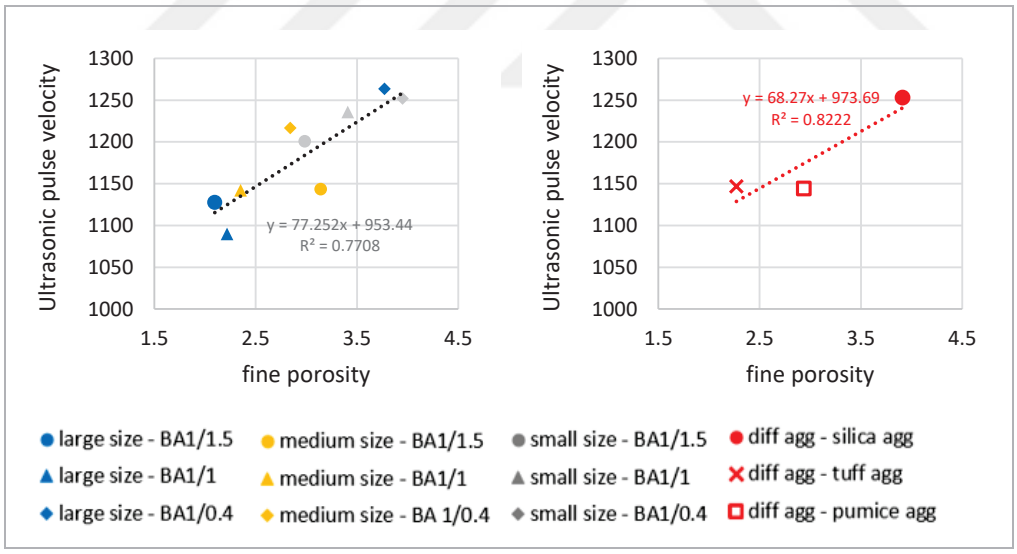


Figure 5.31. Ultrasonic pulse velocity with respect to fine porosity

The dynamic modulus of elasticity is proportional to the density and square of ultrasonic pulse velocity. Figure 5.32 shows the dynamic modulus of elasticity concerning open porosity in the samples.

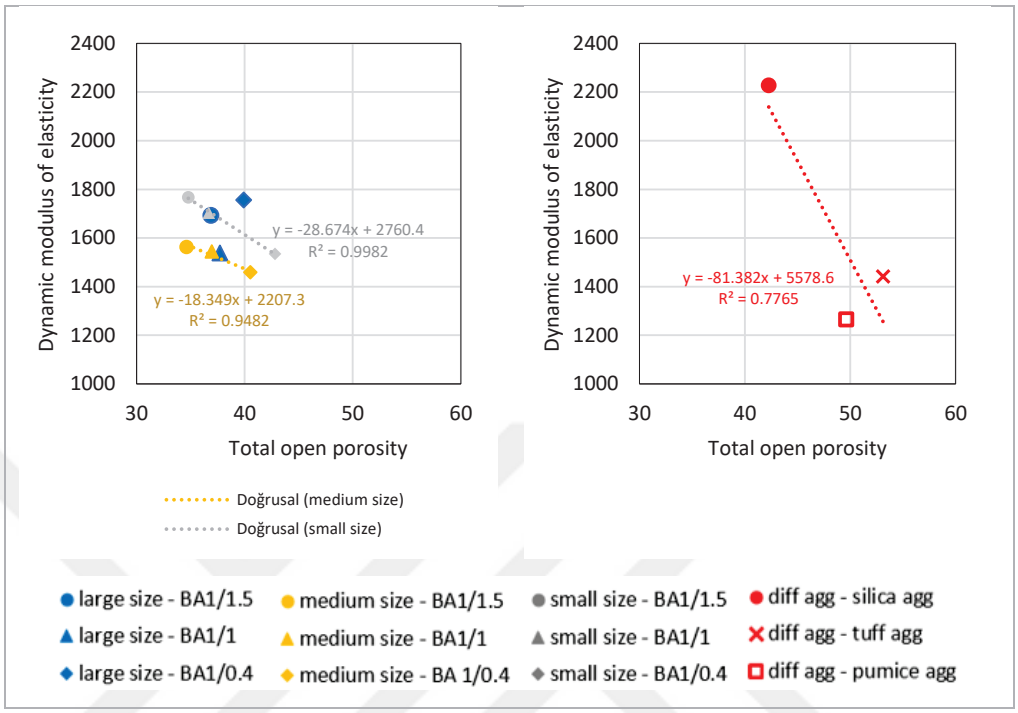


Figure 5.32. Dynamic modulus of elasticity with respect to open porosity

For the first plaster set, for the samples with medium size (0.5-1mm) and small size (0.25-0.5mm) silica aggregates in higher weight amounts, the dynamic modulus of elasticity decreases with the increase of open porosity and BA ratio. The samples containing medium-size aggregates in the dominant amount have a lower dynamic modulus of elasticity than those with small-size aggregates in higher weight amounts. This interrelation can not be observed for the sample of the first set with large-size silica aggregates in higher weight amounts. The plaster samples with lightweight aggregates have the lowest dynamic modulus of elasticity and highest open porosity. In the second set, the dynamic modulus of elasticity also decreases when porosity increases.

The dynamic modulus of elasticity of samples concerning measured fine porosity is given in Figure 5.33. The data is dispersed randomly. Fine porosity values change in a limited range, making it hard to interpret based on minor differences. No relation

is observed between fine porosity and dynamic modulus of elasticity for samples containing larger and medium size aggregates in dominant weight amounts.

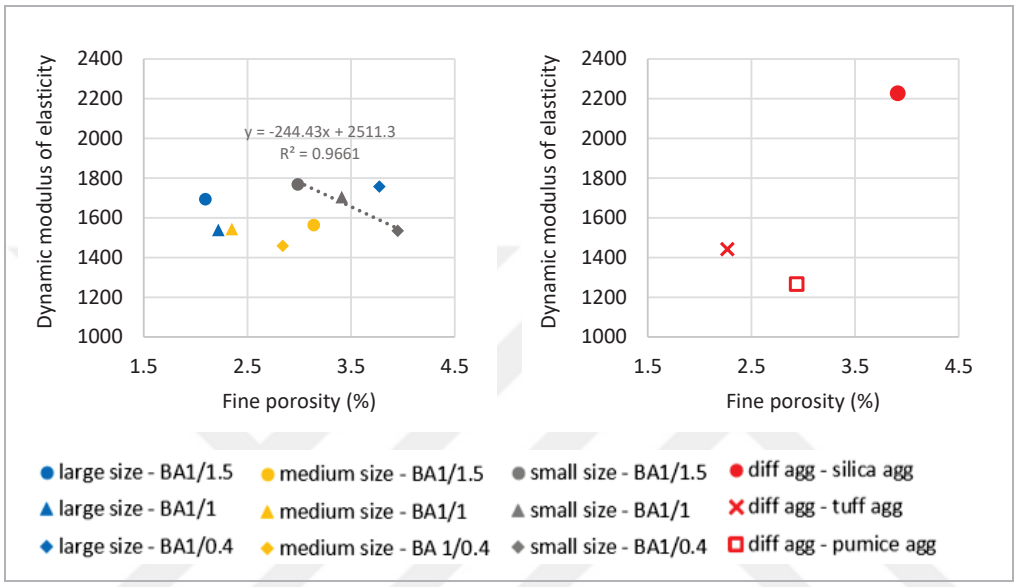


Figure 5.33. Dynamic modulus of elasticity with respect to fine porosity

On the other hand, the dynamic modulus of elasticity of the sample that contains small-size aggregates in higher amounts shows a descending trend as fine porosity increases with the increase of binder amount. It is hard to identify a meaningful relationship between fine porosity and dynamic modulus of elasticity for the second batch of plasters.

The predicted tortuosity is shown in relation to the dynamic modulus of elasticity in Figure 5.34. The relationship between dynamic modulus of elasticity and tortuosity is weak for the first plaster set except for the samples containing medium-size aggregates (1-0.5mm size) dominantly. In this sample group, as the BA ratio gets higher, the tortuosity increases, and the dynamic modulus of elasticity decreases. In the second plaster set, where different types and larger size aggregates (4-0.5mm) are used, the dynamic modulus of elasticity is found to be increased with the increase of tortuosity.

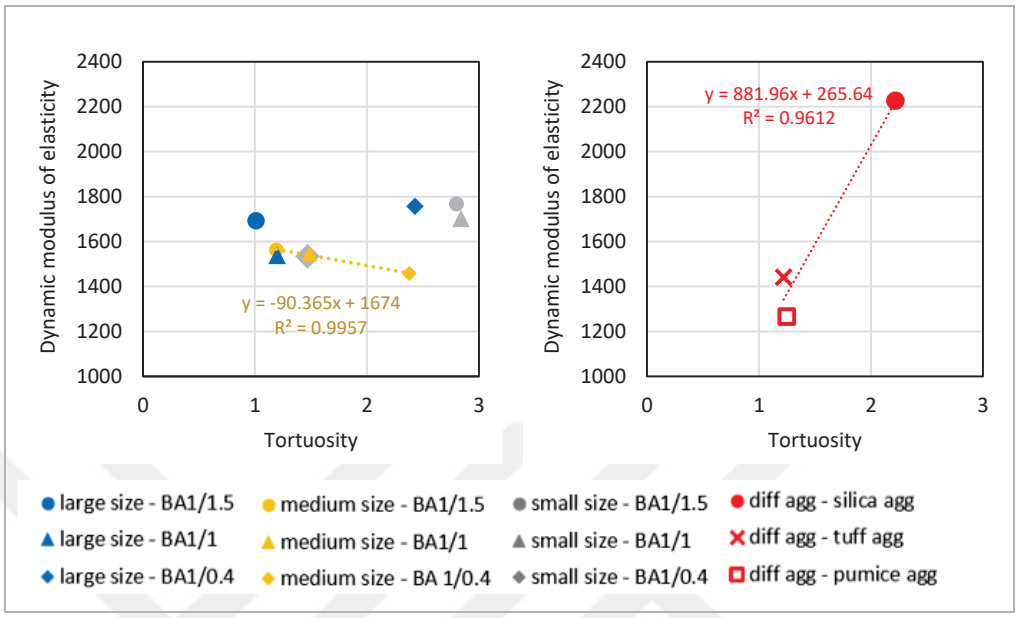


Figure 5.34. Dynamic modulus of elasticity with respect to tortuosity

5.3.3 Discussion of sound absorption performance and pore structure of plasters

The sound absorption of plaster samples is analyzed by considering the compositional ratios and the different aggregate types used in compositions. The measured sound absorption data from 1/3 octave bands is not normally distributed. Based on this fact, a statistical test method named the "Kruskal Wallis Test" is utilized to reveal the significant differences between the sound absorption performance of the first group of samples at any specific 1/3 octave band frequency. As the measured data originates from two different impedance tube setups, the large tube for the frequencies range between 63Hz to 1600Hz, and the small tube for the frequencies range between 1000Hz to 5000Hz, the Kruskal Wallis test is performed on the measured sound absorption coefficients in this two tube separately. The null hypothesis states that "there is no significant difference between the sample groups". If the calculated significance level based on H values is below the significance level (0.05), the null hypothesis is rejected, indicating a significant difference between

groups. A post hoc test (Dunn's test) is also conducted to compare different sample groups pairwise. In this test, the significance results are adjusted with Bonferroni correction to overcome the risk of false positive results. The results of these tests are given in the Appendix.

The adjusted results of the pairwise comparison show a significant difference between the sample group having smaller aggregates under 0.5mm in larger amounts and the sample group having a larger size, 2-1mm, aggregates in higher amounts at 100Hz and 125Hz. The unadjusted significance levels also indicate a difference between the samples having aggregates of size 2-0.5mm in a dominant amount in its content and those with aggregates smaller than 0.5mm in higher content. This difference is assumed to be associated with the use of aggregates under 0.5mm in lesser amounts because the common ground for the groups (Dist group B and M) that differentiate significantly from the group with smaller size aggregates in higher weight amounts (Dist S) is that they both have the same amount aggregates under 0.5mm which is 40%. This amount for aggregates under 0.5mm is 65% for the aggregate distribution group based heavily on small-size aggregates (Dist S). The significance of pairwise comparisons at 100Hz and 125Hz is given in Tables 5.1 and 5.2.

Table 5.1 Pairwise comparison of material samples based on sound absorption data at 100Hz, (a) unadjusted significance results (b) adjusted significance results

(a)

	W-S1-1/1.5-DistB	W-S1-1/1.5-DistB	W-S1-1/1.5-DistB	W-S1-1/1.5-DistB	W-S1-1/1.5-DistB	W-S1-1/1.5-DistB	W-S1-1/1.5-DistB	W-S1-1/1.5-DistB	W-S1-1/1.5-DistB
W-S1-1/1.5-DistB		notsig	notsig	notsig	notsig	notsig	sig	sig	sig
W-S1-1/1.5-DistB			sig	notsig	sig	notsig	sig	sig	sig
W-S1-1/1.5-DistB				notsig	notsig	notsig	sig	sig	sig
W-S1-1/1.5-DistB					notsig	notsig	sig	sig	sig
W-S1-1/1.5-DistB						notsig	notsig	notsig	notsig
W-S1-1/1.5-DistB							sig	sig	sig
W-S1-1/1.5-DistB								notsig	notsig
W-S1-1/1.5-DistB									notsig
W-S1-1/1.5-DistB									

(b)

	W-S1-1/1.5-DistB	W-S1-1/1.5-DistB	W-S1-1/1.5-DistB	W-S1-1/1.5-DistB	W-S1-1/1.5-DistB	W-S1-1/1.5-DistB	W-S1-1/1.5-DistB	W-S1-1/1.5-DistB	W-S1-1/1.5-DistB
W-S1-1/1.5-DistB		notsig	notsig	notsig	notsig	notsig	sig	sig	sig
W-S1-1/1.5-DistB			notsig	notsig	notsig	notsig	sig	sig	sig
W-S1-1/1.5-DistB				notsig	notsig	notsig	sig	sig	sig
W-S1-1/1.5-DistB					notsig	notsig	sig	sig	sig
W-S1-1/1.5-DistB						notsig	notsig	notsig	notsig
W-S1-1/1.5-DistB							notsig	notsig	notsig
W-S1-1/1.5-DistB								notsig	notsig
W-S1-1/1.5-DistB									notsig
W-S1-1/1.5-DistB									

Table 5.2 Pairwise comparison of material samples based on sound absorption data at 125Hz, (a) unadjusted significance results (b) adjusted significance results

(a)

	W-S1-1/1.5-DistB	W-S1-1/1.5-DistB	W-S1-1/1.5-DistB	W-S1-1/1.5-DistB	W-S1-1/1.5-DistB	W-S1-1/1.5-DistB	W-S1-1/1.5-DistB	W-S1-1/1.5-DistB	W-S1-1/1.5-DistB
W-S1-1/1.5-DistB		notsig	notsig	notsig	notsig	notsig	sig	sig	sig
W-S1-1/1-DistB			notsig	notsig	notsig	notsig	sig	sig	sig
W-S1-1/0.4-DistB				notsig	notsig	notsig	sig	sig	sig
W-S1-1/1.5-DistM					notsig	notsig	sig	sig	sig
W-S1-1/1-DistM						notsig	sig	sig	sig
W-S1-1/0.4-DistM							sig	sig	sig
W-S1-1/1.5-DistS								notsig	notsig
W-S1-1/1-DistS									notsig
W-S1-1/0.4-DistS									

(b)

	W-S1-1/1.5-DistB	W-S1-1/1.5-DistB	W-S1-1/1.5-DistB	W-S1-1/1.5-DistB	W-S1-1/1.5-DistB	W-S1-1/1.5-DistB	W-S1-1/1.5-DistB	W-S1-1/1.5-DistB	W-S1-1/1.5-DistB
W-S1-1/1.5-DistB		notsig	notsig	notsig	notsig	notsig	sig	sig	sig
W-S1-1/1-DistB			notsig	notsig	notsig	notsig	sig	sig	sig
W-S1-1/0.4-DistB				notsig	notsig	notsig	sig	sig	sig
W-S1-1/1.5-DistM					notsig	notsig	notsig	notsig	notsig
W-S1-1/1-DistM						notsig	notsig	notsig	notsig
W-S1-1/0.4-DistM							sig	sig	sig
W-S1-1/1.5-DistS								notsig	notsig
W-S1-1/1-DistS									notsig
W-S1-1/0.4-DistS									

The pore structure parameters that may play a role in the significant sound absorption coefficient differences at 100 Hz and 125 Hz for the first set of plasters' sounds are investigated. The mean values of different pore parameters and standard deviations that belong to different aggregate size distribution groups are shown in Figure 5.35. The most remarkable difference between the distribution group B and the distribution group S is observed for the average thermal characteristic length values.

Average fine porosity (%), average fine to total porosity (%), average tortuosity, average airflow resistivity, and average viscous characteristic length of the distribution group S are also different from the distribution group B. However, the average porosity and density values of distribution group S are close to the values of the other distribution groupss.

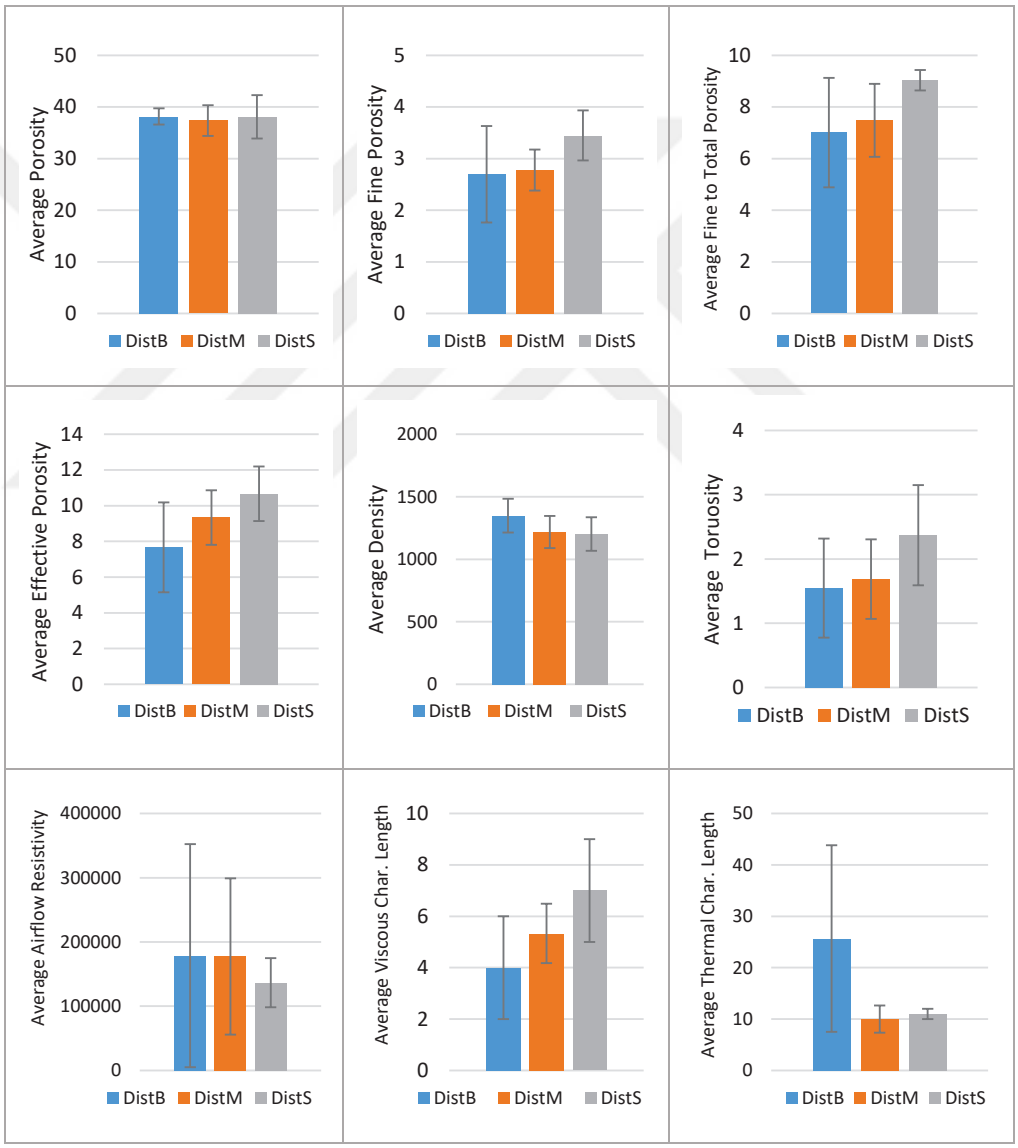


Figure 5.35. Average values of parameters related to pore structure for the first plaster set grouped aggregate size distribution

Similarly, the average values of pore structure parameters based on binder-to-aggregate ratios are also generated to understand the possible differences between groups.

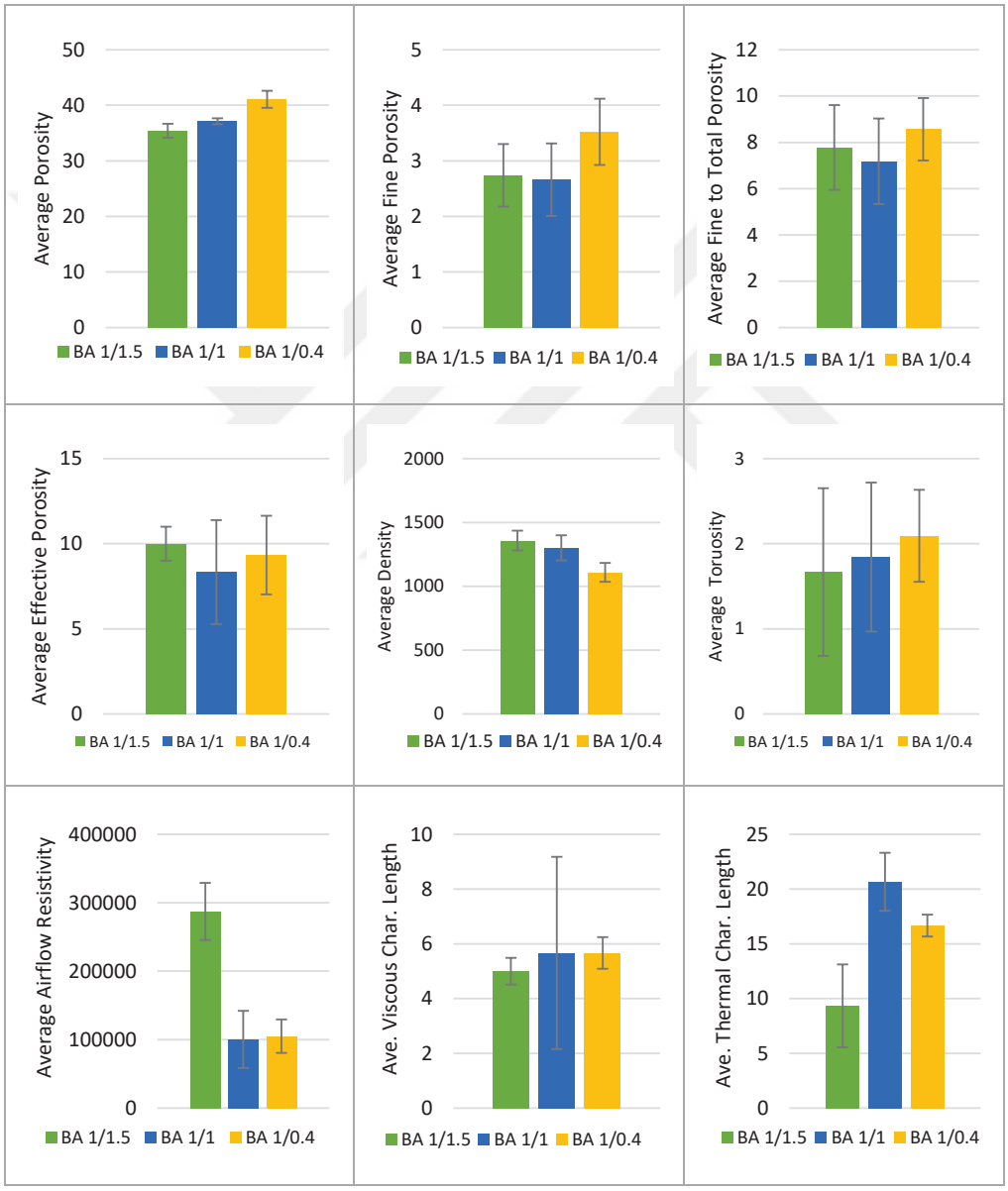


Figure 5.36. Average values of parameters related to pore structure for the first plaster set grouped according to binder to aggregate ratio

The most remarkable differences between groups with varying BA ratios are detected for average airflow resistivity and average thermal characteristic length. While the average airflow resistivity of group BA 1/1.5 is the highest of all groups, the group's average thermal characteristic length is the lowest within the groups. The average fine porosity of samples with a BA ratio of 1/0.4 also distinguishes it from the other groups. These differences based on the BA ratio, on the other hand, do not affect the sound absorption performance of groups significantly.

The Kruskall Wallis test and post hoc "Dunn's test" are also conducted for the second plaster set where different aggregates are used. In this second set, the aggregate size distribution and binder-to-aggregate ratio are set by volumetric quantities and kept the same throughout all samples produced utilizing different aggregate types. The results of the test are given in the Appendix. A brief representation of the pairwise comparisons is shown in Table 5.3. Pairwise comparisons at 80Hz, 160Hz, 200Hz, and 250Hz can not be conducted because the results of the Kruskall-Wallis test do not show any significant variance between sample groups. According to the test, the sound absorption performances of the sample groups do not differ depending on whether the aggregate type used is light or heavy.

It should be noted that except at 2000Hz frequency, the difference between the sound absorption of samples with tuff and pumice is always significant depending on the data from the low and high impedance tube (see Table 5.3, adjusted significance). Until the overlapping frequency range (between 1000Hz and 1600Hz) of two impedance tubes, the sound absorption difference is significant between the samples prepared with silica aggregates and those prepared with tuff aggregates. When we consider the pore structure parameters previously compared in Section 5.1, fine porosity, pore size distribution, and airflow resistivity are the main parameters that show noteworthy differences between the plaster samples with tuff aggregate and the other two with silica or pumice aggregates. Another comparison based on commonly used single number rating systems, SAA and NRC, given in Table 5.4, reveals the differences between the samples with tuff aggregate and the other

samples with silica or pumice aggregates. The sound absorption performance of plasters with tuff aggregate is the lowest.

Table 5.3 Pairwise comparison of second set based on sound absorption data

		Significance result			Adjusted significance result		
	Hz	S-P	S-T	P-T	S-P	S-T	P-T
Low frequency impedance tube range	63	notsig	notsig	sig	notsig	notsig	sig
	80	-	-	-	-	-	-
	100	notsig	notsig	sig	notsig	notsig	sig
	125	notsig	notsig	sig	notsig	notsig	sig
	160	-	-	-	-	-	-
	200	-	-	-	-	-	-
	250	-	-	-	-	-	-
	315	notsig	sig	sig	notsig	sig	sig
	400	notsig	sig	sig	notsig	sig	sig
	500	notsig	sig	sig	notsig	sig	sig
	630	notsig	sig	sig	notsig	sig	sig
	800	notsig	sig	sig	notsig	sig	sig
	1000	notsig	sig	sig	notsig	sig	sig
	1250	notsig	sig	sig	notsig	sig	sig
	1600	notsig	sig	sig	notsig	sig	sig
High frequency impedance tube range	1000	sig	notsig	sig	sig	notsig	sig
	1250	sig	notsig	sig	sig	notsig	sig
	1600	sig	notsig	sig	sig	notsig	sig
	2000	sig	notsig	sig	sig	notsig	notsig
	2500	sig	notsig	sig	notsig	notsig	sig
	3150	sig	notsig	sig	notsig	notsig	sig
	4000	sig	notsig	sig	notsig	notsig	sig
	5000	sig	notsig	sig	notsig	notsig	sig

Table 5.4 SAA and NRC comparison of second set of plasters

Sample Code	SAA (average of 200Hz-2500Hz)	NRC (average of 250Hz, 500Hz, 1kHz and 2kHz)
V-S2-1/0.6-DistSp	0.191	0.194
V-T-1/0.6-DistSp	0.133	0.131
V-P-1/0.6-DistSp	0.177	0.179

CHAPTER 6

CONCLUSION

Knowledge displays evidence that the pore structure of materials plays a crucial role in their acoustical performance. The materials that become the subject of many studies in this context are mostly the ones that are highly sound absorptive such as fibrous materials or cellular materials. Loose or consolidated granular materials are also investigated as their potential to control excessive noise in outdoor spaces as noise barriers is a popular topic of interest. On the other hand, plasters used do not attract much interest due to their less absorptive nature although they are used as a common finish material in construction. The studies on plasters that have been done so far only investigate the effect of compositional properties on sound absorption but do not attempt to analyze the pore structure associated with the sound absorption performance in depth. Moreover not only sound absorption, but also performance properties related to the transport of water vapor or water are related to the porous matrix in the materials.

In this study, by utilizing the the sound absorption data as a starting point, the pore structure of lime-based plasters are analyzed through various measurements at laboratory conditions. In the design of experiment, the variables in the plaster compositions are binder to aggregate ratio, aggregate size distribution and aggregate type. Depending on these variables, compositionally 12 different sets of plasters were prepared. As a result of the study, the measured parameters related to pore structure and those anticipated by the optimization technique based on the Johnson Champoux Allard Sound Propagation Model provide precious insights about the porous network present in the lime plaster samples.

Contribution of study in terms of methodology:

The studies that have been conducted so far on plasters compare the sound absorption performance of compositions based on single number ratings such as sound absorption average (SAA), and noise reduction coefficient (NRC). Although these ratings are practical, such comparisons based on ratings only give a rough estimate of the material performance. In similar studies, granular materials such as mortars with larger aggregates (above 1mm size) are characterized through the curve that shows the sound absorption coefficients at the measured frequency range. The shift of the frequency where the maximum absorption occurs or the changes in the maximum absorption observed at specific frequencies are the main topics of discussion. In these experimental studies, the differences in sound absorption are not questioned in terms of significance based on scientific grounds. In this study, statistical methods are utilized to establish the distinct performance disparities between groups based on binder to aggregate ratio, aggregate size distribution or aggregate type, other than setting individual differences in the samples that may link to a combination of these compositional characteristics. Statistical methods also enable us to make comparisons depending on the data observed in a limited range.

It is speculated that not all open pores effectively contribute to sound absorption. Most of the theoretical sound propagation models are based on the volume of through pores, neglecting the volume of the ones with a dead end. Recent studies aim to account for the sound energy losses observed in these dead-end pores. In studies on the acoustic performance of plasters, the most frequently discussed parameter regarding the pore structure is open porosity. None of these studies, especially the ones on plasters, investigate porosity with a focus on pore typology. Interpreting the sound absorption performance by referring only to differences in open porosity may lead to inaccurate conclusions. In this study, besides the open porosity values measured by the water immersion method, additional parameters related to pore structure predicted through inverse characterization, such as effective porosity

(which resembles the volume of through pores), tortuosity, airflow resistivity, viscous and thermal characteristic length are employed in discussions. The arguments are also reinforced by the visual observations of cross-sectional images of samples.

This study is also a leading attempt to discuss the relation between the pore structure parameters estimated through a sound propagation model with performance properties other than sound absorption, such as water vapor permeability and dynamic elasticity modulus.

The most important results of this experimental study which enrich the knowledge on material characterization are summarized below:

The conclusions about the effect of compositional properties on the pore structure and sound absorption:

- Only at 100 Hz and 125 Hz there is a correlation between the sound absorption capacity and the aggregate size distributions. The sound absorption performance of samples with aggregates of size under 0.5mm in dominant quantity is significantly different from the performance of other groups.
- Using aggregates under 0.5mm in higher weight amount in compositions significantly affects thermal characteristic length if the compared group has larger aggregates of size 2-1mm with a considerable weight amount.
- The primary pore structure metrics strongly associated with the usage of smaller size aggregates under 0.5mm include average tortuosity, average airflow resistivity, average fine porosity (%), average fine to total porosity (%), and average viscous characteristic length.
- The binder to aggregate ratios defined in this study does not considerably change the sound absorption performance.

- The most remarkable differences between groups with varying BA ratios are found in average airflow resistivity and average thermal characteristic length.

The conclusions about the interrelations between pore structure parameters:

- The generally observed trend in all sample groups is that as the fine porosity value increases, the fine to total porosity value also increases.
- For the first group of plasters, where aggregates under 2mm in size are used with varying binder-to-aggregate ratios and aggregate size distributions, no correlation has been observed between the total open and effective porosity values. Effective porosity values are almost identical and found to be lower than the open porosity values. However, there is an inverse relationship between effective porosity and total open porosity in the samples of the second set prepared with different types of aggregates of sizes between 1-4mm.
- It has been found that tortuosity increases with an increase in viscous characteristic length.
- The viscous characteristic length and thermal characteristic length of the first set of plasters are in a similar range. Thermal interaction zone in the first set of plasters is narrower when it is compared to the one found in the second set of plasters. This difference can be attributed to the different aggregate size utilized in these groups. In the second group where 4-1mm size aggregates are used, thermal losses might contribute the absorption more than they do in the first group of plasters.

The conclusions about the relation of water vapor permeability and dynamic bulk modulus to pore structure and compositional properties:

- The water vapor resistance factor is found to be slightly affected by the total open porosity of the samples. Somewhat less strong connections exist between the water vapor resistance factor and other characteristics such fine porosity, airflow resistivity, and tortuosity.

- Different aggregate size distributions seem to generate different water vapor resistance groups. Samples having aggregates of size below 0.5mm in higher amount fall into medium water vapor permeability class depending on their SD value.
- The comparison of UPV values with total open porosity and density shows that especially for the first plaster group in which aggregates smaller than 2mm are used, the findings are opposed to what has been reported in the literature. This result showed that if there is heterogeneity in the material, density and porosity may not be sufficient to describe the propagation of ultrasound within the material. Interfacial energy loss and diffraction of ultrasound due to impedance differences in between binder and aggregate zone could be speculated as the source of this outcome. Further studies should examine the binder interface, the aggregates and also their distribution among the solid part.
- The strongest relationship observed is between dynamic elastic modulus and total open porosity. The dynamic bulk modulus of samples decreases with increasing porosity in general.

Limitations of the study:

There is currently no standard method for measuring the pore structure characteristics related to sound propagation, such as tortuosity, viscous characteristic length, and thermal characteristic length. The measurement procedure necessitates in-depth expertise, and equipment is costly as well. The wavelength that measurements conducted is small compared to the pore sizes which enables/highlights the attenuation of ultrasound waves in the material. This limitations increases the risk of errors in measurements. Due to these facts, inverse estimation method is prefered to estimate these characteristics, as has been established in several prior studies in literature.

Recommendations for Future Research:

Further research on 3D modeling of pore structure based on the image of cross sections or by means of tomograhic imaging may give valuable insights about the formation of pores within the material and their contribution to the propagation of sound within the material.

This study is an organized experimental work that aims to define the complex pore structure within lime plasters using combined methods. Estimation of parameters related to pore structure by sound absorption performance has a high potential to be used as a nondestructive tool for the characterization of the porous network wherever in-situ sound absorption measurement techniques are available.

REFERENCES

Aggelakopoulou, E., Bakolas, A., & Moropoulou, A. (2011). Properties of lime–metakolin mortars for the restoration of historic masonries. *Applied Clay Science*, *53*(1), 15–19. https://doi.org/10.1016/j.clay.2011.04.005

Aggelakopoulou, E., Bakolas, A., & Moropoulou, A. (2019). Lime putty versus hydrated lime powder: Physicochemical and mechanical characteristics of lime based mortars. *Construction and Building Materials*, *225*, 633–641.

Akin, S., & Demiral, B. (1998). Genetic algorithm for estimating multiphase flow functions from unsteady-state displacement experiments. *Computers & Geosciences*, *24*(3), 251–258.

Allard, J. F., Castagnede, B., Henry, M., & Lauriks, W. (1994). Evaluation of tortuosity in acoustic porous materials saturated by air. *Review of Scientific Instruments*, *65*(3), 754–755. https://doi.org/10.1063/1.1145097

Allard, J. F., & Champoux, Y. (1992). New empirical equations for sound propagation in rigid frame fibrous materials. *The Journal of the Acoustical Society of America*, *91*(6), 3346–3353. https://doi.org/10.1121/1.402824

Almeida, L., Santos Silva, A., Veiga, R., & Mirão, J. (2023). 20th Century Mortars: Physical and Mechanical Properties from Awarded Buildings in Lisbon (Portugal)—Studies towards Their Conservation and Repair. *Buildings*, *13*(10), 2468. https://doi.org/10.3390/buildings13102468

Amziane, S., & Sonebi, M. (2016). Overview on biobased building material made with plant aggregate. *RILEM Technical Letters*, *1*, 31–38.

Apostolopoulou, M., Bakolas, A., & Kotsainas, M. (2021). Mechanical and physical performance of natural hydraulic lime mortars. *Construction and Building Materials*, *290*, 123272. https://doi.org/10.1016/j.conbuildmat.2021.123272

Arenas, J. P., & Crocker, M. J. (2010). Recent Trend in Porous Sound Absorbing Materials. *Sound & Vibrations*, *44*(7), 12–18.

Arizzi, A., & Cultrone, G. (2021). Mortars and plasters—How to characterise hydraulic mortars. *Archaeological and Anthropological Sciences*, *13*(9), 144. https://doi.org/10.1007/s12520-021-01404-2

ASTM International. (2013). *Standard test method for materials finer than 75-µm (ASTM C117-13)* (ASTM C117-13). ASTM International. https://doi.org/10.1520/C0117-13

ASTM International. (2014). *Standard specification for lightweight aggregates for structural concrete (ASTM C330/C330M-14)* (ASTM C330/C330M-14). ASTM International. https://doi.org/10.1520/C0330_C0330M

ASTM International. (2015). *Standard test method for relative density (specific gravity) and absorption of fine aggregate (ASTM C128-15)* (ASTM C128-15). ASTM International. https://doi.org/10.1520/C0128-15

ASTM International. (2020). *Standard test method for flow of hydraulic cement mortar (ASTM C1437-20)*. ASTM International.

ASTM International. (2022). *Test Methods for Gravimetric Determination of Water Vapor Transmission Rate of Materials (ASTM E96/E96M − 22)*. ASTM International. https://doi.org/10.1520/E0096_E0096M-22

ASTM International. (2023a). *Standard test method for bulk density and voids in aggregate (ASTM C29/C29M − 23)* (ASTM C29/C29M − 23). ASTM International.

ASTM International. (2023b). *Standard test method for sound absorption and sound absorption coefficients by the reverberation room method (ASTM C423-23)*.

Atalla, Y., & Panneton, R. (2005). Inverse acoustical characterization of open cell porous media using impedance tube measurements. *Canadian Acoustics*, *33*(1), 11–24.

Attenborough, K. (1983). Acoustical characteristics of rigid fibrous absorbents and granular materials. *The Journal of the Acoustical Society of America*, *73*(3), 785–799. https://doi.org/10.1121/1.389045

Aydin, A. (2008). *Acoustical characteristics of historical Turkish baths* [MSc]. Middle East Technical University.

Aydin, A., Tavukcuoglu, A., & Caliskan, M. (2008). *Assessment of acoustical characteristics for historical baths (hammams)*. *123*, 3605–3605. https://doi.org/10.1121/1.2934781

Bágel', L., & Živica, V. (1997). Relationship between pore structure and permeability of hardened cement mortars: On the choice of effective pore structure parameter. *Cement and Concrete Research*, *27*(8), 1225–1235. https://doi.org/10.1016/S0008-8846(97)00111-7

Balksten, K., & Steenari, B.-M. (2010). The Influence of Particle Size and Structure in Hydrated Lime on the Properties of the Lime Putty and Lime

Mortar. *International Journal of Architectural Heritage*, *4*(2), 86–101. https://doi.org/10.1080/15583050902822681

Bansod, P. V., & Mohanty, A. R. (2016). Inverse acoustical characterization of natural jute sound absorbing material by the particle swarm optimization method. *Applied Acoustics*, *112*, 41–52. https://doi.org/10.1016/j.apacoust.2016.05.011

Beranek, L. L. (1947). Acoustical properties of homogeneous, isotropic rigid tiles and flexible blankets. *The Journal of the Acoustical Society of America*, *19*(4), 556–568.

Biot, M. A. (1956a). Theory of propagation of elastic waves in a fluid-saturated porous solid. I. Low frequency range. *The Journal of the Acoustical Society of America*, *28*(2), 168–178. https://doi.org/10.1121/1.1908239

Biot, M. A. (1956b). Theory of propagation of elastic waves in a fluid-saturated porous solid. II. Higher frequency range. *The Journal of the Acoustical Society of America*, *28*(2), 179–191. https://doi.org/10.1121/1.1908241

Böke, H., Akkurt, S., İpekoğlu, B., & Uğurlu, E. (2006). Characteristics of brick used as aggregate in historic brick-lime mortars and plasters. *Cement and Concrete Research*, *36*(6), 1115–1122. https://doi.org/10.1016/j.cemconres.2006.03.011

Bonfiglio, P., & Pompoli, F. (2007). *Comparison of different inversion techniques for determining physical parameters of porous media*. 19th International Congress of Acoustics, Madrid.

Boynton, R. S. (1966). *Chemistry and Technology of Lime and Limestone*. John Wiley&Sons.

Bozkurt, T. S. (2023). Acoustic analyses of mortars prepared with recycled aggregates. *Applied Acoustics*, *205*, 109273. https://doi.org/10.1016/j.apacoust.2023.109273

Bozkurt, T. S., & Demirkale, S. Y. (2018). The laboratory analyses for the plasters prepared with river sand aggregate and hydraulic lime binder. *Construction and Building Materials*, *190*, 691–709. https://doi.org/10.1016/j.conbuildmat.2018.09.073

Bozkurt, T. S., & Demirkale, S. Y. (2019). Laboratory analyses and numerical simulation for sound absorption of plasters in historical buildings. *Journal of Cultural Heritage*, *36*, 103–117. https://doi.org/10.1016/j.culher.2018.09.012

Bozkurt, T. S., & Demirkale, S. Y. (2020a). Investigation and development of sound absorption of plasters prepared with pumice aggregate and natural hydraulic lime binder. *Applied Acoustics*, *170*, 1–18.

Bozkurt, T. S., & Demirkale, S. Y. (2020b). The experimental research of sound absorption in plasters produced with perlite aggregate and natural hydraulic lime binder. *Acoustics Australia*, *48*(3), 375–393. https://doi.org/10.1007/s40857-020-00203-4

British Standards Institute. (1999). *Paints and varnishes—Coating materials and coating systems for exterior masonry and concrete—Part 2: Determination*

and classification of water vapor transmission rate (BS EN ISO 7783-2:1999) (BS EN ISO 7783-2:1999). British Standards Institute.

British Standards Institute. (2004). *Paints and varnishes—Coating materials and coating systems for exterior masonry and concrete—Part 1: Classification (BS EN 1062-1:2004)* (BS EN 1062-1:2004). British Standards Institute.

British Standards Institute. (2016). *Hygrothermal performance of building materials and products. Determination of water vapour transmission properties. Cup method (ISO 12572:2016)*. British Standards Institute. https://doi.org/10.3403/30294357

Brown, R. J. (1980). Connection between formation factor for electrical resistivity and fluid-solid coupling factor in Biot's equations for acoustic waves in fluid-filled porous media. *Geophysics*, *45*(8), 1269–1275.

Caner, E. (2003). *Archaeometrical investigation of some seljuk plasters* [MSc]. Middle East Technical University.

Carbajo, J., Esquerdo-Lloret, T. V., Ramis, J., Nadal-Gisbert, A. V., & Denia, F. D. (2015). Acoustic properties of porous concrete made from arlite and vermiculite lightweight aggregates. *Materiales de Construcción*, *65*(320), e072. https://doi.org/10.3989/mc.2015.01115

Carbajo, J., Esquerdo-Lloret, T. V., Ramis, J., Nadal-Gisbert, A. V., & Denia, F. D. (2017). Acoustic modeling of perforated concrete using the dual porosity theory. *Applied Acoustics*, *115*, 150–157. https://doi.org/10.1016/j.apacoust.2016.09.005

Champoux, Y., & Stinson, M. R. (1992). On acoustical models for sound propagation in rigid frame porous materials and the influence of shape factors. *JASA*, *92*(2), 1120–1131.

Champoux, Y., Stinson, M. R., & Daigle, G. A. (1991). Air-based system for the measurement of porosity. *The Journal of the Acoustical Society of America*, *89*(2), 910–916. https://doi.org/10.1121/1.1894653

Chu, R. K. M., Naguib, H. E., & Atalla, N. (2009). Synthesis and characterization of open-cell foams for sound absorption with rotational molding method. *Polymer Engineering & Science*, *49*(9), 1744–1754. https://doi.org/10.1002/pen.21412

Çizer, Ö. (2004). *Investigation of lime mortar characteristics for the conservation of the Ottoman baths in seferihisar-urla region* [MSc]. İzmir Institute of Technology.

Cobo, P., & Simón, F. (2016). A comparison of impedance models for the inverse estimation of the non-acoustical parameters of granular absorbers. *Applied Acoustics*, *104*, 119–126. https://doi.org/10.1016/j.apacoust.2015.11.006

Cox, T. J., & D'Antonio, P. (2009). *Acoustic absorbers and diffusers: Theory, design and application* (2nd ed). Taylor & Francis.

Cultrone, G., Sebastián, E., & Huertas, M. O. (2005). Forced and natural carbonation of lime-based mortars with and without additives: Mineralogical and textural changes. *Cement and Concrete Research*, *35*(12), 2278–2289. https://doi.org/10.1016/j.cemconres.2004.12.012

Da Silva, M. T. Q. S., Perretto, F., Do Rocio Cardoso, M., & Mazer, W. (2023). Porosity: Some characterization techniques. *Materials Today: Proceedings*, S2214785323017832. https://doi.org/10.1016/j.matpr.2023.03.716

De Castro, E. (1979). Les méthodes de succion dans l'étude de l'altération des pierres. *Alteration et Protection Des Monuments En Pierre. Deterioration and Protection of Stone Monuments. Colloque International. International Symposium. Paris, 5-9 Juin 1978*, 26–26.

Degrave-Lemeurs, M., Glé, P., & Hellouin De Menibus, A. (2018). Acoustical properties of hemp concretes for buildings thermal insulation: Application to clay and lime binders. *Construction and Building Materials*, *160*, 462–474. https://doi.org/10.1016/j.conbuildmat.2017.11.064

Diaz, J., & Menéndez, B. (2020). Sustainable lime restoration mortars: Physical properties and durability assessment. *Monument Future - Decay and Conservation of Stone Proceedings of the 14th International Congress on the Deterioration and Conservation of Stone*. The 14th International Congress on the Deterioration and Conservation of Stone, Göttingen.

Doutres, O., Dauchez, N., Génevaux, J.-M., & Dazel, O. (2007). Validity of the limp model for porous materials: A criterion based on the Biot theory. *The Journal of the Acoustical Society of America*, *122*(4), 2038–2048. https://doi.org/10.1121/1.2769824

Dupont, T., Leclaire, P., Sicot, O., Gong, X. L., & Panneton, R. (2011). Acoustic properties of air-saturated porous materials containing dead-end porosity.

Journal of Applied Physics, *110*(9), 094903. https://doi.org/10.1063/1.3646556

Elsen, J. (2006). Microscopy of historic mortars—A review. *Cement and Concrete Research*, *36*(8), 1416–1424. https://doi.org/10.1016/j.cemconres.2005.12.006

Ergenç, D., Fort, R., Varas−Muriel, M. J., & Alvarez De Buergo, M. (2021). Mortars and plasters—How to characterize aerial mortars and plasters. *Archaeological and Anthropological Sciences*, *13*(11), 197. https://doi.org/10.1007/s12520-021-01398-x

Esen, S., Tunç, N., Telatar, S., Tavukcuoglu, A., Caner Saltık, E. N., & Demirci, Ş. (2004). *Manisa Çukur Hamam'ın onarımına yönelik malzeme çalışmaları*. 494–505.

Eve, S., Gomina, M., Jernot, J.-P., Ozouf, J.-C., & Orange, G. (2007). Microstructure characterization of polyamide fibre/latex-filled plaster composites. *Journal of the European Ceramic Society*, *27*(12), 3517–3525. https://doi.org/10.1016/j.jeurceramsoc.2005.04.026

Fahy, F. (2005). Sound Absorption and Sound Absorbers. In *Foundations of Engineerig Acoustics* (pp. 140–379). Elsevier Academic Press.

Fellah, Z. E. A., Berger, S., Lauriks, W., Depollier, C., Aristégui, C., & Chapelon, J.-Y. (2003). Measuring the porosity and the tortuosity of porous materials via reflected waves at oblique incidence. *The Journal of the Acoustical Society of America*, *113*(5), 2424–2433. https://doi.org/10.1121/1.1567275

Garofano, I., Robador, M. D., & Duran, A. (2014). Materials characteristics of roman and arabic mortars and stuccoes from the patio de banderas in the real Alcazar of Seville. *Archaeometry*, *56*(4), 541–561. https://doi.org/10.1111/arcm.12041

Giese, F., Eigenbrod, C., & Koch, D. (2011). A novel production method for porous sound-absorbing ceramic material for high-temperature applications: A novel production method for porous sound absorbing ceramic material. *International Journal of Applied Ceramic Technology*, *8*(3), 646–652. https://doi.org/10.1111/j.1744-7402.2009.02479.x

Giosuè, C., Mobili, A., Yu, Q. L., Brouwers, H. J. H., Ruello, M. L., & Tittarelli, F. (2019). Properties of multifunctional lightweight mortars containing zeolite and natural fibers. *Journal of Sustainable Cement-Based Materials*, *8*(4), 214–227. https://doi.org/10.1080/21650373.2019.1615012

Glé, P., Gourdon, E., & Arnaud, L. (2011). Acoustical properties of materials made of vegetable particles with several scales of porosity. *Applied Acoustics*, *72*(5), 249–259. https://doi.org/10.1016/j.apacoust.2010.11.003

Goueygou, M., Lafhaj, Z., & Soltani, F. (2009). Assessment of porosity of mortar using ultrasonic Rayleigh waves. *NDT & E International*, *42*(5), 353–360. https://doi.org/10.1016/j.ndteint.2009.01.002

Güney, B. A. (2012). *Development of pozzolanic lime mortars for the repair of historic masonry* [PhD]. Middle East Technical University.

Horoshenkov, K. V., Hughes, D. C., & Cwirzen, A. (2003). The sound speed and attenuation in loose and consolidated granular formulations of high alumina

cements. *Applied Acoustics*, *64*(2), 197–212. https://doi.org/10.1016/S0003-682X(02)00069-5

Horoshenkov, K. V., & Swift, M. J. (2001). The effect of consolidation on the acoustic properties of loose rubber granulates. *Applied Acoustics*.

International Standards Organization. (1991). *Acoustics—Materials for acoustical applications – determination of air flow resistance (ISO 9053:1991)* (ISO 9053:1991).

International Standards Organization. (1997). *Acoustics—Sound absorbers for use in buildings: Rating of sound absorption (ISO 11654:1997)* (ISO 11654:1997). International Standards Organization.

International Standards Organization. (1998). *Acoustics—Determination of sound absorption coefficient and impedance in impedance tubes—Part 2: Transfer-function method (ISO 10534-2:1998)* (ISO 10534-2:1998).

Johnson, D. L., Koplik, J., & Dashen, R. (1987). Theory of dynamic permeability and tortuosity in fluid-saturated porous media. *Journal of Fluid Mechanics*, *176*(1), 379. https://doi.org/10.1017/S0022112087000727

Kim, H., Hong, J., & Pyo, S. (2018). Acoustic characteristics of sound absorbable high performance concrete. *Applied Acoustics*, *138*, 171–178. https://doi.org/10.1016/j.apacoust.2018.04.002

Kim, H. K., & Lee, H. K. (2010a). Acoustic absorption modeling of porous concrete considering the gradation and shape of aggregates and void ratio. *Journal of Sound and Vibration*, *329*(7), 866–879. https://doi.org/10.1016/j.jsv.2009.10.013

Kim, H. K., & Lee, H. K. (2010b). Influence of cement flow and aggregate type on the mechanical and acoustic characteristics of porous concrete. *Applied Acoustics*, *71*(7), 607–615. https://doi.org/10.1016/j.apacoust.2010.02.001

Klisińska-Kopacz, A., Tišlova, R., Adamski, G., & Kozłowski, R. (2010). Pore structure of historic and repair Roman cement mortars to establish their compatibility. *Journal of Cultural Heritage*, *11*(4), 404–410. https://doi.org/10.1016/j.culher.2010.03.002

Knapen, E., Lanoye, R., Vermeir, G., Lauriks, W., & Gemert, D. (2003). Acoustic properties of sound absorbing, polymer-modified porous cement mortars. *The 6. International Conference on Material Science and Restoration*.

Knapen, E., Lanoye, R., Vermeir, G., Lauriks, W., & Gemert, D. (2004). *Sound absorption by polymer-modified porous cement mortars*. 191–200.

Kuczmarski, M. A., & Johnston, J. C. (2011). *Acoustic absorption in porous materials*.

Lafarge, D., Lemarinier, P., Allard, J. F., & Tarnow, V. (1997). Dynamic compressibility of air in porous structures at audible frequencies. *The Journal of the Acoustical Society of America*, *102*(4), 1995–2006. https://doi.org/10.1121/1.419690

Lafhaj, Z., Goueygou, M., Djerbi, A., & Kaczmarek, M. (2006). Correlation between porosity, permeability and ultrasonic parameters of mortar with variable water / cement ratio and water content. *Cement and Concrete Research*, *36*(4), 625–633. https://doi.org/10.1016/j.cemconres.2005.11.009

Lanas, J., Pérez Bernal, J. L., Bello, M. A., & Alvarez Galindo, J. I. (2004). Mechanical properties of natural hydraulic lime-based mortars. *Cement and Concrete Research*, *34*(12), 2191–2201. https://doi.org/10.1016/j.cemconres.2004.02.005

Lawrence, R. M., Mays, T. J., Rigby, S. P., Walker, P., & D'Ayala, D. (2007). Effects of carbonation on the pore structure of non-hydraulic lime mortars. *Cement and Concrete Research*, *37*(7), 1059–1069.

Leclaire, P., Swift, M. J., & Horoshenkov, K. V. (1998). Determining the specific area of porous acoustic materials from water extraction data. *Journal of Applied Physics*, *84*(12), 6886–6890. https://doi.org/10.1063/1.368985

Leclaire, P., Umnova, O., Dupont, T., & Panneton, R. (2015). Acoustical properties of air-saturated porous material with periodically distributed dead-end pores. *The Journal of the Acoustical Society of America*, *137*(4), 1772–1782. https://doi.org/10.1121/1.4916712

Leclaire, P., Umnova, O., Horoshenkov, K. V., & Maillet, L. (2003). Porosity measurement by comparison of air volumes. *Review of Scientific Instruments*, *74*(3), 1366–1370. https://doi.org/10.1063/1.1542666

Lee, I.-S., & Park, Y.-H. (2022). Non-acoustic parameter estimation for multilayer system with porous material by genetic algorithm. *International Journal of Naval Architecture and Ocean Engineering*, *14*, 100469. https://doi.org/10.1016/j.ijnaoe.2022.100469

Leiva, C., Vilches, L. F., Arenas, C., Delgado, S., & Fernández-Pereira, C. (2012). Potential recycling of bottom and fly ashes in acoustic mortars and concretes. *ACI Materials Journal*, *109*(5), 529.

Long, M. (2006). *Architectural Acoustics*. Elsevier Academic Press.

Losa, M., & Leandri, P. (2012). A comprehensive model to predict acoustic absorption factor of porous mixes. *Materials and Structures*, *45*(6), 923–940. https://doi.org/10.1617/s11527-011-9808-8

Lu, T. J., Chen, F., & He, D. (2000). Sound absorption of cellular metals with semiopen cells. *The Journal of the Acoustical Society of America*, *108*(4), 1697–1709. https://doi.org/10.1121/1.1286812

Mahasaranon, S., Horoshenkov, K. V., Khan, A., & Benkreira, H. (2012). The effect of continuous pore stratification on the acoustic absorption in open cell foams. *Journal of Applied Physics*, *111*(8), 084901. https://doi.org/10.1063/1.3701710

Maravelaki-Kalaitzaki, P., Bakolas, A., Karatasios, I., & Kilikoglou, V. (2005). Hydraulic lime mortars for the restoration of historic masonry in Crete. *Cement and Concrete Research*, *35*(8), 1577–1586. https://doi.org/10.1016/j.cemconres.2004.09.001

Maria, S. (2010). Methods for porosity measurement in lime-based mortars. *Construction and Building Materials*, *24*(12), 2572–2578. https://doi.org/10.1016/j.conbuildmat.2010.05.019

Marolf, A., Neithalath, N., Sell, E., Wegner, K., Weiss, J., & Olek, J. (2004). Influence of aggregate size and gradation on acoustic absorption of enhanced porosity concrete. *ACI Materials Journal*, *202*(1), 82–91.

Mati-Baouche, N., De Baynast, H., Michaud, P., Dupont, T., & Leclaire, P. (2016). Sound absorption properties of a sunflower composite made from crushed stem particles and from chitosan bio-binder. *Applied Acoustics*, *111*, 179–187. https://doi.org/10.1016/j.apacoust.2016.04.021

Mosanenzadeh, S. G., Naguib, H. E., Park, C. B., & Atalla, N. (2013). Development, characterization, and modeling of environmentally friendly open-cell acoustic foams. *Polymer Engineering & Science*, *53*(9), 1979–1989. https://doi.org/10.1002/pen.23443

Mosquera, M. J., Silva, B., Prieto, B., & Ruiz-Herrera, E. (2006). Addition of cement to lime-based mortars: Effect on pore structure and vapor transport. *Cement and Concrete Research*, *36*(9), 1635–1642. https://doi.org/10.1016/j.cemconres.2004.10.041

Neithalath, N. (2004). *Development and characterization of acoustically efficient cementitious materials*. Purdue University.

Neithalath, N., Weiss, J., & Olek, J. (2004). Improving the acoustic absorption of enhanced porosity concrete with fiber reinforcement. *International RILEM Symposium on Concrete Science and Engineering: A Tribute to Arnon Bentur*.

Othmani, C., Taktak, M., Zain, A., Hantati, T., Dauchez, N., Elnady, T., Fakhfakh, T., & Haddar, M. (2017). Acoustic characterization of a porous absorber

based on recycled sugarcane wastes. *Applied Acoustics*, *120*, 90–97. https://doi.org/10.1016/j.apacoust.2017.01.010

Palomar, I., & Barluenga, G. (2017). Assessment of lime-cement mortar microstructure and properties by P- and S- ultrasonic waves. *Construction and Building Materials*, *139*, 334–341. https://doi.org/10.1016/j.conbuildmat.2017.02.083

Palomar, I., & Barluenga, G. (2018). A multiscale model for pervious lime-cement mortar with perlite and cellulose fibers. *Construction and Building Materials*, *160*, 136–144. https://doi.org/10.1016/j.conbuildmat.2017.11.032

Palomar, I., & Barluenga, G. (2022). Acoustic Assessment of Multiscale Porous Lime-Cement Mortars. *Materials*, *16*(1), 322. https://doi.org/10.3390/ma16010322

Palomar, I., Barluenga, G., & Puentes, J. (2015). *Assessment by non-destructive testing of new coating mortars for retrofitting the Architectural Heritage*. 357–366. https://doi.org/10.2495/STR150301

Panneton, R. (2007). Comments on the limp frame equivalent fluid model for porous media. *The Journal of the Acoustical Society of America*, *122*(6), EL217–EL222. https://doi.org/10.1121/1.2800895

Panzera, T. H., Christoforo, A. L., De Paiva Cota, F., Ribeiro Borges, P. H., & Bowen, C. R. (2011). Ultrasonic pulse velocity evaluation of cementitious materials. In P. Tesinova (Ed.), *Advances in Composite Materials—*

Analysis of Natural and Man-Made Materials. InTech. https://doi.org/10.5772/17167

Papayianni, I., & Stefanidou, M. (2006). Strength–porosity relationships in lime–pozzolan mortars. *Construction and Building Materials*, *20*(9), 700–705. https://doi.org/10.1016/j.conbuildmat.2005.02.012

Park, S. B., Seo, D. S., & Lee, J. (2005). Studies on the sound absorption characteristics of porous concrete based on the content of recycled aggregate and target void ratio. *Cement and Concrete Research*, *35*(9), 1846–1854. https://doi.org/10.1016/j.cemconres.2004.12.009

Pavlík, Z., Benešová, H., Matiašovský, P., & Pavlíková, M. (2012). *Study on carbonation process of several types of advanced lime-based plasters*. *6*(10).

Pereira, M., Carbajo, J., Godinho, L., Amado-Mendes, P., Mateus, D., & Ramis, J. (2019). Acoustic behavior of porous concrete. Characterization by experimental and inversion methods. *Materiales de Construcción*, *69*(336), 202. https://doi.org/10.3989/mc.2019.03619

Pompoli, F., Bonfiglio, P., Horoshenkov, K. V., Khan, A., Jaouen, L., Bécot, F.-X., Sgard, F., Asdrubali, F., D'Alessandro, F., Hübelt, J., Atalla, N., Amédin, C. K., Lauriks, W., & Boeckx, L. (2017). How reproducible is the acoustical characterization of porous media? *The Journal of the Acoustical Society of America*, *141*(2), 945–955. https://doi.org/10.1121/1.4976087

RILEM. (1980). Recommended tests to measure the deterioration of stone and assess the effectiveness of treatment methods. *Mater. Struct.*, *13*(75).

Rodriguez-Navarro, C. (2012). Binders in historical buildings: Traditional lime in conservation. *Semin. SEM*, *9*, 91–112.

Rodriguez-Navarro, C., Cazalla, O., Elert, K., & Sebastian, E. (2002). Liesegang pattern development in carbonating traditional lime mortars. *Proceedings of the Royal Society of London. Series A: Mathematical, Physical and Engineering Sciences*, *458*(2025), 2261–2273. https://doi.org/10.1098/rspa.2002.0975

Seddeq, H. S. (2009). Factors influencing acoustic performance of sound absorptive materials. *Australian Journal of Basic and Applied Sciences*, *3*(4), 4610–4617.

Stanley, D. R. (2012). Impedance tube specimen preparation and mounting issues. *INTER-NOISE and NOISE-CON Congress and Conference Proceedings*, *2012*(2), 9126–9132.

Stefanidou, M., & Papayianni, I. (2005). The role of aggregates on the structure and properties of lime mortars. *Cement and Concrete Composites*, *27*(9–10), 914–919. https://doi.org/10.1016/j.cemconcomp.2005.05.001

Stinson, M. R., & Champoux, Y. (1992). Propagation of sound and the assignment of shape factors in model porous materials having simple pore geometries. *The Journal of the Acoustical Society of America*, *91*(2), 685–695. https://doi.org/10.1121/1.402530

Sugrañez, R., Álvarez, J. I., Cruz-Yusta, M., Mármol, I., Morales, J., & Sánchez, L. (2013). Controlling microstructure in cement based mortars by adjusting the

particle size distribution of the raw materials. *Construction and Building Materials*, *41*, 139–145. https://doi.org/10.1016/j.conbuildmat.2012.11.090

Swift, M. J., Bris, P., & Horoshenkov, K. V. (1999). Acoustic absorption in recycled rubber granulate. *Applied Acoustics*, *57*(3), 203–212. https://doi.org/10.1016/S0003-682X(98)00061-9

Szűcs, H. (2023). Numerical study to investigate the viscous characteristic length on reconstructed porous media. *Alexandria Engineering Journal*, *66*, 269–286. https://doi.org/10.1016/j.aej.2022.11.022

Thomson, M., Lindqvist, J. E., Elsen, J., & Groot, C. W. (2007). 2. 5 Porosity of Mortars. In *Report 28: Characterisation of Old Mortars with Respect to their Repair-State-of-the-Art Report of RILEM Technical Committee 167-COM*.

Türk Standardları Enstitüsü. (2015). *Yapı kireci—Bölüm 1: Tarifler, özellikler ve uygunluk kriterleri (TS EN 459-1: 2010)* (TS EN 459-1: 2010). Türk Standardları Enstitüsü.

Uğurlu, E. (2005). *Characterization of horasan plasters from some ottoman baths in izmir* [MSc]. İzmir Institute of Technology.

Vasina, M., Hughes, D. C., Horoshenkov, K. V., & Lapcik, J. L. (2006). The acoustical properties of consolidated expanded clay granulates. *Applied Acoustics*, *67*(8), 787–796.

Zhang, Y., Li, H., Abdelhady, A., & Du, H. (2020). Laboratorial investigation on sound absorption property of porous concrete with different mixtures.

Construction and Building Materials, *259*, 120414.

https://doi.org/10.1016/j.conbuildmat.2020.120414

Zwikker, C., & Kosten, C. W. (1949). *Sound Absorbing Materials*. Elsevier.

APPENDICES

A. The results of statistical tests conducted on the first plaster set

Table A. 1 The result of Kruskal Wallis Test for the data of first plaster set received from low frequency impedance tube measurements

	Null Hypothesis	Test	Sig.[a,b]	Decision
1	The distribution of alpha63 is the same across categories of Matgroup.	Independent-Samples Kruskal-Wallis Test	0.000	Reject the null hypothesis.
2	The distribution of alpha80 is the same across categories of Matgroup.	Independent-Samples Kruskal-Wallis Test	0.001	Reject the null hypothesis.
3	The distribution of alpha100 is the same across categories of Matgroup.	Independent-Samples Kruskal-Wallis Test	0.000	Reject the null hypothesis.
4	The distribution of alpha125 is the same across categories of Matgroup.	Independent-Samples Kruskal-Wallis Test	0.000	Reject the null hypothesis.
5	The distribution of alpha160 is the same across categories of Matgroup.	Independent-Samples Kruskal-Wallis Test	0.000	Reject the null hypothesis.
6	The distribution of alpha200 is the same across categories of Matgroup.	Independent-Samples Kruskal-Wallis Test	0.000	Reject the null hypothesis.
7	The distribution of alpha250 is the same across categories of Matgroup.	Independent-Samples Kruskal-Wallis Test	0.000	Reject the null hypothesis.
8	The distribution of alpha315 is the same across categories of Matgroup.	Independent-Samples Kruskal-Wallis Test	0.000	Reject the null hypothesis.
9	The distribution of alpha400 is the same across categories of Matgroup.	Independent-Samples Kruskal-Wallis Test	0.000	Reject the null hypothesis.
10	The distribution of alpha500 is the same across categories of Matgroup.	Independent-Samples Kruskal-Wallis Test	0.000	Reject the null hypothesis.
11	The distribution of alpha630 is the same across categories of Matgroup.	Independent-Samples Kruskal-Wallis Test	0.000	Reject the null hypothesis.
12	The distribution of alpha800 is the same across categories of Matgroup.	Independent-Samples Kruskal-Wallis Test	0.000	Reject the null hypothesis.
13	The distribution of alpha1000 is the same across categories of Matgroup.	Independent-Samples Kruskal-Wallis Test	0.000	Reject the null hypothesis.
14	The distribution of alpha1250 is the same across categories of Matgroup.	Independent-Samples Kruskal-Wallis Test	0.000	Reject the null hypothesis.
15	The distribution of alpha1600 is the same across categories of Matgroup.	Independent-Samples Kruskal-Wallis Test	0.000	Reject the null hypothesis.

a. The significance level is .050.

b. Asymptotic significance is displayed.

Table A. 2 The result of Kruskal Wallis Test for the data of first plaster set received from high frequency impedance tube measurements

	Null Hypothesis	Test	Sig.[a,b]	Decision
1	The distribution of alpha1250 is the same across categories of Matgroup.	Independent-Samples Kruskal-Wallis Test	0.000	Reject the null hypothesis.
2	The distribution of alpha1600 is the same across categories of Matgroup.	Independent-Samples Kruskal-Wallis Test	0.000	Reject the null hypothesis.
3	The distribution of alpha2000 is the same across categories of Matgroup.	Independent-Samples Kruskal-Wallis Test	0.000	Reject the null hypothesis.
4	The distribution of alpha2500 is the same across categories of Matgroup.	Independent-Samples Kruskal-Wallis Test	0.000	Reject the null hypothesis.
5	The distribution of alpha3150 is the same across categories of Matgroup.	Independent-Samples Kruskal-Wallis Test	0.000	Reject the null hypothesis.
6	The distribution of alpha4000 is the same across categories of Matgroup.	Independent-Samples Kruskal-Wallis Test	0.001	Reject the null hypothesis.
7	The distribution of alpha5000 is the same across categories of Matgroup.	Independent-Samples Kruskal-Wallis Test	0.000	Reject the null hypothesis.
a. The significance level is .050.				
b. Asymptotic significance is displayed.				

In pairwise distributions, each row tests the null hypothesis that the Sample 1 and Sample 2 distributions are the same. Asymptotic significances (2-sided tests) are displayed in the tables. The significance level is 0.05. Significance values have been adjusted by the Bonferroni correction for multiple tests.

Table A. 3 Abbreviations used for material codes in statistical tests

Material Code	Abbreviation in Statistical Test
W-S1-1/1.5-DistB	1
W-S1-1/1-DistB	2
W-S1-1/0.4-DistB	3
W-S1-1/1.5-M	4
W-S1-1/1-DistM	5
W-S1-1/0.4-DistM	6
W-S1-1/1.5-DistS	7
W-S1-1/1-DistS	8
W-S1-1/0.4-DistS	9

Table A. 4 Pairwise comparison of samples from the first material set based on sound absorption data at 63Hz received from low frequency impedance tube

Sample 1-Sample 2	Test Statistic	Std. Error	Std. Test Statistic	Sig.	Adj. Sig.[a]
8-7	3.056	10.949	0.279	0.780	1.000
8-9	-5.056	10.949	-0.462	0.644	1.000
8-5	8.333	10.949	0.761	0.447	1.000
8-6	14.167	12.241	1.157	0.247	1.000
8-1	35.136	10.439	3.366	0.001	0.027
8-3	36.409	10.439	3.488	0.000	0.018
8-2	43.591	10.439	4.176	0.000	0.001
8-4	48.056	10.949	4.389	0.000	0.000
7-9	-2.000	10.949	-0.183	0.855	1.000
7-5	5.278	10.949	0.482	0.630	1.000
7-6	11.111	12.241	0.908	0.364	1.000
7-1	32.081	10.439	3.073	0.002	0.076
7-3	33.354	10.439	3.195	0.001	0.050
7-2	40.535	10.439	3.883	0.000	0.004
7-4	45.000	10.949	4.110	0.000	0.001
9-5	3.278	10.949	0.299	0.765	1.000
9-6	9.111	12.241	0.744	0.457	1.000
9-1	30.081	10.439	2.882	0.004	0.142
9-3	31.354	10.439	3.003	0.003	0.096
9-2	38.535	10.439	3.691	0.000	0.008
9-4	43.000	10.949	3.927	0.000	0.003
5-6	-5.833	12.241	-0.477	0.634	1.000
5-1	26.803	10.439	2.568	0.010	0.369
5-3	28.076	10.439	2.689	0.007	0.258
5-2	35.258	10.439	3.377	0.001	0.026
5-4	39.722	10.949	3.628	0.000	0.010
6-1	20.970	11.788	1.779	0.075	1.000
6-3	22.242	11.788	1.887	0.059	1.000
6-2	29.424	11.788	2.496	0.013	0.452
6-4	33.889	12.241	2.768	0.006	0.203
1-3	-1.273	9.904	-0.129	0.898	1.000
1-2	-8.455	9.904	-0.854	0.393	1.000
1-4	-12.919	10.439	-1.238	0.216	1.000
3-2	7.182	9.904	0.725	0.468	1.000
3-4	-11.646	10.439	-1.116	0.265	1.000
2-4	-4.465	10.439	-0.428	0.669	1.000

Table A. 5 Pairwise comparison of samples from the first material set based on sound absorption data at 80Hz received from low frequency impedance tube

Sample 1-Sample 2	Test Statistic	Std. Error	Std. Test Statistic	Sig.	Adj. Sig.[a]
9-8	0.722	11.061	0.065	0.948	1.000
9-7	7.167	11.061	0.648	0.517	1.000
9-5	21.611	11.061	1.954	0.051	1.000
9-1	28.833	10.546	2.734	0.006	0.225
9-2	30.379	10.546	2.881	0.004	0.143
9-6	32.667	12.366	2.642	0.008	0.297
9-4	33.111	11.061	2.994	0.003	0.099
9-3	34.652	10.546	3.286	0.001	0.037
8-7	6.444	11.061	0.583	0.560	1.000
8-5	20.889	11.061	1.889	0.059	1.000
8-1	28.111	10.546	2.666	0.008	0.277
8-2	29.657	10.546	2.812	0.005	0.177
8-6	31.944	12.366	2.583	0.010	0.352
8-4	32.389	11.061	2.928	0.003	0.123
8-3	33.929	10.546	3.217	0.001	0.047
7-5	14.444	11.061	1.306	0.192	1.000
7-1	21.667	10.546	2.055	0.040	1.000
7-2	23.212	10.546	2.201	0.028	0.998
7-6	25.500	12.366	2.062	0.039	1.000
7-4	25.944	11.061	2.346	0.019	0.684
7-3	27.485	10.546	2.606	0.009	0.330
5-1	7.222	10.546	0.685	0.493	1.000
5-2	8.768	10.546	0.831	0.406	1.000
5-6	-11.056	12.366	-0.894	0.371	1.000
5-4	11.500	11.061	1.040	0.298	1.000
5-3	13.040	10.546	1.237	0.216	1.000
1-2	-1.545	10.005	-0.154	0.877	1.000
1-6	-3.833	11.908	-0.322	0.748	1.000
1-4	-4.278	10.546	-0.406	0.685	1.000
1-3	-5.818	10.005	-0.582	0.561	1.000
2-6	-2.288	11.908	-0.192	0.848	1.000
2-4	-2.732	10.546	-0.259	0.796	1.000
2-3	-4.273	10.005	-0.427	0.669	1.000
6-4	0.444	12.366	0.036	0.971	1.000
6-3	1.985	11.908	0.167	0.868	1.000
4-3	1.540	10.546	0.146	0.884	1.000

Table A. 6 Pairwise comparison of samples from the first material set based on sound absorption data at 100Hz received from low frequency impedance tube

Sample 1-Sample 2	Test Statistic	Std. Error	Std. Test Statistic	Sig.	Adj. Sig.[a]
8-9	0.000	11.319	0.000	1.000	1.000
8-4	41.389	11.319	3.657	0.000	0.009
9-7	2.056	11.319	0.182	0.856	1.000
8-7	2.056	11.319	0.182	0.856	1.000
9-6	38.639	12.655	3.053	0.002	0.081
9-3	39.480	10.792	3.658	0.000	0.009
8-1	39.116	10.792	3.625	0.000	0.010
9-1	39.116	10.792	3.625	0.000	0.010
8-6	38.639	12.655	3.053	0.002	0.081
9-5	21.278	11.319	1.880	0.060	1.000
8-5	21.278	11.319	1.880	0.060	1.000
9-4	41.389	11.319	3.657	0.000	0.009
8-3	39.480	10.792	3.658	0.000	0.009
8-2	45.071	10.792	4.176	0.000	0.001
9-2	45.071	10.792	4.176	0.000	0.001
7-5	19.222	11.319	1.698	0.089	1.000
7-6	36.583	12.655	2.891	0.004	0.138
7-1	37.061	10.792	3.434	0.001	0.021
7-3	37.424	10.792	3.468	0.001	0.019
7-4	39.333	11.319	3.475	0.001	0.018
7-2	43.015	10.792	3.986	0.000	0.002
5-6	-17.361	12.655	-1.372	0.170	1.000
5-1	17.838	10.792	1.653	0.098	1.000
5-3	18.202	10.792	1.687	0.092	1.000
5-4	20.111	11.319	1.777	0.076	1.000
5-2	23.793	10.792	2.205	0.027	0.989
6-1	0.477	12.186	0.039	0.969	1.000
6-3	0.841	12.186	0.069	0.945	1.000
6-4	2.750	12.655	0.217	0.828	1.000
6-2	6.432	12.186	0.528	0.598	1.000
1-3	-0.364	10.238	-0.036	0.972	1.000
1-4	-2.273	10.792	-0.211	0.833	1.000
1-2	-5.955	10.238	-0.582	0.561	1.000
3-4	-1.909	10.792	-0.177	0.860	1.000
3-2	5.591	10.238	0.546	0.585	1.000
4-2	3.682	10.792	0.341	0.733	1.000

Table A. 7 Pairwise comparison of samples from the first material set based on sound absorption data at 125Hz received from low frequency impedance tube

Sample 1-Sample 2	Test Statistic	Std. Error	Std. Test Statistic	Sig.	Adj. Sig.[a]
8-9	0.000	11.302	0.000	1.000	1.000
8-4	34.611	11.302	3.062	0.002	0.079
9-7	6.389	11.302	0.565	0.572	1.000
8-7	6.389	11.302	0.565	0.572	1.000
9-3	42.222	10.776	3.918	0.000	0.003
9-6	48.139	12.636	3.810	0.000	0.005
8-1	42.904	10.776	3.981	0.000	0.002
9-1	42.904	10.776	3.981	0.000	0.002
8-6	48.139	12.636	3.810	0.000	0.005
9-5	29.333	11.302	2.595	0.009	0.340
8-5	29.333	11.302	2.595	0.009	0.340
9-4	34.611	11.302	3.062	0.002	0.079
8-3	42.222	10.776	3.918	0.000	0.003
8-2	42.768	10.776	3.969	0.000	0.003
9-2	42.768	10.776	3.969	0.000	0.003
7-5	22.944	11.302	2.030	0.042	1.000
7-4	28.222	11.302	2.497	0.013	0.451
7-3	35.833	10.776	3.325	0.001	0.032
7-2	36.379	10.776	3.376	0.001	0.026
7-1	36.515	10.776	3.389	0.001	0.025
7-6	41.750	12.636	3.304	0.001	0.034
5-4	5.278	11.302	0.467	0.641	1.000
5-3	12.889	10.776	1.196	0.232	1.000
5-2	13.434	10.776	1.247	0.213	1.000
5-1	13.571	10.776	1.259	0.208	1.000
5-6	-18.806	12.636	-1.488	0.137	1.000
4-3	7.611	10.776	0.706	0.480	1.000
4-2	8.157	10.776	0.757	0.449	1.000
4-1	8.293	10.776	0.770	0.442	1.000
4-6	-13.528	12.636	-1.071	0.284	1.000
3-2	0.545	10.223	0.053	0.957	1.000
3-1	0.682	10.223	0.067	0.947	1.000
3-6	-5.917	12.168	-0.486	0.627	1.000
2-1	0.136	10.223	0.013	0.989	1.000
2-6	-5.371	12.168	-0.441	0.659	1.000
1-6	-5.235	12.168	-0.430	0.667	1.000

Table A. 8 Pairwise comparison of samples from the first material set based on sound absorption data at 160Hz received from low frequency impedance tube

Sample 1-Sample 2	Test Statistic	Std. Error	Std. Test Statistic	Sig.	Adj. Sig.[a]
8-9	-2.722	11.090	-0.245	0.806	1.000
8-7	8.167	11.090	0.736	0.461	1.000
8-5	27.944	11.090	2.520	0.012	0.423
8-4	35.944	11.090	3.241	0.001	0.043
8-2	39.091	10.574	3.697	0.000	0.008
8-3	40.182	10.574	3.800	0.000	0.005
8-1	42.364	10.574	4.006	0.000	0.002
8-6	49.833	12.399	4.019	0.000	0.002
9-7	5.444	11.090	0.491	0.623	1.000
9-5	25.222	11.090	2.274	0.023	0.826
9-4	33.222	11.090	2.996	0.003	0.099
9-2	36.369	10.574	3.439	0.001	0.021
9-3	37.460	10.574	3.543	0.000	0.014
9-1	39.641	10.574	3.749	0.000	0.006
9-6	47.111	12.399	3.800	0.000	0.005
7-5	19.778	11.090	1.783	0.075	1.000
7-4	27.778	11.090	2.505	0.012	0.441
7-2	30.924	10.574	2.925	0.003	0.124
7-3	32.015	10.574	3.028	0.002	0.089
7-1	34.197	10.574	3.234	0.001	0.044
7-6	41.667	12.399	3.360	0.001	0.028
5-4	8.000	11.090	0.721	0.471	1.000
5-2	11.146	10.574	1.054	0.292	1.000
5-3	12.237	10.574	1.157	0.247	1.000
5-1	14.419	10.574	1.364	0.173	1.000
5-6	-21.889	12.399	-1.765	0.078	1.000
4-2	3.146	10.574	0.298	0.766	1.000
4-3	4.237	10.574	0.401	0.689	1.000
4-1	6.419	10.574	0.607	0.544	1.000
4-6	-13.889	12.399	-1.120	0.263	1.000
2-3	-1.091	10.031	-0.109	0.913	1.000
2-1	3.273	10.031	0.326	0.744	1.000
2-6	-10.742	11.940	-0.900	0.368	1.000
3-1	2.182	10.031	0.217	0.828	1.000
3-6	-9.652	11.940	-0.808	0.419	1.000
1-6	-7.470	11.940	-0.626	0.532	1.000

Table A. 9 Pairwise comparison of samples from the first material set based on sound absorption data at 200Hz received from low frequency impedance tube

Sample 1-Sample 2	Test Statistic	Std. Error	Std. Test Statistic	Sig.	Adj. Sig.[a]
8-9	0.000	10.765	0.000	1.000	1.000
8-4	32.722	10.765	3.040	0.002	0.085
9-7	14.444	10.765	1.342	0.180	1.000
8-7	14.444	10.765	1.342	0.180	1.000
9-3	36.545	10.264	3.561	0.000	0.013
9-6	43.750	12.036	3.635	0.000	0.010
8-1	46.500	10.264	4.530	0.000	0.000
9-1	46.500	10.264	4.530	0.000	0.000
8-6	43.750	12.036	3.635	0.000	0.010
9-5	18.056	10.765	1.677	0.093	1.000
8-5	18.056	10.765	1.677	0.093	1.000
9-4	32.722	10.765	3.040	0.002	0.085
8-2	26.818	10.264	2.613	0.009	0.323
8-3	36.545	10.264	3.561	0.000	0.013
9-2	26.818	10.264	2.613	0.009	0.323
7-5	3.611	10.765	0.335	0.737	1.000
7-2	12.374	10.264	1.206	0.228	1.000
7-4	18.278	10.765	1.698	0.090	1.000
7-3	22.101	10.264	2.153	0.031	1.000
7-6	29.306	12.036	2.435	0.015	0.536
7-1	32.056	10.264	3.123	0.002	0.064
5-2	8.763	10.264	0.854	0.393	1.000
5-4	14.667	10.765	1.362	0.173	1.000
5-3	18.490	10.264	1.801	0.072	1.000
5-6	-25.694	12.036	-2.135	0.033	1.000
5-1	28.444	10.264	2.771	0.006	0.201
2-4	-5.904	10.264	-0.575	0.565	1.000
2-3	-9.727	9.737	-0.999	0.318	1.000
2-6	-16.932	11.590	-1.461	0.144	1.000
2-1	19.682	9.737	2.021	0.043	1.000
4-3	3.823	10.264	0.372	0.710	1.000
4-6	-11.028	12.036	-0.916	0.360	1.000
4-1	13.778	10.264	1.342	0.179	1.000
3-6	-7.205	11.590	-0.622	0.534	1.000
3-1	9.955	9.737	1.022	0.307	1.000
6-1	2.750	11.590	0.237	0.812	1.000

Table A. 10 Pairwise comparison of samples from the first material set based on sound absorption data at 250Hz received from low frequency impedance tube

Sample 1-Sample 2	Test Statistic	Std. Error	Std. Test Statistic	Sig.	Adj. Sig.[a]
9-8	6.444	10.076	0.640	0.522	1.000
9-7	6.444	10.076	0.640	0.522	1.000
9-2	11.712	9.607	1.219	0.223	1.000
9-3	12.985	9.607	1.352	0.176	1.000
9-5	13.722	10.076	1.362	0.173	1.000
9-6	34.000	11.265	3.018	0.003	0.092
9-4	35.444	10.076	3.518	0.000	0.016
9-1	48.530	9.607	5.052	0.000	0.000
8-4	29.000	10.076	2.878	0.004	0.144
7-5	7.278	10.076	0.722	0.470	1.000
8-5	7.278	10.076	0.722	0.470	1.000
7-6	27.556	11.265	2.446	0.014	0.520
7-1	42.086	9.607	4.381	0.000	0.000
8-6	27.556	11.265	2.446	0.014	0.520
8-1	42.086	9.607	4.381	0.000	0.000
7-8	0.000	10.076	0.000	1.000	1.000
7-2	5.268	9.607	0.548	0.583	1.000
8-2	5.268	9.607	0.548	0.583	1.000
7-3	6.540	9.607	0.681	0.496	1.000
8-3	6.540	9.607	0.681	0.496	1.000
7-4	29.000	10.076	2.878	0.004	0.144
2-3	-1.273	9.114	-0.140	0.889	1.000
2-5	-2.010	9.607	-0.209	0.834	1.000
2-6	-22.288	10.847	-2.055	0.040	1.000
2-4	-23.732	9.607	-2.470	0.013	0.486
2-1	36.818	9.114	4.040	0.000	0.002
3-5	-0.737	9.607	-0.077	0.939	1.000
3-6	-21.015	10.847	-1.937	0.053	1.000
3-4	-22.460	9.607	-2.338	0.019	0.698
3-1	35.545	9.114	3.900	0.000	0.003
5-6	-20.278	11.265	-1.800	0.072	1.000
5-4	21.722	10.076	2.156	0.031	1.000
5-1	34.808	9.607	3.623	0.000	0.010
6-4	1.444	11.265	0.128	0.898	1.000
6-1	14.530	10.847	1.340	0.180	1.000
4-1	13.086	9.607	1.362	0.173	1.000

Table A. 11 Pairwise comparison of samples from the first material set based on sound absorption data at 315Hz received from low frequency impedance tube

Sample 1-Sample 2	Test Statistic	Std. Error	Std. Test Statistic	Sig.	Adj. Sig.[a]
3-2	3.091	9.683	0.319	0.750	1.000
3-5	-5.000	10.207	-0.490	0.624	1.000
3-9	-5.000	10.207	-0.490	0.624	1.000
3-8	-5.000	10.207	-0.490	0.624	1.000
3-7	-16.000	10.207	-1.568	0.117	1.000
3-6	-16.000	11.525	-1.388	0.165	1.000
3-4	-40.667	10.207	-3.984	0.000	0.002
3-1	44.091	9.683	4.553	0.000	0.000
2-8	-1.909	10.207	-0.187	0.852	1.000
2-9	-1.909	10.207	-0.187	0.852	1.000
2-5	-1.909	10.207	-0.187	0.852	1.000
2-7	-12.909	10.207	-1.265	0.206	1.000
2-6	-12.909	11.525	-1.120	0.263	1.000
2-4	-37.576	10.207	-3.681	0.000	0.008
2-1	41.000	9.683	4.234	0.000	0.001
5-1	39.091	10.207	3.830	0.000	0.005
9-1	39.091	10.207	3.830	0.000	0.005
8-1	39.091	10.207	3.830	0.000	0.005
5-4	35.667	10.705	3.332	0.001	0.031
8-4	35.667	10.705	3.332	0.001	0.031
9-4	35.667	10.705	3.332	0.001	0.031
5-8	0.000	10.705	0.000	1.000	1.000
5-9	0.000	10.705	0.000	1.000	1.000
5-6	-11.000	11.969	-0.919	0.358	1.000
5-7	-11.000	10.705	-1.028	0.304	1.000
8-6	11.000	11.969	0.919	0.358	1.000
9-6	11.000	11.969	0.919	0.358	1.000
8-7	11.000	10.705	1.028	0.304	1.000
9-7	11.000	10.705	1.028	0.304	1.000
8-9	0.000	10.705	0.000	1.000	1.000
6-1	28.091	11.525	2.437	0.015	0.533
7-1	28.091	10.207	2.752	0.006	0.213
6-4	24.667	11.969	2.061	0.039	1.000
7-4	24.667	10.705	2.304	0.021	0.764
6-7	0.000	11.969	0.000	1.000	1.000
4-1	3.424	10.207	0.335	0.737	1.000

Table A. 12 Pairwise comparison of samples from the first material set based on sound absorption data at 400Hz received from low frequency impedance tube

Sample 1-Sample 2	Test Statistic	Std. Error	Std. Test Statistic	Sig.	Adj. Sig.[a]
9-2	0.864	10.425	0.083	0.934	1.000
9-5	15.722	10.934	1.438	0.150	1.000
9-3	16.318	10.425	1.565	0.118	1.000
9-7	17.000	10.934	1.555	0.120	1.000
9-6	17.667	12.225	1.445	0.148	1.000
9-8	34.667	10.934	3.171	0.002	0.055
9-4	42.833	10.934	3.917	0.000	0.003
9-1	51.000	10.425	4.892	0.000	0.000
2-5	-14.859	10.425	-1.425	0.154	1.000
2-3	-15.455	9.890	-1.563	0.118	1.000
2-7	-16.136	10.425	-1.548	0.122	1.000
2-6	-16.803	11.772	-1.427	0.153	1.000
2-8	-33.803	10.425	-3.242	0.001	0.043
2-4	-41.970	10.425	-4.026	0.000	0.002
2-1	50.136	9.890	5.069	0.000	0.000
5-3	0.596	10.425	0.057	0.954	1.000
5-7	-1.278	10.934	-0.117	0.907	1.000
5-6	-1.944	12.225	-0.159	0.874	1.000
5-8	-18.944	10.934	-1.733	0.083	1.000
5-4	27.111	10.934	2.480	0.013	0.474
5-1	35.278	10.425	3.384	0.001	0.026
3-7	-0.682	10.425	-0.065	0.948	1.000
3-6	-1.348	11.772	-0.115	0.909	1.000
3-8	-18.348	10.425	-1.760	0.078	1.000
3-4	-26.515	10.425	-2.543	0.011	0.395
3-1	34.682	9.890	3.507	0.000	0.016
7-6	0.667	12.225	0.055	0.957	1.000
7-8	-17.667	10.934	-1.616	0.106	1.000
7-4	25.833	10.934	2.363	0.018	0.653
7-1	34.000	10.425	3.261	0.001	0.040
6-8	-17.000	12.225	-1.391	0.164	1.000
6-4	25.167	12.225	2.059	0.040	1.000
6-1	33.333	11.772	2.832	0.005	0.167
8-4	8.167	10.934	0.747	0.455	1.000
8-1	16.333	10.425	1.567	0.117	1.000
4-1	8.167	10.425	0.783	0.433	1.000

Table A. 13 Pairwise comparison of samples from the first material set based on sound absorption data at 500Hz received from low frequency impedance tube

Sample 1-Sample 2	Test Statistic	Std. Error	Std. Test Statistic	Sig.	Adj. Sig.[a]
2-5	-3.076	10.788	-0.285	0.776	1.000
2-1	12.727	10.234	1.244	0.214	1.000
2-6	-24.576	12.181	-2.018	0.044	1.000
2-3	-28.227	10.234	-2.758	0.006	0.209
2-4	-31.242	10.788	-2.896	0.004	0.136
2-9	-51.909	10.788	-4.812	0.000	0.000
2-7	-56.909	10.788	-5.275	0.000	0.000
2-8	-64.909	10.788	-6.017	0.000	0.000
5-1	9.652	10.788	0.895	0.371	1.000
5-6	-21.500	12.650	-1.700	0.089	1.000
5-3	25.152	10.788	2.331	0.020	0.710
5-4	28.167	11.314	2.489	0.013	0.461
5-9	-48.833	11.314	-4.316	0.000	0.001
5-7	-53.833	11.314	-4.758	0.000	0.000
5-8	-61.833	11.314	-5.465	0.000	0.000
1-6	-11.848	12.181	-0.973	0.331	1.000
1-3	-15.500	10.234	-1.515	0.130	1.000
1-4	-18.515	10.788	-1.716	0.086	1.000
1-9	-39.182	10.788	-3.632	0.000	0.010
1-7	-44.182	10.788	-4.096	0.000	0.002
1-8	-52.182	10.788	-4.837	0.000	0.000
6-3	3.652	12.181	0.300	0.764	1.000
6-4	6.667	12.650	0.527	0.598	1.000
6-9	-27.333	12.650	-2.161	0.031	1.000
6-7	-32.333	12.650	-2.556	0.011	0.381
6-8	-40.333	12.650	-3.188	0.001	0.051
3-4	-3.015	10.788	-0.279	0.780	1.000
3-9	-23.682	10.788	-2.195	0.028	1.000
3-7	-28.682	10.788	-2.659	0.008	0.282
3-8	-36.682	10.788	-3.400	0.001	0.024
4-9	-20.667	11.314	-1.827	0.068	1.000
4-7	-25.667	11.314	-2.268	0.023	0.839
4-8	-33.667	11.314	-2.976	0.003	0.105
9-7	5.000	11.314	0.442	0.659	1.000
9-8	13.000	11.314	1.149	0.251	1.000
7-8	-8.000	11.314	-0.707	0.480	1.000

Table A. 14 Pairwise comparison of samples from the first material set based on sound absorption data at 630Hz received from low frequency impedance tube

Sample 1-Sample 2	Test Statistic	Std. Error	Std. Test Statistic	Sig.	Adj. Sig.[a]
2-7	-28.500	10.879	-2.620	0.009	0.317
2-3	-29.364	10.320	-2.845	0.004	0.160
2-5	-31.167	10.879	-2.865	0.004	0.150
2-1	36.273	10.320	3.515	0.000	0.016
2-9	-41.167	10.879	-3.784	0.000	0.006
2-6	-43.000	12.284	-3.501	0.000	0.017
2-8	-64.500	10.879	-5.929	0.000	0.000
2-4	-66.444	10.879	-6.108	0.000	0.000
7-3	0.864	10.879	0.079	0.937	1.000
7-5	2.667	11.410	0.234	0.815	1.000
7-1	7.773	10.879	0.714	0.475	1.000
7-9	-12.667	11.410	-1.110	0.267	1.000
7-6	14.500	12.756	1.137	0.256	1.000
7-8	-36.000	11.410	-3.155	0.002	0.058
7-4	37.944	11.410	3.326	0.001	0.032
3-5	-1.803	10.879	-0.166	0.868	1.000
3-1	6.909	10.320	0.669	0.503	1.000
3-9	-11.803	10.879	-1.085	0.278	1.000
3-6	-13.636	12.284	-1.110	0.267	1.000
3-8	-35.136	10.879	-3.230	0.001	0.045
3-4	-37.081	10.879	-3.409	0.001	0.024
5-1	5.106	10.879	0.469	0.639	1.000
5-9	-10.000	11.410	-0.876	0.381	1.000
5-6	-11.833	12.756	-0.928	0.354	1.000
5-8	-33.333	11.410	-2.921	0.003	0.125
5-4	35.278	11.410	3.092	0.002	0.072
1-9	-4.894	10.879	-0.450	0.653	1.000
1-6	-6.727	12.284	-0.548	0.584	1.000
1-8	-28.227	10.879	-2.595	0.009	0.341
1-4	-30.172	10.879	-2.773	0.006	0.200
9-6	1.833	12.756	0.144	0.886	1.000
9-8	23.333	11.410	2.045	0.041	1.000
9-4	25.278	11.410	2.215	0.027	0.962
6-8	-21.500	12.756	-1.685	0.092	1.000
6-4	23.444	12.756	1.838	0.066	1.000
8-4	1.944	11.410	0.170	0.865	1.000

Table A. 15 Pairwise comparison of samples from the first material set based on sound absorption data at 800Hz received from low frequency impedance tube

Sample 1-Sample 2	Test Statistic	Std. Error	Std. Test Statistic	Sig.	Adj. Sig.[a]
2-3	-4.773	10.350	-0.461	0.645	1.000
2-6	-12.341	12.319	-1.002	0.316	1.000
2-7	-29.091	10.910	-2.666	0.008	0.276
2-8	-41.091	10.910	-3.766	0.000	0.006
2-5	-45.035	10.910	-4.128	0.000	0.001
2-1	45.182	10.350	4.365	0.000	0.000
2-9	-47.758	10.910	-4.377	0.000	0.000
2-4	-48.591	10.910	-4.454	0.000	0.000
3-6	-7.568	12.319	-0.614	0.539	1.000
3-7	-24.318	10.910	-2.229	0.026	0.929
3-8	-36.318	10.910	-3.329	0.001	0.031
3-5	-40.263	10.910	-3.690	0.000	0.008
3-1	40.409	10.350	3.904	0.000	0.003
3-9	-42.985	10.910	-3.940	0.000	0.003
3-4	-43.818	10.910	-4.016	0.000	0.002
6-7	-16.750	12.793	-1.309	0.190	1.000
6-8	-28.750	12.793	-2.247	0.025	0.886
6-5	32.694	12.793	2.556	0.011	0.382
6-1	32.841	12.319	2.666	0.008	0.277
6-9	-35.417	12.793	-2.768	0.006	0.203
6-4	36.250	12.793	2.833	0.005	0.166
7-8	-12.000	11.443	-1.049	0.294	1.000
7-5	15.944	11.443	1.393	0.163	1.000
7-1	16.091	10.910	1.475	0.140	1.000
7-9	-18.667	11.443	-1.631	0.103	1.000
7-4	19.500	11.443	1.704	0.088	1.000
8-5	3.944	11.443	0.345	0.730	1.000
8-1	4.091	10.910	0.375	0.708	1.000
8-9	-6.667	11.443	-0.583	0.560	1.000
8-4	7.500	11.443	0.655	0.512	1.000
5-1	0.146	10.910	0.013	0.989	1.000
5-9	-2.722	11.443	-0.238	0.812	1.000
5-4	3.556	11.443	0.311	0.756	1.000
1-9	-2.576	10.910	-0.236	0.813	1.000
1-4	-3.409	10.910	-0.312	0.755	1.000
9-4	0.833	11.443	0.073	0.942	1.000

Table A. 16 Pairwise comparison of samples from the first material set based on sound absorption data at 1000Hz received from low frequency impedance tube

Sample 1-Sample 2	Test Statistic	Std. Error	Std. Test Statistic	Sig.	Adj. Sig.[a]
2-3	-3.591	10.304	-0.348	0.727	1.000
2-6	-5.841	12.265	-0.476	0.634	1.000
2-7	-6.258	10.862	-0.576	0.565	1.000
2-8	-22.924	10.862	-2.111	0.035	1.000
2-5	-37.646	10.862	-3.466	0.001	0.019
2-9	-40.924	10.862	-3.768	0.000	0.006
2-4	-44.924	10.862	-4.136	0.000	0.001
2-1	48.455	10.304	4.702	0.000	0.000
3-6	-2.250	12.265	-0.183	0.854	1.000
3-7	-2.667	10.862	-0.246	0.806	1.000
3-8	-19.333	10.862	-1.780	0.075	1.000
3-5	-34.056	10.862	-3.135	0.002	0.062
3-9	-37.333	10.862	-3.437	0.001	0.021
3-4	-41.333	10.862	-3.805	0.000	0.005
3-1	44.864	10.304	4.354	0.000	0.000
6-7	-0.417	12.737	-0.033	0.974	1.000
6-8	-17.083	12.737	-1.341	0.180	1.000
6-5	31.806	12.737	2.497	0.013	0.451
6-9	-35.083	12.737	-2.755	0.006	0.212
6-4	39.083	12.737	3.069	0.002	0.077
6-1	42.614	12.265	3.474	0.001	0.018
7-8	-16.667	11.392	-1.463	0.143	1.000
7-5	31.389	11.392	2.755	0.006	0.211
7-9	-34.667	11.392	-3.043	0.002	0.084
7-4	38.667	11.392	3.394	0.001	0.025
7-1	42.197	10.862	3.885	0.000	0.004
8-5	14.722	11.392	1.292	0.196	1.000
8-9	-18.000	11.392	-1.580	0.114	1.000
8-4	22.000	11.392	1.931	0.053	1.000
8-1	25.530	10.862	2.350	0.019	0.675
5-9	-3.278	11.392	-0.288	0.774	1.000
5-4	7.278	11.392	0.639	0.523	1.000
5-1	10.808	10.862	0.995	0.320	1.000
9-4	4.000	11.392	0.351	0.725	1.000
9-1	7.530	10.862	0.693	0.488	1.000
4-1	3.530	10.862	0.325	0.745	1.000

Table A. 17 Pairwise comparison of samples from the first material set based on sound absorption data at 1250Hz received from low frequency impedance tube

Sample 1-Sample 2	Test Statistic	Std. Error	Std. Test Statistic	Sig.	Adj. Sig.[a]
2-6	-4.545	12.165	-0.374	0.709	1.000
2-3	-14.545	10.221	-1.423	0.155	1.000
2-7	-14.712	10.774	-1.366	0.172	1.000
2-8	-25.712	10.774	-2.387	0.017	0.612
2-5	-34.879	10.774	-3.237	0.001	0.043
2-9	-44.879	10.774	-4.166	0.000	0.001
2-1	52.955	10.221	5.181	0.000	0.000
2-4	-56.045	10.774	-5.202	0.000	0.000
6-3	10.000	12.165	0.822	0.411	1.000
6-7	-10.167	12.633	-0.805	0.421	1.000
6-8	-21.167	12.633	-1.675	0.094	1.000
6-5	30.333	12.633	2.401	0.016	0.588
6-9	-40.333	12.633	-3.193	0.001	0.051
6-1	48.409	12.165	3.979	0.000	0.002
6-4	51.500	12.633	4.077	0.000	0.002
3-7	-0.167	10.774	-0.015	0.988	1.000
3-8	-11.167	10.774	-1.036	0.300	1.000
3-5	-20.333	10.774	-1.887	0.059	1.000
3-9	-30.333	10.774	-2.816	0.005	0.175
3-1	38.409	10.221	3.758	0.000	0.006
3-4	-41.500	10.774	-3.852	0.000	0.004
7-8	-11.000	11.299	-0.973	0.330	1.000
7-5	20.167	11.299	1.785	0.074	1.000
7-9	-30.167	11.299	-2.670	0.008	0.273
7-1	38.242	10.774	3.550	0.000	0.014
7-4	41.333	11.299	3.658	0.000	0.009
8-5	9.167	11.299	0.811	0.417	1.000
8-9	-19.167	11.299	-1.696	0.090	1.000
8-1	27.242	10.774	2.529	0.011	0.412
8-4	30.333	11.299	2.684	0.007	0.261
5-9	-10.000	11.299	-0.885	0.376	1.000
5-1	18.076	10.774	1.678	0.093	1.000
5-4	21.167	11.299	1.873	0.061	1.000
9-1	8.076	10.774	0.750	0.454	1.000
9-4	11.167	11.299	0.988	0.323	1.000
1-4	-3.091	10.774	-0.287	0.774	1.000

Table A. 18 Pairwise comparison of samples from the first material set based on sound absorption data at 1600Hz received from low frequency impedance tube

Sample 1-Sample 2	Test Statistic	Std. Error	Std. Test Statistic	Sig.	Adj. Sig.[a]
6-2	2.114	12.133	0.174	0.862	1.000
6-3	7.750	12.133	0.639	0.523	1.000
6-7	-28.250	12.600	-2.242	0.025	0.898
6-5	35.417	12.600	2.811	0.005	0.178
6-8	-36.417	12.600	-2.890	0.004	0.139
6-9	-47.472	12.600	-3.768	0.000	0.006
6-1	56.705	12.133	4.674	0.000	0.000
6-4	58.083	12.600	4.610	0.000	0.000
2-3	-5.636	10.194	-0.553	0.580	1.000
2-7	-26.136	10.745	-2.432	0.015	0.540
2-5	-33.303	10.745	-3.099	0.002	0.070
2-8	-34.303	10.745	-3.192	0.001	0.051
2-9	-45.359	10.745	-4.221	0.000	0.001
2-1	54.591	10.194	5.355	0.000	0.000
2-4	-55.970	10.745	-5.209	0.000	0.000
3-7	-20.500	10.745	-1.908	0.056	1.000
3-5	-27.667	10.745	-2.575	0.010	0.361
3-8	-28.667	10.745	-2.668	0.008	0.275
3-9	-39.722	10.745	-3.697	0.000	0.008
3-1	48.955	10.194	4.802	0.000	0.000
3-4	-50.333	10.745	-4.684	0.000	0.000
7-5	7.167	11.270	0.636	0.525	1.000
7-8	-8.167	11.270	-0.725	0.469	1.000
7-9	-19.222	11.270	-1.706	0.088	1.000
7-1	28.455	10.745	2.648	0.008	0.291
7-4	29.833	11.270	2.647	0.008	0.292
5-8	-1.000	11.270	-0.089	0.929	1.000
5-9	-12.056	11.270	-1.070	0.285	1.000
5-1	21.288	10.745	1.981	0.048	1.000
5-4	22.667	11.270	2.011	0.044	1.000
8-9	-11.056	11.270	-0.981	0.327	1.000
8-1	20.288	10.745	1.888	0.059	1.000
8-4	21.667	11.270	1.923	0.055	1.000
9-1	9.232	10.745	0.859	0.390	1.000
9-4	10.611	11.270	0.942	0.346	1.000
1-4	-1.379	10.745	-0.128	0.898	1.000

Table A. 19 Pairwise comparison of samples from the first material set based on sound absorption data at 1000Hz received from high frequency impedance tube

Sample 1-Sample 2	Test Statistic	Std. Error	Std. Test Statistic	Sig.	Adj. Sig.[a]
6-8	-4.500	10.863	-0.414	0.679	1.000
6-5	22.667	10.863	2.087	0.037	1.000
6-7	-27.167	10.863	-2.501	0.012	0.446
6-4	34.000	10.863	3.130	0.002	0.063
6-1	39.833	10.863	3.667	0.000	0.009
6-2	41.000	14.574	2.813	0.005	0.177
6-9	-45.000	10.863	-4.143	0.000	0.001
6-3	53.167	10.863	4.894	0.000	0.000
8-5	18.167	9.716	1.870	0.062	1.000
8-7	22.667	9.716	2.333	0.020	0.707
8-4	29.500	9.716	3.036	0.002	0.086
8-1	35.333	9.716	3.637	0.000	0.010
8-2	36.500	13.740	2.656	0.008	0.284
8-9	-40.500	9.716	-4.168	0.000	0.001
8-3	48.667	9.716	5.009	0.000	0.000
5-7	-4.500	9.716	-0.463	0.643	1.000
5-4	11.333	9.716	1.166	0.243	1.000
5-1	17.167	9.716	1.767	0.077	1.000
5-2	18.333	13.740	1.334	0.182	1.000
5-9	-22.333	9.716	-2.299	0.022	0.775
5-3	30.500	9.716	3.139	0.002	0.061
7-4	6.833	9.716	0.703	0.482	1.000
7-1	12.667	9.716	1.304	0.192	1.000
7-2	13.833	13.740	1.007	0.314	1.000
7-9	-17.833	9.716	-1.835	0.066	1.000
7-3	26.000	9.716	2.676	0.007	0.268
4-1	5.833	9.716	0.600	0.548	1.000
4-2	7.000	13.740	0.509	0.610	1.000
4-9	-11.000	9.716	-1.132	0.258	1.000
4-3	19.167	9.716	1.973	0.049	1.000
1-2	-1.167	13.740	-0.085	0.932	1.000
1-9	-5.167	9.716	-0.532	0.595	1.000
1-3	-13.333	9.716	-1.372	0.170	1.000
2-9	-4.000	13.740	-0.291	0.771	1.000
2-3	-12.167	13.740	-0.885	0.376	1.000
9-3	8.167	9.716	0.841	0.401	1.000

Table A. 20 Pairwise comparison of samples from the first material set based on sound absorption data at 1250Hz received from high frequency impedance tube

Sample 1-Sample 2	Test Statistic	Std. Error	Std. Test Statistic	Sig.	Adj. Sig.[a]
6-8	-9.500	10.811	-0.879	0.380	1.000
6-4	13.500	10.811	1.249	0.212	1.000
6-1	19.000	10.811	1.757	0.079	1.000
6-5	28.500	10.811	2.636	0.008	0.302
6-7	-35.500	10.811	-3.284	0.001	0.037
6-2	40.500	14.505	2.792	0.005	0.188
6-3	41.000	10.811	3.792	0.000	0.005
6-9	-43.500	10.811	-4.024	0.000	0.002
8-4	4.000	9.670	0.414	0.679	1.000
8-1	9.500	9.670	0.982	0.326	1.000
8-5	19.000	9.670	1.965	0.049	1.000
8-7	26.000	9.670	2.689	0.007	0.258
8-2	31.000	13.675	2.267	0.023	0.842
8-3	31.500	9.670	3.258	0.001	0.040
8-9	-34.000	9.670	-3.516	0.000	0.016
4-1	5.500	9.670	0.569	0.570	1.000
4-5	-15.000	9.670	-1.551	0.121	1.000
4-7	-22.000	9.670	-2.275	0.023	0.824
4-2	27.000	13.675	1.974	0.048	1.000
4-3	27.500	9.670	2.844	0.004	0.160
4-9	-30.000	9.670	-3.102	0.002	0.069
1-5	-9.500	9.670	-0.982	0.326	1.000
1-7	-16.500	9.670	-1.706	0.088	1.000
1-2	-21.500	13.675	-1.572	0.116	1.000
1-3	-22.000	9.670	-2.275	0.023	0.824
1-9	-24.500	9.670	-2.534	0.011	0.406
5-7	-7.000	9.670	-0.724	0.469	1.000
5-2	12.000	13.675	0.877	0.380	1.000
5-3	12.500	9.670	1.293	0.196	1.000
5-9	-15.000	9.670	-1.551	0.121	1.000
7-2	5.000	13.675	0.366	0.715	1.000
7-3	5.500	9.670	0.569	0.570	1.000
7-9	-8.000	9.670	-0.827	0.408	1.000
2-3	-0.500	13.675	-0.037	0.971	1.000
2-9	-3.000	13.675	-0.219	0.826	1.000
3-9	-2.500	9.670	-0.259	0.796	1.000

Table A. 21 Pairwise comparison of samples from the first material set based on sound absorption data at 1600Hz received from high frequency impedance tube

Sample 1-Sample 2	Test Statistic	Std. Error	Std. Test Statistic	Sig.	Adj. Sig.[a]
8-6	3.000	10.701	0.280	0.779	1.000
8-4	5.000	9.572	0.522	0.601	1.000
8-5	5.000	9.572	0.522	0.601	1.000
8-2	12.000	13.536	0.887	0.375	1.000
8-1	15.333	9.572	1.602	0.109	1.000
8-7	33.667	9.572	3.517	0.000	0.016
8-3	38.667	9.572	4.040	0.000	0.002
8-9	-40.333	9.572	-4.214	0.000	0.001
6-4	2.000	10.701	0.187	0.852	1.000
6-5	2.000	10.701	0.187	0.852	1.000
6-2	9.000	14.357	0.627	0.531	1.000
6-1	12.333	10.701	1.153	0.249	1.000
6-7	-30.667	10.701	-2.866	0.004	0.150
6-3	35.667	10.701	3.333	0.001	0.031
6-9	-37.333	10.701	-3.489	0.000	0.017
4-1	10.333	9.572	1.080	0.280	1.000
5-1	10.333	9.572	1.080	0.280	1.000
4-5	0.000	9.572	0.000	1.000	1.000
4-2	7.000	13.536	0.517	0.605	1.000
4-3	33.667	9.572	3.517	0.000	0.016
5-2	7.000	13.536	0.517	0.605	1.000
5-3	33.667	9.572	3.517	0.000	0.016
4-7	-28.667	9.572	-2.995	0.003	0.099
4-9	-35.333	9.572	-3.691	0.000	0.008
5-7	-28.667	9.572	-2.995	0.003	0.099
5-9	-35.333	9.572	-3.691	0.000	0.008
2-1	3.333	13.536	0.246	0.805	1.000
2-7	-21.667	13.536	-1.601	0.109	1.000
2-3	-26.667	13.536	-1.970	0.049	1.000
2-9	-28.333	13.536	-2.093	0.036	1.000
1-7	-18.333	9.572	-1.915	0.055	1.000
1-3	-23.333	9.572	-2.438	0.015	0.532
1-9	-25.000	9.572	-2.612	0.009	0.324
7-3	5.000	9.572	0.522	0.601	1.000
7-9	-6.667	9.572	-0.697	0.486	1.000
3-9	-1.667	9.572	-0.174	0.862	1.000

Table A. 22 Pairwise comparison of samples from the first material set based on sound absorption data at 2000Hz received from high frequency impedance tube

Sample 1-Sample 2	Test Statistic	Std. Error	Std. Test Statistic	Sig.	Adj. Sig.[a]
8-5	7.500	9.545	0.786	0.432	1.000
8-6	15.000	10.672	1.406	0.160	1.000
8-2	22.500	13.499	1.667	0.096	1.000
8-4	25.000	9.545	2.619	0.009	0.317
8-7	32.333	9.545	3.387	0.001	0.025
8-1	33.333	9.545	3.492	0.000	0.017
8-9	-38.500	9.545	-4.034	0.000	0.002
8-3	45.833	9.545	4.802	0.000	0.000
5-6	-7.500	10.672	-0.703	0.482	1.000
5-2	15.000	13.499	1.111	0.266	1.000
5-4	17.500	9.545	1.833	0.067	1.000
5-7	-24.833	9.545	-2.602	0.009	0.334
5-1	25.833	9.545	2.706	0.007	0.245
5-9	-31.000	9.545	-3.248	0.001	0.042
5-3	38.333	9.545	4.016	0.000	0.002
6-2	7.500	14.318	0.524	0.600	1.000
6-4	10.000	10.672	0.937	0.349	1.000
6-7	-17.333	10.672	-1.624	0.104	1.000
6-1	18.333	10.672	1.718	0.086	1.000
6-9	-23.500	10.672	-2.202	0.028	0.996
6-3	30.833	10.672	2.889	0.004	0.139
2-4	-2.500	13.499	-0.185	0.853	1.000
2-7	-9.833	13.499	-0.728	0.466	1.000
2-1	10.833	13.499	0.803	0.422	1.000
2-9	-16.000	13.499	-1.185	0.236	1.000
2-3	-23.333	13.499	-1.729	0.084	1.000
4-7	-7.333	9.545	-0.768	0.442	1.000
4-1	8.333	9.545	0.873	0.383	1.000
4-9	-13.500	9.545	-1.414	0.157	1.000
4-3	20.833	9.545	2.183	0.029	1.000
7-1	1.000	9.545	0.105	0.917	1.000
7-9	-6.167	9.545	-0.646	0.518	1.000
7-3	13.500	9.545	1.414	0.157	1.000
1-9	-5.167	9.545	-0.541	0.588	1.000
1-3	-12.500	9.545	-1.310	0.190	1.000
9-3	7.333	9.545	0.768	0.442	1.000

Table A. 23 Pairwise comparison of samples from the first material set based on sound absorption data at 2500Hz received from high frequency impedance tube

Sample 1-Sample 2	Test Statistic	Std. Error	Std. Test Statistic	Sig.	Adj. Sig.[a]
8-5	7.778	9.767	0.796	0.426	1.000
8-7	16.556	9.767	1.695	0.090	1.000
8-6	18.889	10.920	1.730	0.084	1.000
8-9	-20.056	9.767	-2.053	0.040	1.000
8-4	40.889	9.767	4.186	0.000	0.001
8-2	44.889	13.813	3.250	0.001	0.042
8-1	47.389	9.767	4.852	0.000	0.000
8-3	54.889	9.767	5.620	0.000	0.000
5-7	-8.778	9.767	-0.899	0.369	1.000
5-6	-11.111	10.920	-1.018	0.309	1.000
5-9	-12.278	9.767	-1.257	0.209	1.000
5-4	33.111	9.767	3.390	0.001	0.025
5-2	37.111	13.813	2.687	0.007	0.260
5-1	39.611	9.767	4.056	0.000	0.002
5-3	47.111	9.767	4.823	0.000	0.000
7-6	2.333	10.920	0.214	0.831	1.000
7-9	-3.500	9.767	-0.358	0.720	1.000
7-4	24.333	9.767	2.491	0.013	0.458
7-2	28.333	13.813	2.051	0.040	1.000
7-1	30.833	9.767	3.157	0.002	0.057
7-3	38.333	9.767	3.925	0.000	0.003
6-9	-1.167	10.920	-0.107	0.915	1.000
6-4	22.000	10.920	2.015	0.044	1.000
6-2	26.000	14.651	1.775	0.076	1.000
6-1	28.500	10.920	2.610	0.009	0.326
6-3	36.000	10.920	3.297	0.001	0.035
9-4	20.833	9.767	2.133	0.033	1.000
9-2	24.833	13.813	1.798	0.072	1.000
9-1	27.333	9.767	2.799	0.005	0.185
9-3	34.833	9.767	3.566	0.000	0.013
4-2	4.000	13.813	0.290	0.772	1.000
4-1	6.500	9.767	0.666	0.506	1.000
4-3	14.000	9.767	1.433	0.152	1.000
2-1	2.500	13.813	0.181	0.856	1.000
2-3	-10.000	13.813	-0.724	0.469	1.000
1-3	-7.500	9.767	-0.768	0.443	1.000

Table A. 24 Pairwise comparison of samples from the first material set based on sound absorption data at 3150Hz received from high frequency impedance tube

Sample 1-Sample 2	Test Statistic	Std. Error	Std. Test Statistic	Sig.	Adj. Sig.[a]
8-5	9.222	9.672	0.953	0.340	1.000
8-7	20.222	9.672	2.091	0.037	1.000
8-9	-21.222	9.672	-2.194	0.028	1.000
8-4	27.944	9.672	2.889	0.004	0.139
8-2	31.889	13.678	2.331	0.020	0.710
8-1	32.556	9.672	3.366	0.001	0.027
8-6	39.639	10.814	3.666	0.000	0.009
8-3	42.889	9.672	4.434	0.000	0.000
5-7	-11.000	9.672	-1.137	0.255	1.000
5-9	-12.000	9.672	-1.241	0.215	1.000
5-4	18.722	9.672	1.936	0.053	1.000
5-2	22.667	13.678	1.657	0.097	1.000
5-1	23.333	9.672	2.412	0.016	0.570
5-6	-30.417	10.814	-2.813	0.005	0.177
5-3	33.667	9.672	3.481	0.000	0.018
7-9	-1.000	9.672	-0.103	0.918	1.000
7-4	7.722	9.672	0.798	0.425	1.000
7-2	11.667	13.678	0.853	0.394	1.000
7-1	12.333	9.672	1.275	0.202	1.000
7-6	19.417	10.814	1.796	0.073	1.000
7-3	22.667	9.672	2.344	0.019	0.688
9-4	6.722	9.672	0.695	0.487	1.000
9-2	10.667	13.678	0.780	0.435	1.000
9-1	11.333	9.672	1.172	0.241	1.000
9-6	18.417	10.814	1.703	0.089	1.000
9-3	21.667	9.672	2.240	0.025	0.903
4-2	3.944	13.678	0.288	0.773	1.000
4-1	4.611	9.672	0.477	0.634	1.000
4-6	-11.694	10.814	-1.081	0.279	1.000
4-3	14.944	9.672	1.545	0.122	1.000
2-1	0.667	13.678	0.049	0.961	1.000
2-6	-7.750	14.508	-0.534	0.593	1.000
2-3	-11.000	13.678	-0.804	0.421	1.000
1-6	-7.083	10.814	-0.655	0.512	1.000
1-3	-10.333	9.672	-1.068	0.285	1.000
6-3	3.250	10.814	0.301	0.764	1.000

Table A. 25 Pairwise comparison of samples from the first material set based on sound absorption data at 4000Hz received from high frequency impedance tube

Sample 1-Sample 2	Test Statistic	Std. Error	Std. Test Statistic	Sig.	Adj. Sig.[a]
4-8	-0.333	9.735	-0.034	0.973	1.000
4-1	2.833	9.735	0.291	0.771	1.000
4-2	4.833	13.768	0.351	0.726	1.000
4-5	-7.667	9.735	-0.787	0.431	1.000
4-3	19.167	9.735	1.969	0.049	1.000
4-9	-20.667	9.735	-2.123	0.034	1.000
4-7	-27.167	9.735	-2.790	0.005	0.189
4-6	-40.833	10.885	-3.751	0.000	0.006
8-1	2.500	9.735	0.257	0.797	1.000
8-2	4.500	13.768	0.327	0.744	1.000
8-5	7.333	9.735	0.753	0.451	1.000
8-3	18.833	9.735	1.935	0.053	1.000
8-9	-20.333	9.735	-2.089	0.037	1.000
8-7	26.833	9.735	2.756	0.006	0.210
8-6	40.500	10.885	3.721	0.000	0.007
1-2	-2.000	13.768	-0.145	0.885	1.000
1-5	-4.833	9.735	-0.496	0.620	1.000
1-3	-16.333	9.735	-1.678	0.093	1.000
1-9	-17.833	9.735	-1.832	0.067	1.000
1-7	-24.333	9.735	-2.499	0.012	0.448
1-6	-38.000	10.885	-3.491	0.000	0.017
2-5	-2.833	13.768	-0.206	0.837	1.000
2-3	-14.333	13.768	-1.041	0.298	1.000
2-9	-15.833	13.768	-1.150	0.250	1.000
2-7	-22.333	13.768	-1.622	0.105	1.000
2-6	-36.000	14.603	-2.465	0.014	0.493
5-3	11.500	9.735	1.181	0.238	1.000
5-9	-13.000	9.735	-1.335	0.182	1.000
5-7	-19.500	9.735	-2.003	0.045	1.000
5-6	-33.167	10.885	-3.047	0.002	0.083
3-9	-1.500	9.735	-0.154	0.878	1.000
3-7	-8.000	9.735	-0.822	0.411	1.000
3-6	-21.667	10.885	-1.991	0.047	1.000
9-7	6.500	9.735	0.668	0.504	1.000
9-6	20.167	10.885	1.853	0.064	1.000
7-6	13.667	10.885	1.256	0.209	1.000

Table A. 26 Pairwise comparison of samples from the first material set based on sound absorption data at 5000Hz received from high frequency impedance tube

Sample 1-Sample 2	Test Statistic	Std. Error	Std. Test Statistic	Sig.	Adj. Sig.[a]
8-5	4.500	9.794	0.459	0.646	1.000
8-9	-22.333	9.794	-2.280	0.023	0.813
8-7	25.500	9.794	2.604	0.009	0.332
8-4	28.667	9.794	2.927	0.003	0.123
8-1	32.667	9.794	3.335	0.001	0.031
8-6	34.417	10.950	3.143	0.002	0.060
8-2	37.167	13.851	2.683	0.007	0.262
8-3	52.333	9.794	5.343	0.000	0.000
5-9	-17.833	9.794	-1.821	0.069	1.000
5-7	-21.000	9.794	-2.144	0.032	1.000
5-4	24.167	9.794	2.468	0.014	0.490
5-1	28.167	9.794	2.876	0.004	0.145
5-6	-29.917	10.950	-2.732	0.006	0.227
5-2	32.667	13.851	2.358	0.018	0.661
5-3	47.833	9.794	4.884	0.000	0.000
9-7	3.167	9.794	0.323	0.746	1.000
9-4	6.333	9.794	0.647	0.518	1.000
9-1	10.333	9.794	1.055	0.291	1.000
9-6	12.083	10.950	1.104	0.270	1.000
9-2	14.833	13.851	1.071	0.284	1.000
9-3	30.000	9.794	3.063	0.002	0.079
7-4	3.167	9.794	0.323	0.746	1.000
7-1	7.167	9.794	0.732	0.464	1.000
7-6	8.917	10.950	0.814	0.415	1.000
7-2	11.667	13.851	0.842	0.400	1.000
7-3	26.833	9.794	2.740	0.006	0.221
4-1	4.000	9.794	0.408	0.683	1.000
4-6	-5.750	10.950	-0.525	0.600	1.000
4-2	8.500	13.851	0.614	0.539	1.000
4-3	23.667	9.794	2.416	0.016	0.564
1-6	-1.750	10.950	-0.160	0.873	1.000
1-2	-4.500	13.851	-0.325	0.745	1.000
1-3	-19.667	9.794	-2.008	0.045	1.000
6-2	2.750	14.691	0.187	0.852	1.000
6-3	17.917	10.950	1.636	0.102	1.000
2-3	-15.167	13.851	-1.095	0.274	1.000

B. The resulst of statistical tests conducted on the second plaster set

Table B. 1 The results of Kruskal-Wallis test for the data of second plaster set received from low frequency impedance tube measurements

	Null Hypothesis	Test	Sig.[a,b]	Decision
1	The distribution of alpha63 is the same across categories of matgroup.	Independent-Samples Kruskal-Wallis Test	0.024	Reject the null hypothesis.
2	The distribution of alpha80 is the same across categories of matgroup.	Independent-Samples Kruskal-Wallis Test	0.069	Retain the null hypothesis.
3	The distribution of alpha100 is the same across categories of matgroup.	Independent-Samples Kruskal-Wallis Test	0.036	Reject the null hypothesis.
4	The distribution of alpha125 is the same across categories of matgroup.	Independent-Samples Kruskal-Wallis Test	0.041	Reject the null hypothesis.
5	The distribution of alpha160 is the same across categories of matgroup.	Independent-Samples Kruskal-Wallis Test	0.090	Retain the null hypothesis.
6	The distribution of alpha200 is the same across categories of matgroup.	Independent-Samples Kruskal-Wallis Test	0.278	Retain the null hypothesis.
7	The distribution of alpha250 is the same across categories of matgroup.	Independent-Samples Kruskal-Wallis Test	0.063	Retain the null hypothesis.
8	The distribution of alpha315 is the same across categories of matgroup.	Independent-Samples Kruskal-Wallis Test	0.000	Reject the null hypothesis.
9	The distribution of alpha400 is the same across categories of matgroup.	Independent-Samples Kruskal-Wallis Test	0.001	Reject the null hypothesis.
10	The distribution of alpha500 is the same across categories of matgroup.	Independent-Samples Kruskal-Wallis Test	0.001	Reject the null hypothesis.
11	The distribution of alpha630 is the same across categories of matgroup.	Independent-Samples Kruskal-Wallis Test	0.004	Reject the null hypothesis.
12	The distribution of alpha800 is the same across categories of matgroup.	Independent-Samples Kruskal-Wallis Test	0.004	Reject the null hypothesis.
13	The distribution of alpha1000 is the same across categories of matgroup.	Independent-Samples Kruskal-Wallis Test	0.001	Reject the null hypothesis.
14	The distribution of alpha1250 is the same across categories of matgroup.	Independent-Samples Kruskal-Wallis Test	0.000	Reject the null hypothesis.
15	The distribution of alpha1600 is the same across categories of matgroup.	Independent-Samples Kruskal-Wallis Test	0.000	Reject the null hypothesis.

a. The significance level is .050.

b. Asymptotic significance is displayed.

Table B. 2 The results of Kruskal-Wallis test for the data of second plaster set received from high frequency impedance tube measurements

	Null Hypothesis	Test	Sig.[a,b]	Decision
1	The distribution of alpha1000 is the same across categories of matgroup.	Independent-Samples Kruskal-Wallis Test	0.003	Reject the null hypothesis.
2	The distribution of alpha1250 is the same across categories of matgroup.	Independent-Samples Kruskal-Wallis Test	0.004	Reject the null hypothesis.
3	The distribution of alpha1600 is the same across categories of matgroup.	Independent-Samples Kruskal-Wallis Test	0.004	Reject the null hypothesis.
4	The distribution of alpha2000 is the same across categories of matgroup.	Independent-Samples Kruskal-Wallis Test	0.021	Reject the null hypothesis.
5	The distribution of alpha2500 is the same across categories of matgroup.	Independent-Samples Kruskal-Wallis Test	0.015	Reject the null hypothesis.
6	The distribution of alpha3150 is the same across categories of matgroup.	Independent-Samples Kruskal-Wallis Test	0.009	Reject the null hypothesis.
7	The distribution of alpha4000 is the same across categories of matgroup.	Independent-Samples Kruskal-Wallis Test	0.015	Reject the null hypothesis.
8	The distribution of alpha5000 is the same across categories of matgroup.	Independent-Samples Kruskal-Wallis Test	0.006	Reject the null hypothesis.
a. The significance level is .050.				
b. Asymptotic significance is displayed.				

In pairwise distributions, each row tests the null hypothesis that the Sample 1 and Sample 2 distributions are the same. Asymptotic significances (2-sided tests) are displayed in the tables. The significance level is 0.05. Significance values have been adjusted by the Bonferroni correction for multiple tests.

Table B. 3 Abbreviations used for material codes in statistical tests

Material Code	Abbreviation in Statistical Test
V-S2-1/0.6-DistSp	S
V-T-1/0.6-DistSp	T
V-P-1/0.6-DistSp	P

Table B. 4 Pairwise comparison of samples from the second material set based on sound absorption data at 63Hz received from low frequency impedance tube

Sample 1-Sample 2	Test Statistic	Std. Error	Std. Test Statistic	Sig.	Adj. Sig.[a]
P-K	5.600	3.780	1.482	0.138	0.415
P-T	-10.267	3.780	-2.716	0.007	0.020
K-T	-4.667	3.878	-1.203	0.229	0.686

Table B. 5 Pairwise comparison of samples from the second material set based on sound absorption data at 100Hz received from low frequency impedance tube

Sample 1-Sample 2	Test Statistic	Std. Error	Std. Test Statistic	Sig.	Adj. Sig.[a]
P-K	5.944	3.780	1.573	0.116	0.347
P-T	-9.611	3.780	-2.543	0.011	0.033
K-T	-3.667	3.878	-0.946	0.344	1.000

Table B. 6 Pairwise comparison of samples from the second material set based on sound absorption data at 125Hz received from low frequency impedance tube

Sample 1-Sample 2	Test Statistic	Std. Error	Std. Test Statistic	Sig.	Adj. Sig.[a]
P-K	5.089	3.780	1.346	0.178	0.535
P-T	-9.533	3.780	-2.522	0.012	0.035
K-T	-4.444	3.878	-1.146	0.252	0.755

Table B. 7 Pairwise comparison of samples from the second material set based on sound absorption data at 315Hz received from low frequency impedance tube

Sample 1-Sample 2	Test Statistic	Std. Error	Std. Test Statistic	Sig.	Adj. Sig.[a]
T-K	10.333	3.878	2.665	0.008	0.023
T-P	14.500	3.780	3.836	0.000	0.000
K-P	-4.167	3.780	-1.102	0.270	0.811

Table B. 8 Pairwise comparison of samples from the second material set based on sound absorption data at 400Hz received from low frequency impedance tube

Sample 1-Sample 2	Test Statistic	Std. Error	Std. Test Statistic	Sig.	Adj. Sig.[a]
T-K	11.667	3.878	3.009	0.003	0.008
T-P	13.300	3.780	3.519	0.000	0.001
K-P	-1.633	3.780	-0.432	0.666	1.000

Table B. 9 Pairwise comparison of samples from the second material set based on sound absorption data at 500Hz received from low frequency impedance tube

Sample 1-Sample 2	Test Statistic	Std. Error	Std. Test Statistic	Sig.	Adj. Sig.[a]
T-P	12.400	3.780	3.281	0.001	0.003
T-K	12.667	3.878	3.266	0.001	0.003
P-K	0.267	3.780	0.071	0.944	1.000

Table B. 10 Pairwise comparison of samples from the second material set based on sound absorption data at 630Hz received from low frequency impedance tube

Sample 1-Sample 2	Test Statistic	Std. Error	Std. Test Statistic	Sig.	Adj. Sig.[a]
T-K	10.667	3.878	2.751	0.006	0.018
T-P	11.400	3.780	3.016	0.003	0.008
K-P	-0.733	3.780	-0.194	0.846	1.000

Table B. 11 Pairwise comparison of samples from the second material set based on sound absorption data at 800Hz received from low frequency impedance tube

Sample 1-Sample 2	Test Statistic	Std. Error	Std. Test Statistic	Sig.	Adj. Sig.[a]
T-K	10.667	3.878	2.751	0.006	0.018
T-P	11.400	3.780	3.016	0.003	0.008
K-P	-0.733	3.780	-0.194	0.846	1.000

Table B. 12 Pairwise comparison of samples from the second material set based on sound absorption data at 1000Hz received from low frequency impedance tube

Sample 1-Sample 2	Test Statistic	Std. Error	Std. Test Statistic	Sig.	Adj. Sig.[a]
T-P	12.400	3.780	3.281	0.001	0.003
T-K	12.667	3.878	3.266	0.001	0.003
P-K	0.267	3.780	0.071	0.944	1.000

Table B. 13 Pairwise comparison of samples from the second material set based on sound absorption data at 1250Hz received from low frequency impedance tube

Sample 1-Sample 2	Test Statistic	Std. Error	Std. Test Statistic	Sig.	Adj. Sig.[a]
T-P	13.400	3.780	3.545	0.000	0.001
T-K	14.667	3.878	3.782	0.000	0.000
P-K	1.267	3.780	0.335	0.738	1.000

Table B. 14 Pairwise comparison of samples from the second material set based on sound absorption data at 1600Hz received from low frequency impedance tube

Sample 1-Sample 2	Test Statistic	Std. Error	Std. Test Statistic	Sig.	Adj. Sig.[a]
T-K	13.667	3.878	3.524	0.000	0.001
T-P	14.300	3.780	3.783	0.000	0.000
K-P	-0.633	3.780	-0.168	0.867	1.000

Table B. 15 Pairwise comparison of samples from the second material set based on sound absorption data at 1000Hz received from high frequency impedance tube

Sample 1-Sample 2	Test Statistic	Std. Error	Std. Test Statistic	Sig.	Adj. Sig.[a]
K-T	-7.222	3.742	-1.930	0.054	0.161
K-P	-12.778	3.742	-3.415	0.001	0.002
T-P	5.556	3.742	1.485	0.138	0.413

Table B. 16 Pairwise comparison of samples from the second material set based on sound absorption data at 1250Hz received from high frequency impedance tube

Sample 1-Sample 2	Test Statistic	Std. Error	Std. Test Statistic	Sig.	Adj. Sig.[a]
K-T	-3.000	3.742	-0.802	0.423	1.000
K-P	-12.000	3.742	-3.207	0.001	0.004
T-P	9.000	3.742	2.405	0.016	0.048

Table B. 17 Pairwise comparison of samples from the second material set based on sound absorption data at 1600Hz received from high frequency impedance tube

Sample 1-Sample 2	Test Statistic	Std. Error	Std. Test Statistic	Sig.	Adj. Sig.[a]
K-T	-3.000	3.742	-0.802	0.423	1.000
K-P	-12.000	3.742	-3.207	0.001	0.004
T-P	9.000	3.742	2.405	0.016	0.048

Table B. 18 Pairwise comparison of samples from the second material set based on sound absorption data at 2000Hz received from high frequency impedance tube

Sample 1-Sample 2	Test Statistic	Std. Error	Std. Test Statistic	Sig.	Adj. Sig.[a]
K-T	-0.667	3.742	-0.178	0.859	1.000
K-P	-9.333	3.742	-2.494	0.013	0.038
T-P	8.667	3.742	2.316	0.021	0.062

Table B. 19 Pairwise comparison of samples from the second material set based on sound absorption data at 2500Hz received from high frequency impedance tube

Sample 1-Sample 2	Test Statistic	Std. Error	Std. Test Statistic	Sig.	Adj. Sig.[a]
T-K	0.889	3.742	0.238	0.812	1.000
T-P	9.778	3.742	2.613	0.009	0.027
K-P	-8.889	3.742	-2.376	0.018	0.053

Table B. 20 Pairwise comparison of samples from the second material set based on sound absorption data at 3150Hz received from high frequency impedance tube

Sample 1-Sample 2	Test Statistic	Std. Error	Std. Test Statistic	Sig.	Adj. Sig.[a]
T-K	3.778	3.742	1.01	0.313	0.938
T-P	11.222	3.742	2.999	0.003	0.008
K-P	-7.444	3.742	-1.99	0.047	0.14

Table B. 21 Pairwise comparison of samples from the second material set based on sound absorption data at 4000Hz received from high frequency impedance tube

Sample 1-Sample 2	Test Statistic	Std. Error	Std. Test Statistic	Sig.	Adj. Sig.[a]
T-K	3.111	3.742	0.831	0.406	1.000
T-P	10.556	3.742	2.821	0.005	0.014
K-P	-7.444	3.742	-1.990	0.047	0.140

Table B. 22 Pairwise comparison of samples from the second material set based on sound absorption data at 5000Hz received from high frequency impedance tube

Sample 1-Sample 2	Test Statistic	Std. Error	Std. Test Statistic	Sig.	Adj. Sig.[a]
T-K	3.333	3.742	0.891	0.373	1.000
T-P	11.667	3.742	3.118	0.002	0.005
K-P	-8.333	3.742	-2.227	0.026	0.078

CURRICULUM VITAE

Surname, Name: Meriç Nursal, Işın

EDUCATION

Degree	Institution	Year of Graduation
PhD	METU Building Science	2024
MS	İTÜ Environmental Control and Building Science	2009
BS	İTÜ Architecture	2006
High School	Ankara Atatürk Anadolu Lisesi, Ankara	2002

WORK EXPERIENCE

Date	Company
07/2012-	Mezzo Stüdyo Ltd. Şti. Architect and Acoustics Consultant
09/2009 – 09/2010	Ses Görüntü Prodüksiyon Hiz. Ltd. Şti. Architect and Acoustics Consultant
07/2009 – 11/2009	Talayman Akustik Müh. Ltd. Şti. Architect and Acoustics Consultant
10/2008 – 11/2008 02/2009 – 07/2009	Fores Akustik Elektronik Müh. San. Ve Tic. Ltd. Şti. Architect and Acoustics Consultant

RESEARCH PROJECTS INVOLVED

Date	Project
01/2015-06/2017	METU – Faculty of Architecture University Funded Scientific Research Project (BAP-02-01-2015-001) "Investigating the relation between sound absorption characteristics and pore structure parameters of lime based plaster/mortars”
01/2013-12/2013	METU – Faculty of Architecture

	University Funded Scientific Research Project (BAP-02-01-2013-003) " The technological properties of building materials used in traditional timber framed housing in the vicinity of Ankara: Mudbrick and plasters”
09/2006 – 07/2007	İTÜ – Faculty of Architecture University Funded Scientific Research Project “Field survey about the existing acoustical problems of the elementary school buildings and investigating the acoustical solutions”

ORGANIZATIONS INVOLVED

Date	**Organization**
02-05/06/2014	MONUBASIN’9 - 9th International Symposium on Conservation of Monuments in Mediterranean Basin *Support Team Member*

FOREIGN LANGUAGES

Advanced English

CONFERANCE PUBLICATIONS

1. Bayazit, N. T., Kucukciftci, S. & Meric, I. (2007, August). Noise levels of the elementary schools in Istanbul. Paper presented at INTER-NOISE 2007, Istanbul, Turkey.

2. Meric, I., Erdil, M., Madani, N., Alam, B., Tavukcuoglu, A. & Caner Saltik, E. N. (2013, September). Technological properties of earthen building materials in traditional timber frame structures. Paper presented at Kerpic’13 – New Generation Earthen Architecture: Learning from Heritage, Istanbul, Turkey.

3. Meric, I. & Caliskan, M. (2013, September). Acoustics education for architects: Developing a base of knowledge for professional experience. Paper presented at INTER-NOISE 2013, Innsbruck, Austria.

4. Meric, I., Tavukcuoglu, A. & Caliskan, M. (2014, April). Malzemelerin mikro yapi özelliklerinin akustik performansa etkisi: gözeneklilik yapisi ile ses yutma

özellikleri arasindaki ilişki. Paper presented at 1. Ulusal Yapı Fiziği ve Çevre Kontrolü Kongresi, Istanbul, Turkey.

5. Meriç, I., Erdil, M., Madani, N., Alam, B. A, Tavukçuoğlu, A. & Caner Saltık, E.N. (2014, June). Material characterization of mudbrick and neighbouring plasters in traditional timber framed structures. Paper presented at MONUBASIN'9 - 9th International Symposium on Conservation of Monuments in Mediterranean Basin, Ankara, Turkey.

6. Meric Nursal, I.M., Tavukcuoglu, A. & Caliskan M. (2015, August). The role of pore structure in sound absorption performance of lime based plasters. Paper presented at INTER-NOISE 2015, San Francisco, CA, USA.

7. Meric Nursal, I., Tavukcuoglu, A. & Caliskan, M. (2016, May). Kireç esaslı sıvalarda karışım oranlarının gözenek yapısı ve ses yutma özelliklerine etkisi. Paper presented at 2. Ulusal Yapı Fiziği ve Çevre Kontrolü Kongresi, Istanbul, Turkey.

8. Su Gul, Z., Odabas, E., Meric Nursal, I. & Caliskan, M. (2016, September). Acoustical design of Awaza Convention Center. Paper presented at ICA 2016 – 22nd International Congress on Acoustics. Buenos Aires, Argentina.

9. Su Gul, Z., Meric Nursal, I., Bora, Z. & Caliskan, M. (2016, September). Acoustical design of İzmir Opera House. Paper presented at ISMRA 2016 – International Symposium on Musical and Room Acoustics. Buenos Aires, Argentina.

10. Nursal, I. M., Eşmebaşı, M., Erdem, E. and Sü Gül, Z. (2018, October). Acoustic Design and Analysis Methods of Underground Subway Stations. Paper presented at 13th National Acoustics Congress (TAKDER), Diyarbakır, Turkey.